RIVISTA DEL NUOVO CIMENTO Vol. 38, N. 11 2015
DOI 10.1393/ncr/i2015-10118-8

# The discovery of the Higgs boson at the Large Hadron Collider

A. Nisati([1]) and G. Tonelli([2])

([1]) *INFN, Sezione di Roma - Roma, Italy*
([2]) *Dipartimento di Fisica, Università di Pisa and INFN, Sezione di Pisa - Pisa, Italy*

received 27 July 2015

**Summary.** — This paper summarises the work done by the ATLAS and CMS collaborations, and by the teams of the Large Hadron Collider at CERN, that led to the discovery of a new particle, with mass near 125 GeV and properties consistent with the ones predicted for the Standard Model Higgs boson. An overview of the Standard Model, with a description of the role of the Higgs boson in the theory, and a summary of the searches for this particle prior to the LHC operations is also given. The paper presents the results obtained by ATLAS and CMS from the analysis of the full data set produced in the first physics run of LHC. After a short discussion on the implications of the discovery, the future prospects for the precision study of the new particle are lastly discussed.

PACS `12.60.-i` – Models beyond the standard model.
PACS `13.66.Fg` – Gauge and Higgs boson production in $e^-e^+$ interactions.
PACS `13.85.-t` – Hadron-induced high- and super-high-energy interactions (energy $> 10\,\text{GeV}$).
PACS `14.80.Bn` – Standard-model Higgs bosons.

## 1. – Introduction

The Standard Model (SM) of particle physics describes accurately a lot of experimental data that probe elementary particles interactions up to a energy scale of a few hundred GeV (the electroweak energy scale). At the end of 2011, all elementary constituents predicted by the theory (quarks, leptons and gauge bosons) had been discovered, except one: the Higgs boson. This particle with spin 0 plays a fundamental role in the SM: it is responsible of the electroweak symmetry breaking, therefore allowing the gauge bosons, $W^\pm$ and $Z$ to become massive; in addition it provides fermions their distinctive masses through the Yukawa interaction with the Higgs field.

Intensive experimental searches were conducted over many decades since the formulation of the Higgs mechanism in 1964. Given that no significant evidence was found, experiments were able only to set limits on its mass. In particular, the combination of the results of the four LEP experiments yielded a limit $m_H > 114.4\,\mathrm{GeV}$ at 95% confidence level while additional limits were set by experiments at the Tevatron Collider.

With the start-up of the operations at the CERN Large Hadron Collider (LHC), ATLAS and CMS, the two general-purpose experiments, took the lead of the search.

After a first evidence, shown in a seminar held at CERN at the end of 2011, in July 2012 the two experiments announced the discovery of a new, neutral particle of mass of about 125 GeV. The properties of the new particle were shown to be consistent with those predicted for the SM Higgs boson. These results were lastly confirmed by the analysis of the full data sample corresponding to the first physics run of LHC (Run 1).

With the discovery of the Higgs boson the picture appears complete: all fundamental constituents of the Standard Model have been realised in nature. However, precision measurements of the properties of the new particle will be crucial tests to establish the level of consistency of experimental data with the values predicted by the theory. These measurements could probe for possible effects from New Physics at a scale larger than the electroweak scale.

This paper reviews the most important steps that led to the discovery of the Higgs boson. Section **2** gives a concise review of the Standard Model theory, with a particular attention to the Brout-Englert-Higgs mechanism, given in sect. **3**. The most important direct searches prior to the start-up of LHC, including results from LEP and the Tevatron collider, are summarised in sect. **4**. Section **5** summarises the constraints to the SM Higgs boson using precision measurements performed in past experiments, in particular at LEP and SLC. The LHC machine and the ATLAS and CMS experiments are presented in sect. **6**, while sect. **7** illustrates the SM Higgs boson production processes in proton-proton collisions at the LHC energies, as well as the decay final states as a function of its mass. The study of the SM processes at LHC, a major milestone in understanding the new energy regime and some of the most important backgrounds to the Higgs boson search, is presented in sect. **8**. sect. **9** reports the early searches on 7 TeV data, and sect. **10** shows the results producing a first evidence of a new, neutral particle of about 125 GeV mass. The most important steps that led to the observation of the SM-like Higgs boson in 2012 are presented in sect. **11**. The legacy results presented by ATLAS and CMS based on the whole 2011-2012 data set are reported in sect. **12**, while sect. **13** presents the measurement of the mass and some of the most important analyses performed to determine the properties of the new particle. The results of the searches for other Higgs-like bosons at the LHC are summarised in sect. **14**. Lastly, some of the implications of this discovery are briefly discussed in sect. **15**, while the future prospects concerning the physics studies of this new particle, and the future investigations associated to this boson in the domain of high-energy physics are discussed in sect. **16**.

## 2. – The Standard Model of fundamental interactions

The *Standard Model* is a theoretical framework, built in the early 1970's from experimental results, that allows correlating a large set of new data [1-4]. A nice overview of this model is available in [5].

The fundamental elements of matter can be grouped in two distinct families, each composed by three pairs of elementary particles: the *quarks* (*up* and *down*; *charm* and *strange*; *top* and *bottom*) and the *leptons* (*electron* and *electron neutrino*; *muon* and *muon neutrino*; *tau* and *tau neutrino*). For each one of these particles the corresponding antiparticle exists; antiparticles are grouped as particles. The list of these particles, and their most important properties, are shown in fig. 1.

Electrons, muons and taus have the same electric charge, ($e = 1.60217657 \times 10^{-19}$ C), while neutrino have no electric charge. Up-like quarks have fractional electric charge $+2/3e$, while down-type quarks have $-1/3e$ electric charge.

Neglecting from now onwards the gravitational force, charged leptons are subject to

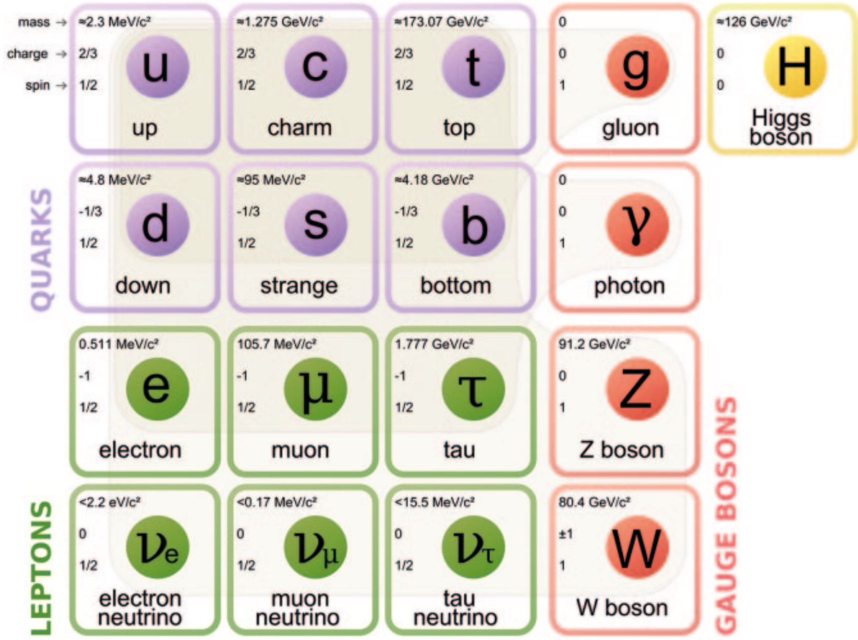


Fig. 1. – Elementary particles of the Standard Model: fermions, gauge bosons and the Higgs boson.

electromagnetic and weak nuclear forces. Neutrinos are subject to the weak nuclear force only. Quarks are sensitive also to the strong nuclear force, in addition to the other two. The quantum number associated to strong interactions between quarks is called *colour*. There are three possible colour states.

Antiparticles have the same mass of the corresponding particle, but opposite electric charge and opposite colour (anticolour), in case of antiquarks.

Leptons and quarks have half-integer spin$(1/2)\hbar$ (or just $1/2$), hence they follow the Fermi-Dirac statistics. All particle with half-integer spin are called *fermions*.

In quantum mechanics, interactions between particles are mediated by spin-1 elementary particles: the *gauge bosons* (particles with integer spin —including spin$\,=0$— follow the Bose-Einstein statistics and are called bosons). In the Standard Model these are the photon $\gamma$, the $W^{\pm}$ and $Z$, and eight types of gluons, $g$. The photon propagates the electromagnetic forces, it is electrically neutral, has vanishing mass and is well-described by the renormalizable theory called Quantum ElectroDynamics, or QED.

The charged $W^{\pm}$ and neutral $Z$ vector bosons propagate the weak nuclear interaction, and have large mass: $80.385 \pm 0.015\,\text{GeV}$ for $W^{\pm}$ and $91.1876 \pm 0.021\,\text{GeV}$ for $Z$ [6]. Gluons are massless, and in contrast to the electrically neutral photon, they carry colour-anticolour charge and hence they couple each other. Furthermore, the strength of the interaction between particles with colour quantum numbers increases with increasing distance: quarks and gluons cannot be observed as free particles: they are subject to colour confinement and appear only as bound states. Quarks are confined with other quarks or antiquarks to compose hadrons: baryons and mesons. The Quantum ChromoDynamics, or QCD, is the theory in the Standard Model that describes the strong interaction of coloured particles, with $SU(3)$ symmetry.

Although at a low energy scale experimentally they appear very different, electromagnetic and weak interactions arise as two different aspects of the same force. Above energies of $\mathcal{O}(100\,\text{GeV})$, they merge into a unified *electroweak* force and the gauge bosons $\gamma$, $W^{\pm}$ and $Z$ are the mediators of this unique force, the *electroweak* interaction. The electroweak interaction is described by the Yang-Mills gauge theory based on the symmetry group $U(1) \times SU(2)_L$. $SU(2)_L$ refers to the weak isospin, $T$, with the subscript $L$ indicating that it involves left-handed fields: under $SU(2)_L$ the left-handed fields transform as doublets, while the right-handed ones do not transform at all. $U(1)_Y$ refers to the weak hypercharge, $Y$, which is defined by the relation:

$$Q = T_3 + \frac{1}{2}Y, \tag{1}$$

where $Q$ is the electric charge, $T_3$ is the third component of the weak isospin [2].

## 3. – The Brout-Englert-Higgs mechanism

The most important historical developments in Higgs physics over the past half-century are nicely reviewed in papers [7-9].

In theories involving gauge invariance, gauge bosons are described by field equations of massless particles. In this framework gauge bosons are massless and the forces have a long range, which is in contrast with the experimental observation.

A very important theoretical breakthrough of the early 1970's was the proof that Yang-Mills theories are renormalisable, and that this property still holds if the gauge symmetry is spontaneously broken [10, 4]. In other words, the Lagrangian of the interaction is gauge invariant while the vacuum state and the spectrum of particles described by the model are not. A physics example is given by a ferromagnet for which the lowest-energy configuration has electron spins aligned. All alignment directions are equally possible, *i.e.* the system has a rotational symmetry, but nature in the end chooses one direction, randomly, that is not possible to predict. This "breaks" that symmetry, because after this "choice" the system has lost the initial symmetry.

In quantum field theory, the simplest way to introduce spontaneous symmetry breaking is the so-called Brout-Englert-Higgs mechanism, reported hereafter simply as the *Higgs mechanism*. A simple model of spontaneous $U(1)$ symmetry breaking [11] with a single complex scalar field $\phi = |\phi| \exp(i\theta)$, whose gauge invariant potential field is described by the function

$$\begin{aligned} V(\phi) &= \mu^2 \left(\phi^\dagger \phi\right) + \lambda \left(\phi^\dagger \phi\right)^2 \\ &= \mu^2 |\phi|^2 + \lambda |\phi|^4 \end{aligned} \tag{2}$$

is illustrated in fig. 2.

This potential has a minimum at $|\phi| = (1/\sqrt{2}) \times \mu/\sqrt{-\lambda} = v$, but is independent of the phase $\theta$. The nature's choice for the angle $\theta$ breaks the symmetry. The value of $v$ is the *vacuum value*, or *vacuum expectation value (vev)*. Quantum excitations along $\phi$ describe a massive particle. The phase $\theta$ of the field $\phi$ is, however, undetermined. Quantum excitations along this parameter around the ground state cost no energy, and they are associated to massless and spinless particles called *Goldstone bosons*.

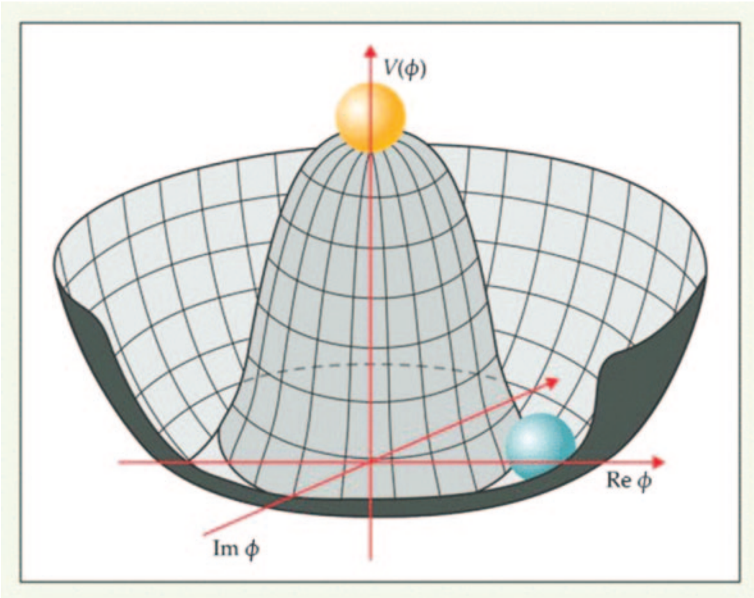


Fig. 2. – Mexican hat shape of the Higgs potential described by eq. (2) that leads to "spontaneous" symmetry breaking. The vacuum, *i.e.* the lowest-energy state, is described by a randomly chosen point around the bottom of the brim of the hat. The Higgs boson is a massive spin-zero particle corresponding to quantum fluctuations in the radial direction, oscillating between the centre and the side of the hat.

In the context of a $SU(2)_L \times U(1)_Y$ symmetry, the Higgs mechanism is implemented introducing a $SU(2)_L$ isospin doublet of complex scalar field with hypercharge $Y = +1$:

$$\phi = \begin{pmatrix} \phi^+ \\ \phi^0 \end{pmatrix} = \frac{1}{\sqrt{2}} \begin{pmatrix} \phi_1 + i\phi_2 \\ \phi_3 + i\phi_4 \end{pmatrix}. \tag{3}$$

The Lagrangian describing the dynamics of this field $\phi$ is then

$$\mathcal{L}_H = (D_\mu \phi)^\dagger (D^\mu \phi) - V(\phi). \tag{4}$$

The symmetry breaking is obtained through the form of the scalar $V$ potential controlled by the parameters $\lambda$ and $\mu$ in eq. (2) and $D_\mu$ is the covariant derivative.

If $\mu^2 > 0$, the ground state corresponds to $\phi = 0$; *i.e.* to the vacuum. For values $\mu^2 < 0$, a non-vanishing vacuum expectation value for $|\phi|^2$ in the physical vacuum state is obtained: the Lagrangian has a mass term with negative sign for the field $\phi$ and the minimum energy is not at $\phi = 0$. The potential assumes a shape with a local maximum at $\phi = 0$. The vacuum is not stable, as it does not correspond to a system with the lowest possible energy.

Minimisation of the vacuum fixes the field $\phi_0$ in the ground state: $|\phi_0| = (1/\sqrt{2}) \times \mu/\sqrt{-\lambda} = v$.

The symmetry can be broken describing the field $\phi$ around the value $\phi_0$, *e.g.*

$$\phi(x) = \begin{pmatrix} 0 \\ \frac{v+H(x)}{\sqrt{2}} \end{pmatrix}, \tag{5}$$

where $H$ is a physical scalar field, whose quantum excitation is the Higgs boson.

Using this field expansion in eq. (4), four physical fields are obtained. Two charged fields for which mass terms naturally appear, and that can be associated to the $W^{\pm}$ bosons. Moreover, two more neutral fields are found, where only one shows a mass term while the other one remains massless; these fields are associated to the $Z$ boson and the photon, respectively.

A gauge boson mass $m$ is determined by its coupling $g$ to the Higgs field and the vacuum value $v$. Since gauge couplings are universal, they also determine the Fermi constant $G_F$: $m = gv/2$; $G_F/\sqrt{2} = g^2/(8m^2) = v^2/2$. From the constant $G_F = 1.16637(1) \times 10^{-5}\,\mathrm{GeV}^{-2}$ the vacuum expectation value is estimated to be $v \simeq 246\,\mathrm{GeV}$.

Also the Higgs field $H$ acquires a mass after the symmetry breaking. The mass of the associated boson, $m_H$, is given by $m_H = 2\sqrt{-\lambda^2}$. The value of the parameter $\lambda$ is not predicted by the SM theory, therefore the Higgs boson mass remains a free parameter of the model.

The mass term of elementary fermions cannot be added in the Lagrangian "by hand", as also in the case of the gauge bosons $W^{\pm}$ and Z, since it would violate the $U(1) \times SU(2)_L$ symmetry. However, it is possible to add the gauge invariant Yukawa term introducing the interaction of the fermionic field with the Higgs field doublet in eq. (3). After symmetry breaking, see eq. (5), the fermion fields acquire a mass. The value of the mass for each fermionic field, however, is not predicted by the theory, it can be determined only through experimental observations.

## 4. – Searches for the Standard Model Higgs boson at the start-up of LHC

The search for the particle responsible of the electroweak symmetry breaking has been extremely challenging since the very beginning. First of all, the existence of the new particle was not granted at all. The electroweak symmetry could have been broken dynamically or through other mechanisms. Even assuming the Brout-Englert-Higgs mechanism, there is no stringent limit preventing the new particle to be extremely light, in the range of a few MeV or less, or extremely heavy, up to 1 TeV. Depending on the mass of the scalar particle, different production mechanisms must be considered, as well as different decay modes. Furthermore, within the Standard Model, the width of the Higgs boson grows significantly with the mass, while the lifetime is not negligible only for very small values of the mass, yielding altogether an incredibly complex range of experimental signatures to be addressed.

**4·1.** *First indirect limits.* – The first limits produced on the Higgs mass came from indirect searches. The presence of a new scalar boson, initially called $\phi$ after Weinberg, was assumed to be responsible of a discrepancy between theory and experiment in the studies of X-rays from high-$Z$ muonic atoms [12]. Other constraints were derived considering the effect of a Higgs boson exchange on neutron- and electron-deuteron scattering yielding a lower limit $m_H > 0.6\,\mathrm{MeV}$ [13]. Constraints from astrophysical considerations, *i.e.* emission of Higgs bosons from neutron stars, led to a lower bound in the same range $m_H > 0.7\,\mathrm{MeV}$ [14]. The most stringent indirect limits came from the non-observation of possible Higgs production in $J^P = 0^+ \to 0^-$ nuclear transitions ($1.03\,\mathrm{MeV} < m_H < 18.3\,\mathrm{MeV}$ [15]) and from data on neutron-nucleus scattering ($m_H > 15\,\mathrm{MeV}$ [16]).

With the discovery of the neutral currents in 1973 [17, 18] and the appearance of a new quark, the *charm* in 1974 [19,20] the Standard Model gained momentum and a large series of experiments started checking carefully its predictions, including the presence of a scalar boson. Experimentalists were guided by the phenomenological profile of the new particle published in 1975, that contained the first comprehensive accounting of Higgs branching fractions up to a mass of 100 GeV [21]. The conclusion of the paper is still worth mentioning: *We apologize to experimentalists for having no idea what is the mass of the Higgs boson, unlike the case for charm, and for not being sure of its coupling to other particles, except that they are probably all very small. For these reasons we do not want to encourage big experimental searches for the Higgs boson, but we do feel that people performing experiments vulnerable to the Higgs boson should know how it may turn up.*

**4·2.** *The early direct searches.* – The early direct searches were conducted in the 1980's at DORIS-II, an $e^+e^-$ collider at DESY (Germany) that in 1982-83 was upgraded to run at an energy in the center-of-mass of 11.2 GeV. The very first data sets ($10.7\,\mathrm{pb}^{-1}$ at the $\Upsilon(1s)$ and $64.5\,\mathrm{pb}^{-1}$ at the $\Upsilon(2s)$) was used by the Crystal Ball NaI(Tl) detector to look for the radiative decays of the $\Upsilon$

$$\Upsilon \to X + \gamma. \tag{6}$$

A new scalar particle would have appeared as a bump in the inclusive spectrum of photons associated to hadrons. Indeed, they found a significant excess of events both in the high multiplicity channel, where they reported a signal with a significance of 4.2 standard deviations (s.d.), and in the low multiplicity one, where the significance was found to be 3.0 s.d. Assuming the two channels to be completely independent, the combination of them would have led to a signal exceeding the 5.0 s.d. necessary to claim a discovery. The result was reported as preliminary evidence of a narrow state of mass 8.33 GeV at the XXII International Conference on High Energy Physics, Leipzig, 1984 [22]. However, interpreting the results as the production of the Higgs boson would have implied different production mechanisms and/or anomalous decay modes with respect to the ones expected within the Standard Model: the observed rates were two orders of magnitude larger with respect to predictions for this particular branching ratio. Unfortunately the signal disappeared as soon as new data were collected and the negative result was confirmed by an independent search in the same channels conducted at the Cornell Electron Storage Ring (CESR at Syracuse, NY, USA) [23].

Additional searches at CESR, performed by the CLEO Collaboration, investigated the possibility to discover the Higgs boson among the decay products of $B$ mesons through the reaction

$$B \to X + H. \tag{7}$$

They looked at different decay modes of the scalar particle $H \to \mu^+\mu^-$, or $\pi^+\pi^-$ or $K^+K^-$ but no signal was found [24].

Other searches were performed at the proton cyclotron of the Paul Scherrer Institute (Villigen, Switzerland) where the SINDRUM Collaboration explored the very-low-mass region searching for the decay

$$\pi^+ \to e^+ \nu_e H, \tag{8}$$

with $H \to e^+e^-$ and, again, it was possible only to set limits [25]. At the end of this first round of experimental searches, when in 1989, the Large Electron Positron Collider (LEP) was inaugurated at CERN (Geneva, Switzerland), the mass of the Higgs was expected to be larger than 5 GeV.

**4·3.** *Searches at LEP.* – The Large Electron Positron collider (LEP) was a gigantic accelerator colliding electrons and positrons at a center-of-mass energy that was initially fixed at the $Z$ peak, 91.18 GeV (LEP-I, 1989-1994). In the second period of running, between 1995 and 2000, the energy of the machine was raised up to 209 GeV (LEP-II).

The direct production of Higgs bosons via electron-positron annihilation is negligible due to the extremely small coupling of the Higgs to the electron(positron). The most important process to search for the Higgs at LEP-I is the splitting of $Z$ into a $H$ and $Z^*$, with the latter producing fermion pairs

$$e^+e^- \to Z \to H + Z^* \to H + f\bar{f}. \tag{9}$$

Clean signatures can be looked for if we assume that $H$ decays into $b\bar{b}$ jets and $Z^*$ goes into electrons or muons. Larger branching fractions can also be explored asking the $Z^*$ to produce *invisible* final states such as $\nu\bar{\nu}$. Since no signal was found for these processes, the LEP-I experiments set lower limits on the mass of the Higgs boson $m_H >$ 63.9 GeV [26-29].

At LEP-II the most important process for the production of a Higgs boson becomes the associated production of a Higgs with an on-shell $Z$

$$e^+e^- \to Z + H. \tag{10}$$

Various decays modes of the $Z^0$ and of the $H$ were explored by the LEP-II experiments. The four major final states were

$$e^+e^- \to \nu\bar{\nu} + b\bar{b}; \quad e^+e^- \to l^+l^- + b\bar{b}; \quad e^+e^- \to q\bar{q} + \tau^+\tau^-; \quad e^+e^- \to q\bar{q} + b\bar{b}. \tag{11}$$

Starting in 1995, LEP raised steadily its collision energy to measure precisely the $W$ mass at the threshold of $W$ pair production (LEP-II). Searches performed at the new energies did not yield any signal pushing therefore the limits on the Higgs boson mass to $m_H > 107.8$ GeV at 95% C.L. [30]. At the end of the LEP-II lifetime, an extraordinary effort was put in place to increase the energy of the machine well beyond the design value. The machine reached a record energy of 209 GeV and some Higgs-like events were observed corresponding to a mass $m_H \sim 115$ GeV. The run period was extended for some weeks and a few other candidates were collected, but not enough to convince that a major discovery was within reach. The LEP-II was shut down in November 2000 to allow the start-up of the installation of the Large Hadron Collider in the tunnel. The lower limit on the Higgs mass coming from the direct searches of LEP-II was set at $m_H > 114.4$ GeV with 95% C.L. [31].

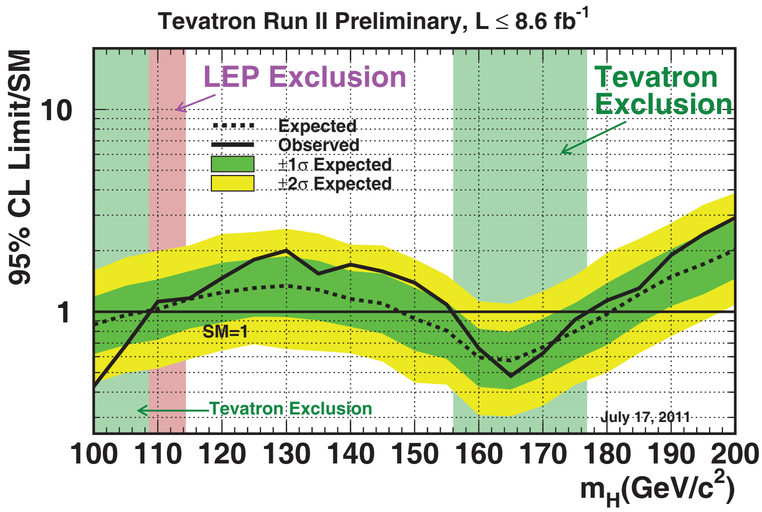


Fig. 3. – Tevatron exclusion limits *vs.* mass of the Higgs boson [32].

4·4. *Searches at the Tevatron collider.* – The Tevatron collider at Fermilab (Batavia, IL USA) led the searches for the Higgs boson in the period between the year 2000, when LEP was shut-down, up to 2010 when LHC started producing its first physics results. The Tevatron collider was a proton-antiproton accelerator in operation since 1987. The maximum collision energy was 1.96 TeV.

The dominant Higgs production mechanism at the Tevatron Collider is Higgs-strahlung in association with a $W^\pm$ or a $Z$. The most sensitive channel is the decay of the Higgs in $b\bar{b}$ jets, a channel that could be explored thanks to the excellent $b$-tagging performance of CDF and D0, the two general purpose experiments.

In July 2011 CDF and D0 presented individual results, based on a statistics of 8.6 fb$^{-1}$ of data, and a combination of their searches (fig. 3). They were able to exclude, at 95% C.L., a range of Higgs masses between 156 and 177 GeV [32]. The Tevatron Collider was shut down in September 2011.

## 5. – Constraints from the global electroweak fit

The huge amount of precision measurements of the electroweak parameters performed at LEP and SLC allowed to establish firmly the validity of the Standard Model. The properties of the $W$ and $Z$ bosons and many other observables were measured with unprecedented precision, in many cases at, or better than, the per-mil level. These measurements were complemented by the observation of the top quark with a precision measurement of its mass, performed by the CDF and DO experiments at the Tevatron Collider, where also the mass of the $W$ was measured with an accuracy challenging the LEP-II results. Assuming the validity of the Standard Model, these electroweak parameters can be combined to extract indirect information on $m_H$ through the dependence of the radiative corrections on the Higgs mass:

$$m_W^2 = \frac{\pi\alpha_{\rm em}}{G_F\sqrt{2}}\frac{1}{\sin^2\theta_W(1-\Delta r)}\,. \tag{12}$$

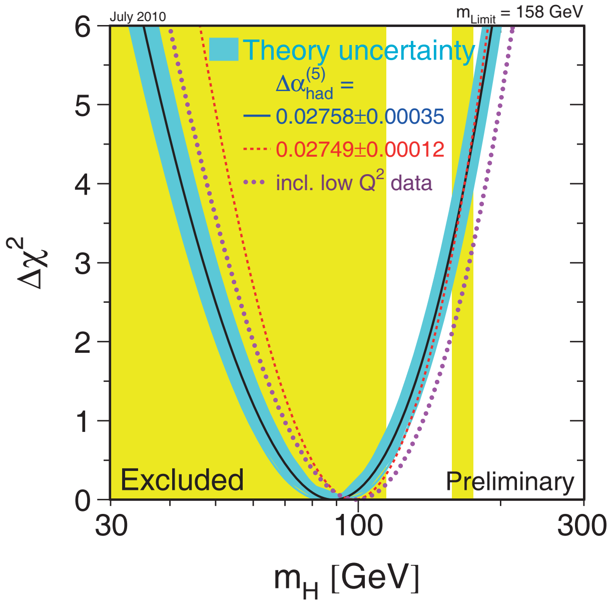


Fig. 4. – Indirect determination of the mass of the Higgs boson $m_H$ from the global electroweak fit [33].

The term $\Delta r$ depends quadratically on the mass of the *top* quark and logarithmically on the mass of the Higgs. Once the mass of the top quark was measured experimentally at the Tevatron Collider, it was possible to extract valuable information on the mass of the Higgs with a global fit to the electroweak parameters that was performed assuming the validity of the Standard Model and leaving $m_H$ as the only free parameter.

An example is shown in fig. 4, where the $\Delta\chi^2$ of the fit is plotted as a function of $m_H$. The black curve is the result of the fit while the blue band represents the theoretical uncertainty due to higher-order corrections. The yellow areas show the region below 114.4 GeV excluded by direct searches at LEP-II and the narrow band of exclusion (158–175 GeV) produced by the Tevatron experiments at the time of the fit (July 2010). The minimum of the curve corresponds to $m_H = 84^{+30}_{-23}$ GeV where the errors correspond to the experimental uncertainty at 68% C.L. and do not consider the theoretical uncertainty. An upper limit on the Higgs boson mass of 158 GeV was set at 95% C.L. Including in the fit the exclusion limits produced by the direct searches, the most probable Higgs mass becomes $m_H = 121^{+17}_{-6}$ GeV [33]. These results are clearly model-dependent, since only contributions from known physics are considered in the loop corrections. However, the strong indication must be noted in favour of a light Higgs boson coming from the global electroweak fit at the time in which LHC experiments started their first physics run.

## 6. – The Large Hadron Collider and its general purpose detectors: ATLAS and CMS

The Large Hadron Collider is to date the largest and highest-energy particle accelerator ever built. The first ideas on a hadron collider with center-of-mass energy in the multi-TeV domain were discussed in the Lausanne Workshop [34] in 1984. Approved


Fig. 5. – Aerial view of the CERN LHC area. The LHC ring is placed at about 100 m under the surface, between the Geneva lake (top-right hand side) and the Jura mountains (opposite side).

by the CERN Council of December 1994, the construction of this accelerator started in 1998, in the LEP tunnel. A nice recollection is available in ref. [35]. The machine was designed primarily to collide protons at a centre-of-mass energy $\sqrt{s} = 14\,\text{TeV}$ with a nominal luminosity of $\mathcal{L} = 1 \times 10^{34}\,\text{cm}^{-2}\,\text{s}^{-1}$ and a bunch spacing of 25 ns. Details on the design of this accelerator can be found in refs. [36-38].

The LHC is located about 100 m below the surface in the 27 km LEP tunnel, between the Jura Mountains and the Geneva lake, see fig. 5. The CERN accelerator complex up to the Super Proton Synchrotron (SPS) machine is used to inject proton beams in the LHC with energy of 450 GeV; see also fig. 6.

A total of about 9600 superconducting magnets are distributed along the circumference of the accelerator. Among these, 1232 dipoles are used to bend the proton trajectory to follow the circular orbit. Each dipole is 14.3 m long and provides a uniform constant magnetic field of 8.3 T for a 7 TeV proton beam. The core of the dipoles is cooled down to 1.9 K in a superfluid liquid-helium bath (a temperature lower than the one in the intergalactic space).

The nominal beam structure consists of 2808 bunches, each one containing $1.15 \times 10^{11}$ protons distributed on a length of 7.6 cm and with a transverse dimension in the final focus of about 16 $\mu$m. As already mentioned, the nominal bunch-to-bunch separation is set to $\Delta t = 25\,\text{ns}$.

The start-up of the Large Hadron Collider on September 10, 2008, was a great success. Unfortunately, just nine days later, a faulty inter-dipole bus-bar splice triggered a severe incident that severely damaged many machine elements in sector "3-4". Actions were taken immediately to repair the damage and to implement the necessary actions to prevent further incidents. It took more than one year to re-commission the accelerator.

In response to the incident, it was decided to implement in the future a complete revision of the splices and other important machine protection measures in order to be

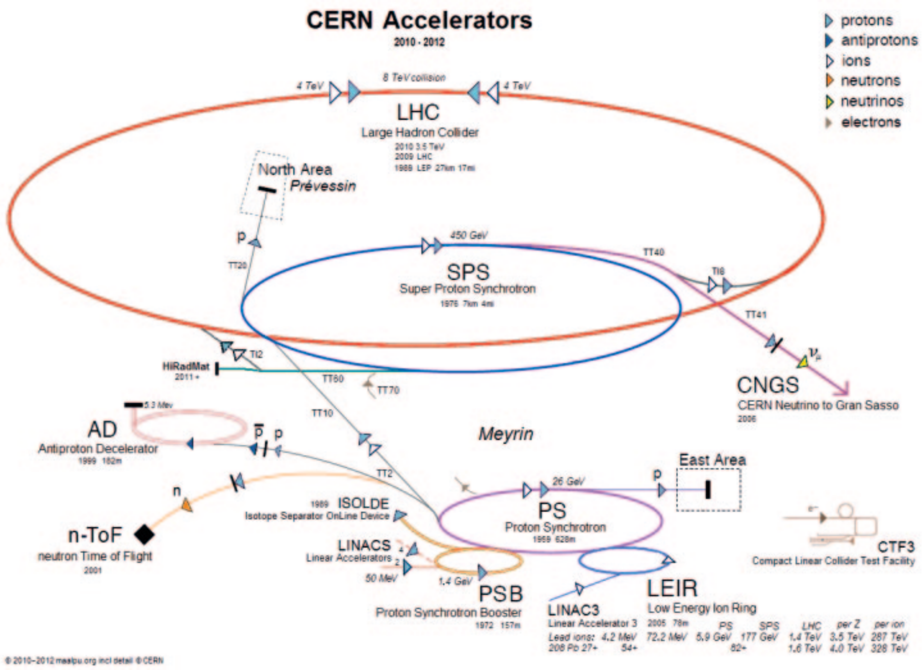


Fig. 6. – Protons accelerated by a linear accelerator (LINACS) to 50 MeV are transferred to a Booster and then to the Proton Synchroton (PS) from where they get out with an energy of 26 GeV. Finally, they are accelerated by the Super Proton Synchroton (SPS) to 450 GeV before being injected to the LHC, where they reach the final energy.

able to run the accelerator at the nominal energy of 7 TeV per beam. Meanwhile, as a precautionary measure, it was decided to run the machine at about one half of the design value *i.e.* 3.5–4.0 TeV per beam.

For the first physics run of LHC (2010-12) the collision energy was therefore first set at 7 TeV, the bunches were separated by $\Delta t = 50\,\text{ns}$, a factor 2 less than nominal, and a maximum number of 1380 bunches was used for a single proton beam. However, the density of protons in a bunch exceeded the design parameter, reaching the value of $1.7 \times 10^{11}$ protons. This value, coupled to close-to-nominal focusing conditions, yielded a record instantaneous luminosity of $\mathcal{L} = 0.77 \times 10^{34}\,\text{cm}^{-2}\,\text{s}^{-1}$. The large inter-bunch separation ensured excellent machine stability and hence long periods of smooth data taking. However, having pushed the bunch population well beyond nominal values, implied a high number of interactions per crossing, "event pileup" (or just pileup) *i.e.* uninteresting collisions superimposed to the events under study. Handling this extremely complex environment was another challenge for ATLAS and CMS. The distribution of the mean number of pileup events in the two main periods of data taking at LHC is shown in fig. 7. The operating parameters of LHC in the first years of operation are compared to the design values in table I.

It should be lastly mentioned that the physics program of LHC includes high-energy collisions of heavy ions. Four main experiments have been installed around the ring: the two general purpose detectors, ATLAS [39] and CMS [40], LHCb [41], a specialised detector for precision studies in the heavy flavour sector, and ALICE [42] a detector

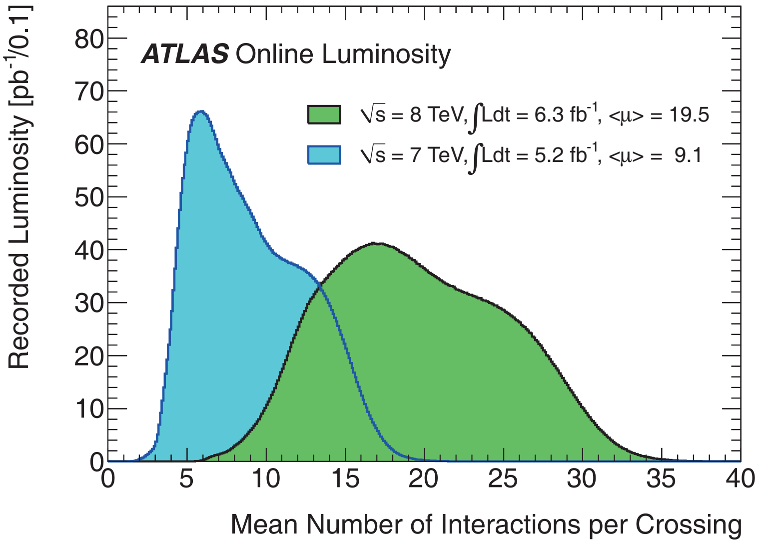


Fig. 7. – Distribution of the average values of $\mu$. The parameter $\mu$ is the average number of additional proton-proton collisions per bunch crossing, as measured by the ATLAS experiment (`https://atlas.web.cern.ch/Atlas/GROUPS/DATAPREPARATION/InteractionsperCrossing/muplot/2012/mu_2011_2012.eps`).

optimised for the physics of heavy ions. Two more experiments, TOTEM [43] dedicated in particular to the measurement of the total *pp* cross section, and LHCf [44], designed to study the production of neutral particles emitted at low angle in *pp* collisions, have been also installed on the ring of the machine. LHC operations started in December 2009.

**6·1.** *The ATLAS experiment.* – The ATLAS (A Toroidal LHC ApparatuS) detector, with its 44 m length, 25 m diameter and a weight of about 7000 tons, is the largest collider detector ever built. A schematic view of this detector is shown in fig. 8.

The innermost system of ATLAS, the *Inner Detector* (ID), is immersed in a 2 T axial field produced by a superconducting solenoidal magnet. Silicon pixel and strip detectors

Table I. – *The main machine parameters of the Large Hadron Collider during the operations in* 2011 *and* 2012*, compared to the design values* [36-38].

| Parameter | 2011 | 2012 | Nominal |
|---|---|---|---|
| Beam energy (TeV) | 3.5 | 4.0 | 7.0 |
| Bunch spacing (ns) | 50 | 50 | 25 |
| Number of bunches per beam | 1380 | 1380 | 2808 |
| $\beta^*$ (m) | 1.0 | 0.6 | 0.55 |
| Protons/bunch | $1.45 \times 10^{11}$ | $1.70 \times 10^{11}$ | $1.15 \times 10^{11}$ |
| Norm. emittance (mm $\times$ mrad) | $\simeq 2.4$ | $\simeq 2.5$ | 3.75 |
| Peak luminosity (cm$^{-2}$ s$^{-1}$) | $3.7 \times 10^{33}$ | $7.7 \times 10^{33}$ | $1.0 \times 10^{34}$ |

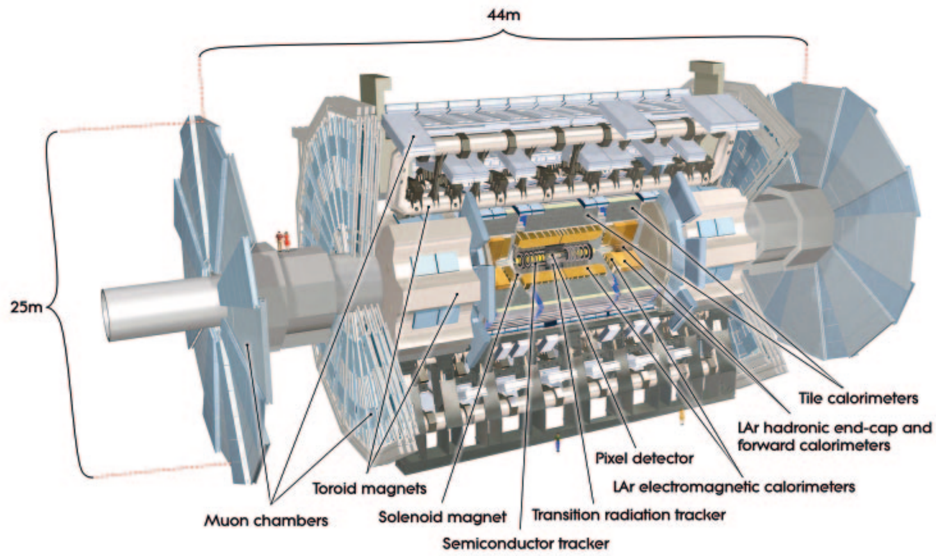


Fig. 8. – Cut-away view of the ATLAS detector. The dimensions of the detector are 25 m in height and 44 m in length [39]. The overall weight of the detector is approximately 7000 tons.

allow the reconstruction and the measurement of charged particles produced in proton-proton collisions in the pseudorapidity range $|\eta| < 2.5$ ($\eta = \log(\tan(\theta/2))$, where $\theta$ is the polar angle). The system is complemented by a straw-tube tracker in the region $|\eta| < 2.0$, which enhances the electron identification through the detection of transition radiation.

The ID is surrounded by the calorimeters system, composed of an electromagnetic and a hadronic calorimeter. The high-granularity, sampling electromagnetic calorimeter is based on a liquid argon and lead technology (LAr). It is made of a central module ($|\eta| < 1.475$) and two endcap ($1.375 < |\eta| < 3.2$) ones. The LAr calorimeter is surrounded by the Hadron Calorimeter (HC) which uses different technologies: scintillating tiles plus iron for $|\eta| < 1.7$, liquid argon plus iron for $1.5 < |\eta| < 3.2$, and liquid argon plus tungsten for $3.1 < |\eta| < 4.9$.

The muon spectrometer is the most external system of ATLAS. It is a large system instrumented with tracking detectors immersed in a toroidal magnetic field of about 1 T in average, produced by three air-core superconducting magnets. The Monitored Drift Tubes (MDTs) are drift detectors capable of precise muon detection and momentum measurement in the region $|\eta| < 2.7$. The MDT system is organised in three measurement stations, each one at a constant distance from the nominal $pp$ interaction point. The innermost station of the endcap system is instrumented with Cathode Strip Chambers (CSCs), because of a better capability to operate in an environment with high particle flux. Resistive Plate Chambers (RPCs) in the barrel ($|\eta| < 1.05$) and Thin Gap Chambers (TGCs) in the endcap ($1 < |\eta| < 2.4$) are used to provide fast measurements for triggering purposes and to contribute to the precision measurement of muons by MDTs and CSCs. More details are available in ref. [39].

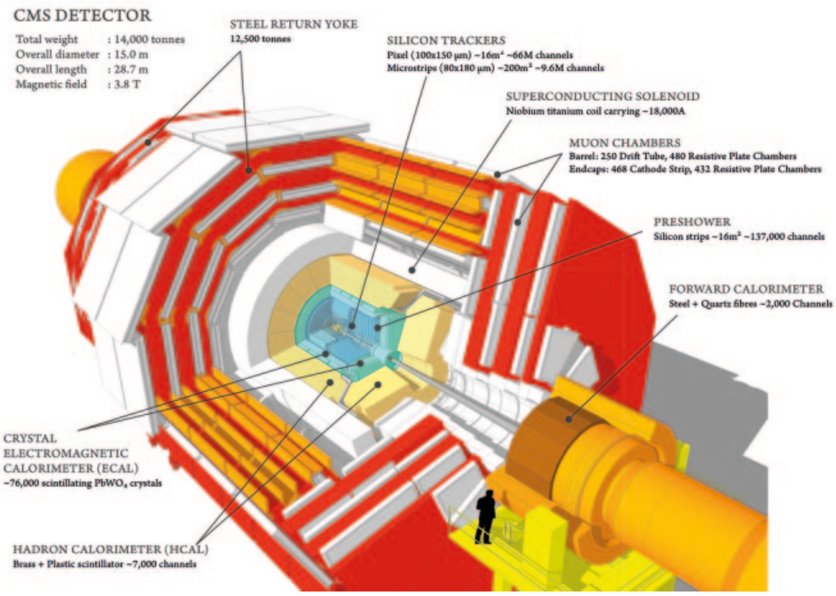


Fig. 9. – Cut-away view of the CMS detector. The dimensions of the detector are 15 m in height and less than 29 m in length. The overall weight of the detector is approximately 14000 tons (`http://cms.web.cern.ch/news/cms-detector-design`).

**6**˙2. *The CMS experiment*. – The CMS (Compact Muon Solenoid) detector, with its 29 m of length and 15 m of diameter, is another gigantic device but more compact than ATLAS. A schematic view of the experiment is shown in fig. 9. The driving idea of this apparatus is the choice of a single, strong magnet, a large central solenoid capable of providing a 3.8 T magnetic field. The central solenoid contains both the inner tracking detector and the electromagnetic and hadronic calorimetry. Charged-particle trajectories are measured by the silicon pixel and strip tracker with full azimuthal coverage within $|\eta| < 2.4$. On the contrary to ATLAS, the CMS ID does not use gas detector technology and is fully based on silicon devices. A lead-tungstate crystal electromagnetic calorimeter (ECAL) and brass/scintillator hadron calorimeter (HCAL) surround the inner tracker. A quartz-fiber Cherenkov calorimeter (HF) extends the coverage of this system to $|\eta| = 5.0$.

Also for CMS, the outermost component of the detector is the muon system, consisting of gas detectors interleaved with thick iron plates. The iron is also used as support structure and return yoke of the central solenoid, therefore contributing significantly to the large weight of the apparatus (about 14000 tonnes). Drift Tubes (DT), RPC and CSC detectors are used to trigger on muons and to measure them precisely with a full azimuthal coverage in the pseudorapidity region $|\eta| < 2.4$. More details are available in ref. [40].

The nominal momentum and energy resolution of the central tracker, the muon system and the calorimeter of ATLAS and CMS are summarised in table II.

## 7. – Production and decay modes of the Standard Model Higgs boson at LHC

While the Higgs boson mass is not predicted by the theory, within the Standard Model its couplings to fermions and bosons must be proportional to the corresponding

TABLE II. – *Performance of the main components of the ATLAS and CMS detectors.*

| Subsystem | ATLAS | CMS |
|---|---|---|
| Magnetic field | 2 T central solenoid; Air-core muon toroids: 0.5 T barrel and 1 T endcap | 3.8 T central solenoid + return yoke |
| Central tracking momentum resolution $\sigma(p_T)/p_T$ | $5 \times 10^{-4} p_T \oplus 0.01$ ($p_T$ in GeV) | $1.5 \times 10^{-4} p_T \oplus 0.005$ ($p_T$ in GeV) |
| Muon system momentum resolution $\sigma(p_T)/p_T$ | 2% for $p_T = 50\,\text{GeV}$ 10% for $p_T = 1\,\text{TeV}$ | 1% for $p_T = 100\,\text{GeV}$ 5% for $p_T = 1\,\text{TeV}$ |
| Electromagnetic calorimeter $\sigma(E)/E$ | $0.10/\sqrt{E} \oplus 0.007$ ($E$ in GeV) | $0.03/\sqrt{E} \oplus 0.005$ ($E$ in GeV) |
| Hadronic calorimeter $\sigma(E)/E$ | $0.50/\sqrt{E} \oplus 0.03$ ($E$ in GeV) | $1/\sqrt{E} \oplus 0.05$ ($E$ in GeV) |

particle masses (for fermions) or squared masses (for bosons). For this reason, the Higgs boson production and decay are dominated by channels involving heavy particles, mainly the $W$ and $Z$ bosons and the third-generation fermions. The Higgs does not couple to photons and gluons at tree level, but only through one-loop graphs. For the $gg \to H$ channel the main contribution is given by the $t\bar{t}$ and $b\bar{b}$ loops. For the $\gamma\gamma \to H$ channel the dominant contributions come from $W$ loops and again from loops of third-generation fermions, dominated by loops of top quarks.

The main processes contributing to the Higgs boson production at a proton-proton collider are gluon-gluon fusion, vector boson fusion, associated production with a $W$ or $Z$ and Higgs radiation off a *top* quark. The corresponding cross sections are shown in fig. 10, for a centre-of-mass energy of 7 TeV, the initial energy of LHC [45]. It must be noted that the total production cross sections at 7 TeV are about one order of magnitude lower than the nominal LHC beam energy. While a continuous effort is ongoing on improving the accuracy of the theoretical predictions on the production cross section, in the following we shall focus our attention on the status of the computations at the start-up of LHC.

**7·1.** *Gluon-gluon fusion.* – The gluon-gluon fusion is the dominating mechanism for the Higgs boson production at the LHC over the whole mass range. The dominant Feynman diagram for the process is shown in fig. 11(a). Results available for this process at the beginning of LHC include next-to-next-to-leading order (NNLO) QCD contributions, complemented with next-to-next-to-leading log (NNLL) resummation, and

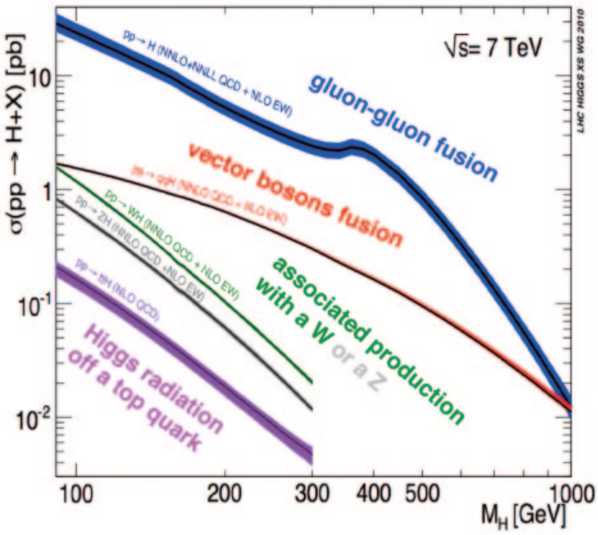


Fig. 10. – Higgs production cross sections for various production mechanisms at 7 TeV as a function of the Higgs mass [45].

next-to-leading order (NLO) electroweak corrections. An uncertainty of 15–20% on the calculation of this cross section is assumed, mostly depending on the choice of the parton distribution functions (PDFs), and on higher-order QCD radiative corrections.

**7**.2. *Vector-boson fusion.* – The vector-boson fusion (VBF) cross sections are about one order of magnitude lower with respect to gluon-gluon fusion for a large range of $m_H$ values. The two processes become comparable only for masses of the order of 1 TeV. Nevertheless, this channel is very interesting because of its clear experimental signature: the presence of two spectator jets with high invariant mass in the forward region provides a powerful tool to tag the signal events and discriminate the backgrounds, thus improving the signal-to-background ratio. Also for this process, NNLO QCD and NLO EW calculations are available. The uncertainties are in general lower (of the order of 5%) than those typical of the gluon-gluon fusion mode. The dominant Feynman diagrams for this process are shown in fig. 11(b).

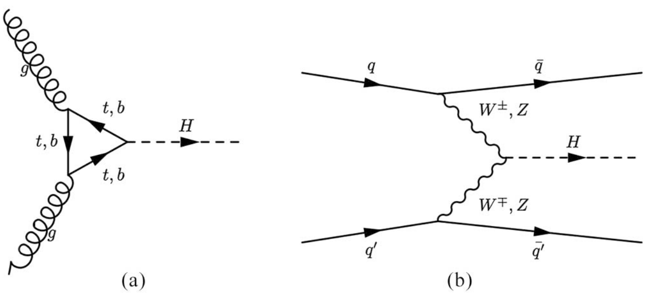


Fig. 11. – Feynman diagrams for the Higgs boson production at hadron colliders via (a) gluon-gluon fusion and (b) vector-boson fusion.

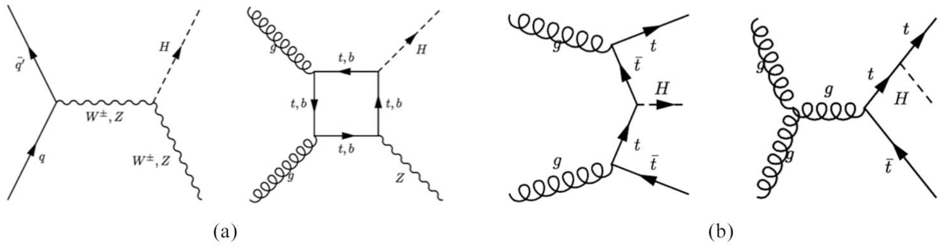


Fig. 12. – Feynman diagrams for the Higgs boson production at hadron colliders associated with (a) a $W$ or $Z$ and (b) with a pair of top quarks.

**7**˙3. *Associated production with W and Z*. – In the Higgs-strahlung process the Higgs boson is produced in association with a $W$ or $Z$ boson (VH), which can be used to tag the event. The typical cross sections are orders of magnitude lower than those of gluon-gluon fusion and are known at the NNLO QCD and NLO EW level. The inclusion of these available contributions increases the LO cross section by about 20–25%. The typical size of the uncertainty for this process is $\sim 5\%$. The dominant Feynman diagrams for the process are shown in fig. 12(a).

**7**˙4. *Associated production with a $t\bar{t}$ pair*. – The last process is the associated production of a Higgs boson with a $t\bar{t}$ pair. Also for this process, despite cross sections much lower than the previous ones, the presence of a pair of *top* quarks in the final state can be used as an experimental signature. For this process, only NLO QCD calculations are available and the typical uncertainty on the cross section is $\sim 10\%$. The dominant Feynman diagrams for this process are shown in fig. 12(b).

**7**˙5. *Higgs width and decay modes*. – The strategy for the Higgs boson identification depends heavily on its mass, since, not only the production mechanisms, but also its width and decay modes change dramatically with $m_H$ across the full mass range. The total width of the Higgs boson is shown in fig. 13 as a function of $m_H$. At low mass, below the $2m_W$ threshold, the Higgs boson is a very narrow resonance, with a width of a few MeV, orders of magnitude smaller than experimental mass resolution of detectors at hadron colliders. The width rapidly increases with mass reaching 1 GeV for $m_H \sim 200$.

For $m_H > 2m_Z$, the total Higgs boson width is dominated by the $W^+W^-$ and $ZZ$ partial widths that can be expressed as follows:

$$\Gamma_{H\to W^+W^-} = \frac{g^2 m_H^3}{64\pi m_W^2}\sqrt{1-x_W}\left(1 - x_W + \frac{3}{4}x_w^2\right), \tag{13}$$

$$\Gamma_{H\to ZZ} = \frac{g^2 m_H^3}{128\pi m_W^2}\sqrt{1-x_Z}\left(1 - x_Z + \frac{3}{4}x_Z^2\right), \tag{14}$$

with

$$x_W = \frac{4m_W^2}{m_H^2}, \qquad x_Z = \frac{4m_Z^2}{m_H^2}, \tag{15}$$

For large $m_H$, $x_W$ and $x_Z \to 0$ and the Higgs width grows as $m_H^3$.

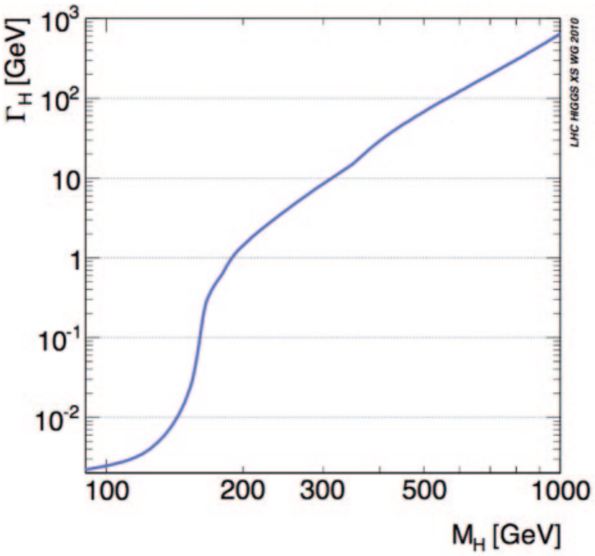


Fig. 13. – SM Higgs boson width as a function of the mass under the relativistic Breit-Wigner assumption [45].

Summing together the two bosonic widths for large mass we get the simple expression

$$\Gamma_{H\to VV} = \frac{3m_H^3}{32\pi v^2}\,. \tag{16}$$

For very large $m_H$ the width of the boson is comparable to its mass ($\Gamma_H \simeq m_H$ at $\sim 1.4\,\mathrm{TeV}$) and the definition of particle becomes meaningless. Experimentally, if the Higgs boson were very heavy, it would have been extremely difficult to separate the Higgs "resonance" from the $VV$ continuum.

Figure 14 shows the branching ratios as a function of the SM Higgs boson mass. The partial width to fermions is proportional to the mass of the fermions squared while the partial width to intermediate vector bosons is proportional to the fourth power of the mass. Therefore, the fermionic decay modes dominate the branching ratio only in the low-mass region (up to about $m_H = 150\,\mathrm{GeV}$). In particular, the channel $H \to b\bar{b}$ is here the largest decay mode, since the bottom quark is the heaviest fermion available in this region, and is followed by the $H \to \tau\tau$ mode. With respect to the low-mass region, the importance of the bosonic decay modes ($H \to \gamma\gamma$ $H \to ZZ^{(*)} \to llll$ $H \to WW^{(*)} \to l\nu l\nu$) must be noted. Even if their branching fraction is much smaller with respect to the dominant $b\bar{b}$ mode, these channels have very clean experimental signatures. When the decay channels into vector-boson pairs open up, they quickly dominate. A peak in the $H \to W^+W^-$ decay is visible around $m_H = 160\,\mathrm{GeV}$, when the production of two on-shell $W$ bosons becomes possible and the production of a real $ZZ$ pair is still not allowed. At high masses, above $m_H = 350\,\mathrm{GeV}$, also $t\bar{t}$ pairs can be produced but still the bosonic decay modes dominate the full range up to 1 TeV.

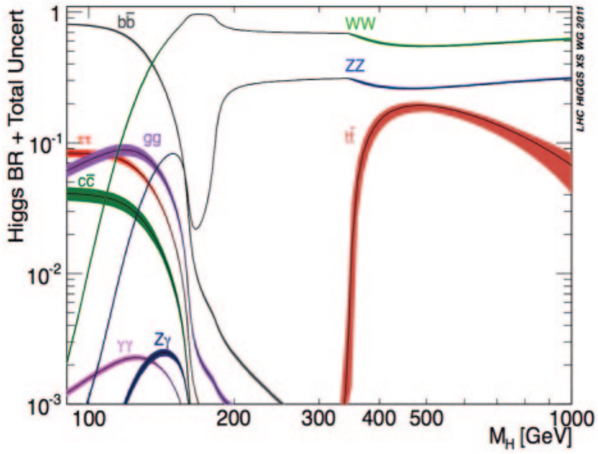


Fig. 14. – SM Higgs boson branching ratio in various decay modes as a function of the mass [45].

## 8. – The start-up of LHC: Rediscovering the Standard Model at $\sqrt{s} = 7\,\text{TeV}$

The first LHC collisions were recorded by the experiments on November 23, 2009, at a centre-of-mass energy $\sqrt{s} = 900\,\text{GeV}$ [46]. During this early physics run, the accelerator and the experiments performed exceptionally, resulting in impressive preliminary results that showed excellent detector performance. The first results on charged particle production were published after a very short time, and compared with existing results from the CERN S$p\bar{p}$S and the Tevatron at Fermilab.

On February 27, 2010, the LHC was commissioned with 3.5 TeV proton beams. The very first collision data at $\sqrt{s} = 7\,\text{TeV}$ were recorded on March 30. From then onwards, data were collected with increasing instantaneous luminosities. At the end of the 2010 proton-proton run, about $45\,\text{pb}^{-1}$ of data per experiment were recorded by ATLAS and CMS. With this data sample, the two experiments were able to perform preliminary detector calibration, in particular the alignment of the inner tracker and of the muon system, and the calibration of the calorimeter energy scale.

The first data sample taken at $\sqrt{s} = 7\,\text{TeV}$ was essential to "re-discover" the fundamental particles of the Standard Model. Production of jets, $W$ and $Z$ bosons, as well as top quarks, were measured and compared to Standard Model predictions. Moreover, the understanding of the Standard Model processes was crucial not only to test this theory at an unprecedented energy scale, but also to control the background processes affecting Higgs boson and New Physics searches.

This section collects examples of the most important early studies performed by the general purpose experiments with the first data taken at the early collision energy provided by LHC. Figure 15(a) shows the Jacobian peak of the $W \to e\nu$ decay as reconstructed in ATLAS [47], while fig. 15(b) shows the measured rate of the $W$ and $Z$ leptonic decays by CMS [48], compared to the Standard Model expectation. The total inclusive $W$- and $Z$-boson production cross section times the leptonic branching fractions were measured with an experimental uncertainty smaller than 4%. The measurements were found in agreement with Standard Model predictions within this experimental uncertainty and the theory uncertainty (about 5%).

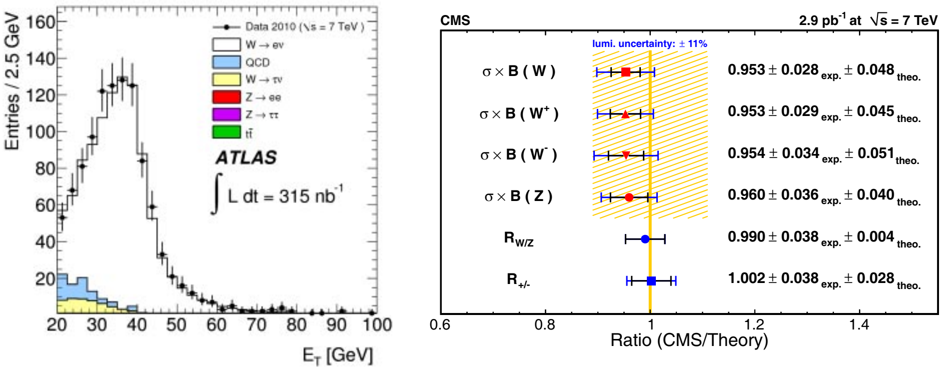


(a) (b)

Fig. 15. – (a) ATLAS distribution of the electron $E_T$ of the $W$ candidates after final selection. The data are compared to Monte Carlo simulation, broken down into the signal and various background components [47]. (b) Summary of the ratios of the CMS measurements to their theoretical predictions. The luminosity uncertainty ($\pm 11\%$), which affects only the cross section times branching ratio measurements, is represented by a shaded area [48].

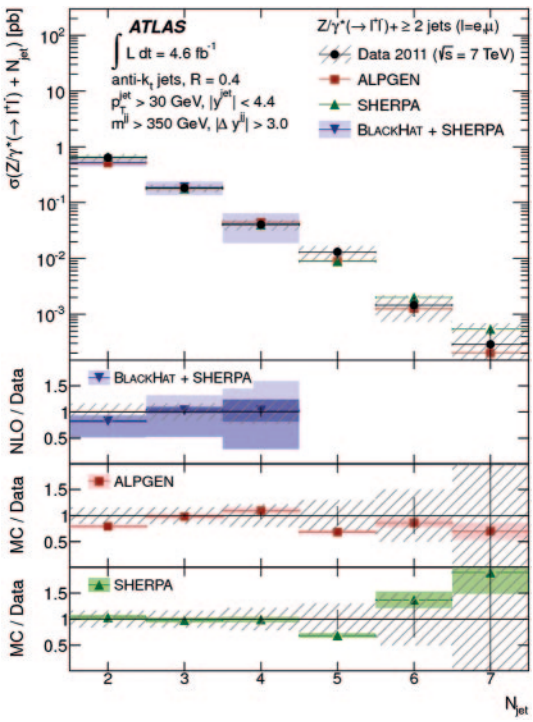


Fig. 16. – Measured cross section by ATLAS for $Z \to ll + \text{jets}$ as a function of the exclusive jet multiplicity, $N_{\text{jets}}$, in events passing the VBF selection (at least two jets with transverse momentum larger than 30 GeV, rapidity larger than 4.4 units, invariant mass larger than 350 GeV and with a rapidity separation larger than 3 units) [49].

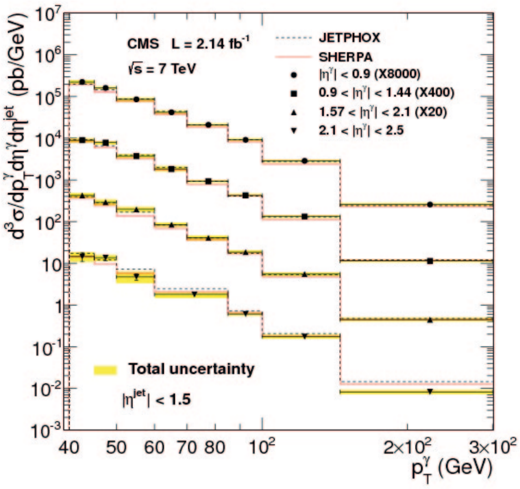


Fig. 17. – Photon differential production cross section as a function of its transverse momentum $p_T^\gamma$ in the presence of accompanying jets produced in the central rapidity region $|\eta_{\mathrm{jet}}| < 1.5$ [50]. The measured cross sections (markers) in four different ranges of the photon rapidity $\eta_\gamma$ are compared with the SHERPA tree-level MC (solid line) and the NLO perturbative QCD calculation from JETPHOX (dashed line). The cross sections for the most central photons are scaled by factors of 20 to 8000 for better visibility. Error bars are statistical uncertainties and the shaded bands correspond to the total experimental uncertainties.

The associated production of vector bosons with high-$p_T$ jets is one of the most important background processes to Higgs boson searches. Furthermore, the production of vector bosons plus jets is an important test of the SM perturbative QCD. Production cross sections as a function of the inclusive and exclusive jet multiplicities and their ratios, as well as differential cross sections as a function of transverse momenta and rapidity of the jets including angular separation between the leading jets, were studied by ATLAS. The studies considered inclusive and VBF selections [49]. Figure 16 presents the absolute cross section as a function of the exclusive jet multiplicity observed by ATLAS in $Z+$jets events after a selection optimised to enhance events due to vector-boson fusion processes. The data are found to be consistent with BLACKHAT+SHERPA predictions.

Photon+jets (direct photon) events are a major source of background to Standard Model measurements, most notably for the search for a light, neutral Higgs boson in the decay channel $H \to \gamma\gamma$. Furthermore, studies of events containing a photon and one or more jets in the final state provide a direct probe of quantum chromodynamics. The production cross sections, examined for various angular configurations, are sensitive to contributions from the QCD hard-scattering subprocesses and to parton distribution functions (PDFs) of the proton. Measurements of these cross sections serve to constrain PDF models and provide information for improving phenomenological Monte Carlo models, and for testing the applicability of fixed-order perturbative calculations over a wide range of kinematic regions. Figure 17 shows the measurement of the triple-differential cross section ($\mathrm{d}^3\sigma/\mathrm{d}p_T^\gamma \mathrm{d}\eta^\gamma \mathrm{d}\eta^{\mathrm{jet}}$) for $|\eta_{\mathrm{jet}}| < 1.5$, as measured by CMS [50]. Although predictions from SHERPA were observed to be lower than those from JETPHOX, the measured cross sections were found to be consistent with both MC predictions within systematic uncertainties over most of the measured kinematic regions.

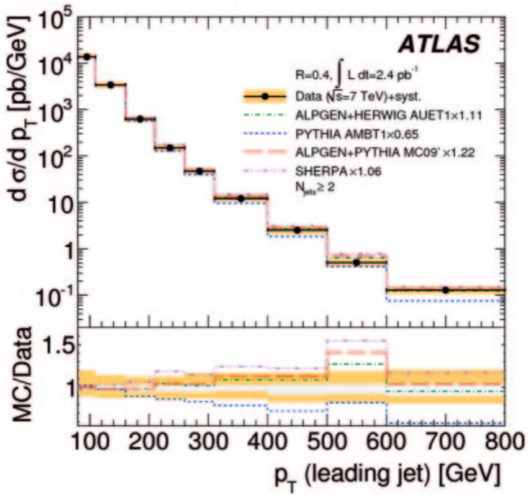


Fig. 18. – ATLAS differential cross section as a function of the leading jet $p_T$ for events with at least two reconstructed jets in the event. The results are compared to different leading-order Monte Carlo simulations normalised to the measured inclusive two-jet cross section [51].

In addition to their role in testing QCD, jet events are an important background in searches for new particles and interactions at high energies. For this reasons, early studies of jet production at LHC were conducted with care by ATLAS and CMS. Figure 18 shows the differential cross section, measured by ATLAS, as a function of the leading jet $p_T$ for events with at least two reconstructed jets in the pseudorapidity region $|\eta| < 2.8$, with $p_T > 30\,\text{GeV}$ [51]. The comparison to leading-order Monte Carlo simulation shows reasonable agreement between data and predictions.

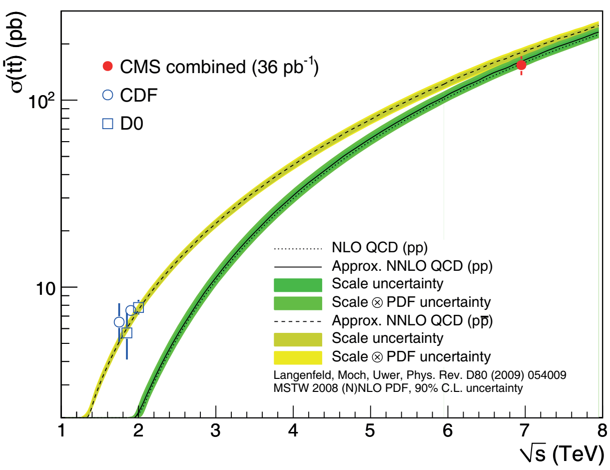


Fig. 19. – CMS measurement of the $t\bar{t}$ production cross section at 7 TeV and comparison with the Tevatron results at 1.96 TeV and with the theoretical predictions for proton-proton(antiproton) collisions as a function of $\sqrt{s}$ [52].

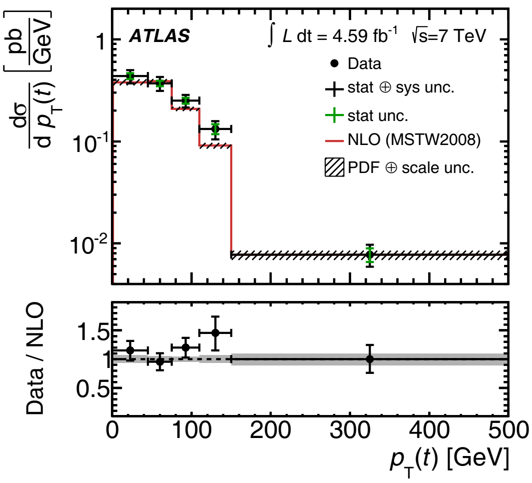


Fig. 20. – Differential cross section as a function of transverse momentum of the top quark $p_T$ (t). The differential distribution measured by ATLAS [53] is compared to the QCD NLO calculation. The black vertical error bars on the data points denote the total combined uncertainty, the green error bars denote the statistical uncertainty, while the red band denotes the theory predictions calculated at NLO using MCFM. Uncertainties on the predicted values include the PDF and scale uncertainties. The horizontal error bars indicate the bin width.

The top quark was first observed in the proton-antiproton collision at $\sqrt{s} = 1.8\,\text{TeV}$ at the Fermilab Tevatron collider. At the LHC, the $t\bar{t}$ production mechanism is expected to be dominated by the gluon fusion process. Measurements of the top quark production at this collider are important to understand the production mechanism of this quark. This was a crucial component of the early LHC physics programme, since many signatures of New Physics models, as well as many Higgs boson search final states, either suffer from top quark production as a significant background, or contain top quark themselves. Figure 19 shows the measurement of the inclusive cross section production of the $t\bar{t}$ pairs performed by CMS [52] and compared to the findings at the Tevatron collider. Similar results were obtained also by ATLAS. These measurements were found to be in good agreement with the QCD predictions, based on full NLO matrix element calculation.

At hadron colliders, alternative production modes contribute to the production of single top quark final states. These modes can be grouped in three basic subprocesses: the exchange of a virtual $W$ boson in the $t$-channel ($q'g \to tq\bar{b}$), or in the $s$-channel ($q\bar{q} \to tb$), and the associated production of a top quark and an on-shell $W$ boson ($bq \to Wt$). The single top quark production represents a background source to Higgs boson searches that cannot be neglected. It is also sensitive to many BSM physics processes. Furthermore, it provides a direct probe of the $W$-$t$-$b$ coupling. As an example of many studies performed at LHC, fig. 20 shows the ATLAS result on the differential production cross section of the single top quark as a function of its transverse momentum. The measurement is compared to the theory prediction, based on MCFM [53].

The understanding of diboson ($VV$) production in proton-proton collisions is a crucial test of the Standard Model. $VV$ processes are sensitive to self-interactions between gauge boson via trilinear gauge couplings (TGC). The values of these couplings are fully fixed in SM, and hence any deviation would indicate presence of New Physics at the LHC energy scale.

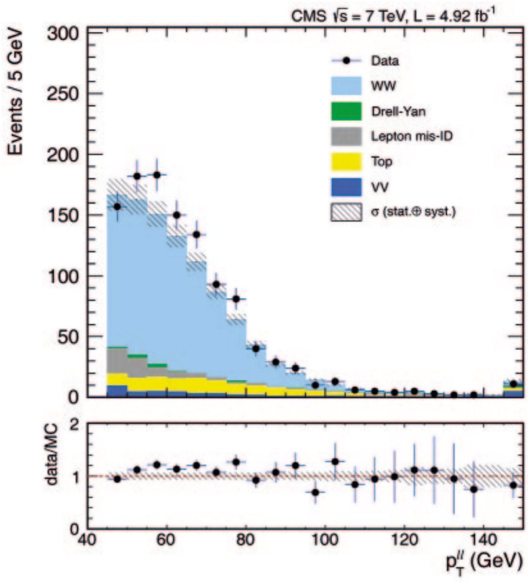


Fig. 21. – Distributions of the dilepton transverse momentum $p_T^{ll}$ from the selection of $W^+W^- \to l^+\nu l^-\bar{\nu}$ events by CMS [54]. Some of the backgrounds have been rescaled to the estimates based on control samples in data, as described in the text. All leptonic channels are combined, and the uncertainty band corresponds to the statistical and systematic uncertainties in the predicted yield. The last bin includes the overflow. In the box below, the ratio of the observed CMS event yield to the total SM prediction is shown.

Measurements were performed by ATLAS and CMS with the full 7 TeV data sample, and both found consistency with the Standard Model predictions; see for example [54,55] and fig. 21, where the transverse momentum of dileptons for events selected to measure $W^+W^- \to l^+\nu l^-\bar{\nu}$ processes in CMS is compared to theory predictions.

Figure 22 summarises the main results on SM measurements obtained by ATLAS and compared to the theory predictions; 8 TeV data are also included in the plot. Similar results were obtained by CMS.

LHC produced proton-proton collisions till the end of October 2010. After the first week of November, the machine was used to collide Pb ions at the centre-of-mass energy $\sqrt{s_{NN}} = 2.76$ TeV per nucleon pair. The data collected by ATLAS and CMS allowed the first direct observation of jet quenching in heavy ion collisions [56, 57]. This was one of the first important results of the LHC physics programme.

LHC operations started again in spring 2011, with 4.0 TeV beam energy, till about the end of the year.

Higgs boson searches were performed by ATLAS and CMS with the 7 and 8 TeV data. The results on this search are described in the next sections.

## 9. – Early Higgs boson hunting at $\sqrt{s} = 7$ TeV

As soon as it was evident that LHC would have run for several years only at about half of the nominal energy and with instantaneous luminosity lower than the nominal $\mathcal{L} = 1 \times 10^{34}\,\mathrm{cm^{-2}\,s^{-1}}$, the chances to discover quickly the new boson were considered by many extremely low. As a matter of fact, all physics studies performed in preparation

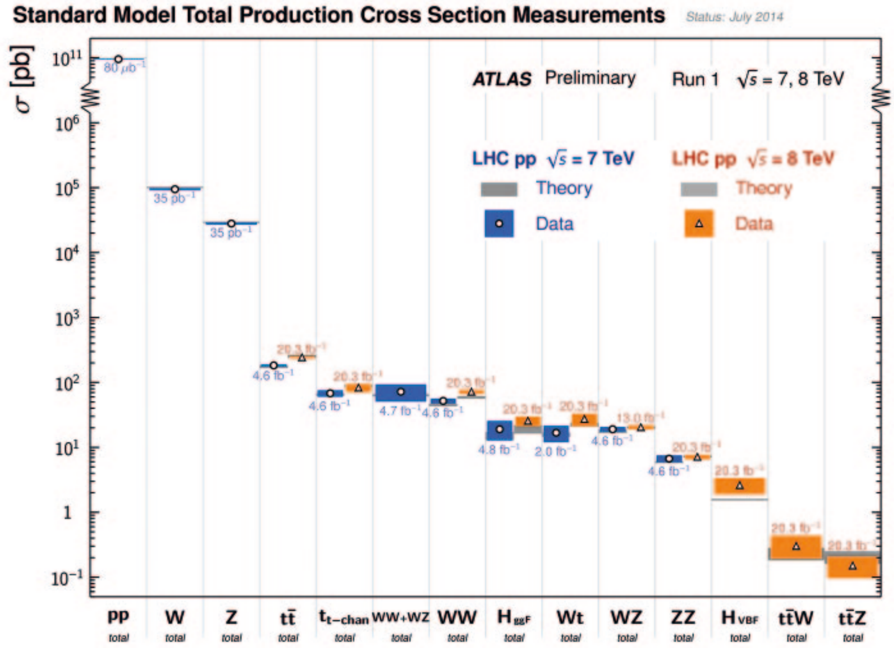


Fig. 22. – Summary of several Standard Model total production cross section measurements, corrected for leptonic branching fractions, compared to the corresponding theoretical expectations. All theoretical expectations were calculated at NLO or higher order. The $W$ and $Z$ vector-boson inclusive cross sections were measured with $35\,\text{pb}^{-1}$ of integrated luminosity from the 2010 dataset. All other measurements were performed using the 2011 dataset or the 2012 dataset. The luminosity used for each measurement is indicated close to the data point. Uncertainties for the theoretical predictions are quoted from the original ATLAS publications (they were not always evaluated using the same prescriptions for PDFs and scales, see `https://atlas.web.cern.ch/Atlas/GROUPS/PHYSICS/CombinedSummaryPlots/SM/ATLAS_a_SMSummary_TotalXsect/history.html`).

for the new machine assumed the large production cross sections at 14 TeV and such a huge statistics of data that would have allowed the discovery of the new particle in the full range of mass in a single channel.

As an example of these studies, fig. 23 shows the expected signal for a Higgs boson in the low-mass region as reconstructed by the ATLAS detector in the decay mode $H \to \gamma\gamma$, with LHC running at 14 TeV and $100\,\text{fb}^{-1}$ of data [58]. It is clear that, with such a large statistics, a single experiment would have had the potential of a clean $5\sigma$ discovery in a single channel, namely $H \to \gamma\gamma$, if the Higgs boson mass had been below 140 GeV. Similarly, clear signals would have been achievable for masses between 130 and 500 GeV using $H \to ZZ^{(*)} \to llll$ while, in the high mass region, one could have used the decay mode $H \to ZZ \to lljj$, which is basically background-free for masses exceeding 500 GeV.

With LHC running at 7 TeV, and the perspective of getting an integrated luminosity in the range of a few $\text{fb}^{-1}$, even for the most promising decay modes, a handful of events was expected over significant backgrounds. No single channel could have led to signals strong enough to claim an observation. Therefore, a new strategy for hunting the Higgs boson was definitely needed.

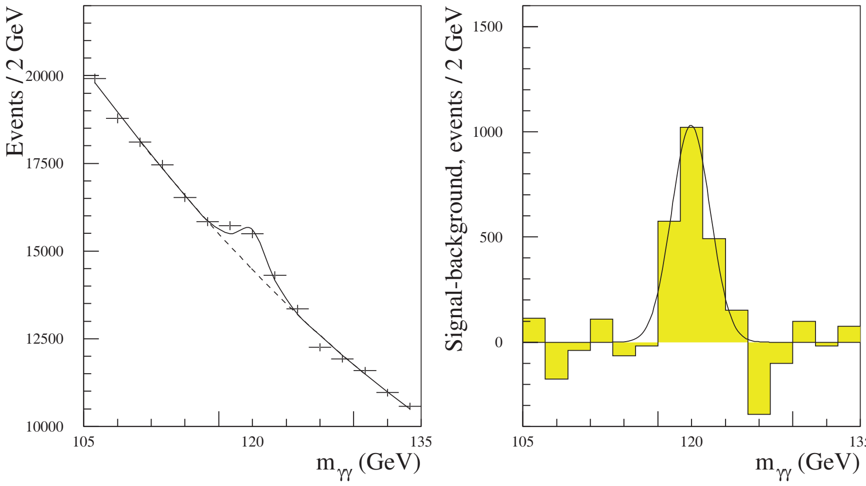


Fig. 23. – Invariant mass distribution of di-photon events in ATLAS in the presence of a Higgs signal at 120 GeV for $100\,\mathrm{fb}^{-1}$ of data at 14 TeV [58].

Several new studies were performed in the second half of 2010, and the results were officially adopted by the two collaborations at the end of that year, when the target of discovering the SM Higgs boson, or definitely exclude it, using the 7 TeV data of LHC was set as an official goal of the two collaborations.

A key element of the new strategy was the challenging proposal of improving by all means the sensitivity of each individual search to combine together, for each mass region, the largest possible set of decay channels.

In the high mass region the studies were based on the $H \to WW$ and $H \to ZZ$ decay modes each one reconstructed in several channels *i.e.* $H \to WW \to l^+\nu q\bar{q}$ combined with $H \to WW \to l^+\nu l^-\nu$ and $H \to ZZ \to l^+l^-q\bar{q}$ combined with $H \to ZZ \to l^+l^-\nu\nu$ and $H \to ZZ \to l^+l^-l^+l^-$.

In the low-mass region the sensitivity of the two bosonic modes, $H \to WW^* \to l^+\nu l^-\nu$ and $H \to ZZ^* \to l^+l^-l^+l^-$ was extended down to 120 GeV while they were combined with the other well-known bosonic channel $H \to \gamma\gamma$. In the attempt to leave no stone unturned, both collaborations deployed a substantial effort to address even the two extremely challenging fermionic modes: $H \to b\bar{b}$ and $H \to \tau\tau$.

It must be considered that, for each one of these channels, several independent sub-channels were carefully studied considering signatures enhancing different production mechanisms (*i.e.* vector-boson fusion or associate production) and various decay modes of the decay products (*i.e.* different decay modes of the $\tau$ leptons in the channel $H \to \tau\tau$). Many new studies were simply organised from scratch using collision data to improve the understanding of the major physics tools.

The complex and challenging new strategy was made possible thanks to the efforts of many hundreds of physicists fully devoted to produce an in-depth revision of the previously performed studies, in addition to the deployment and validation of several innovative analysis techniques.

An example of the new approach is shown in fig. 24. The plot summarises in (a) the potential of the CMS experiment in excluding the presence of the Standard Model Higgs boson with just $5\,\mathrm{fb}^{-1}$ of data at 7 TeV for various mass hypothesis. It is evident that, by

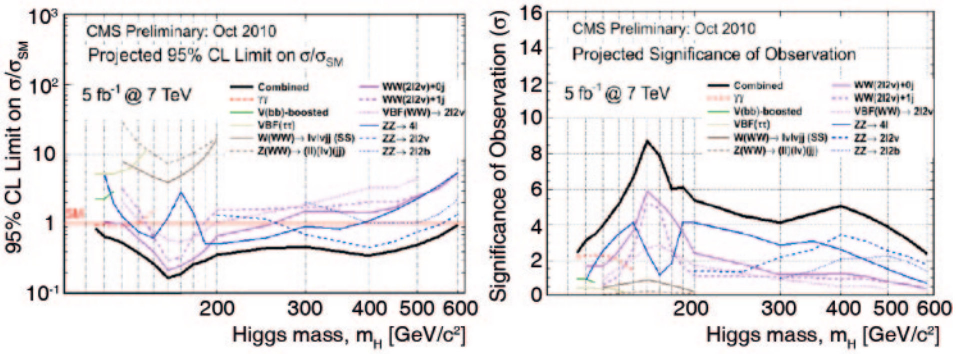


(a) (b)

Fig. 24. – (a) Projected exclusion limits at 95% C.L. for the presence of a Standard Model Higgs boson in the mass region between 120 and 600 GeV with $5\,\mathrm{fb}^{-1}$ of data at $\sqrt{s} = 7\,\mathrm{TeV}$. (b) Projected significance of the observation of a Standard Model Higgs boson in the same mass region and with the same statistics [59].

combining together a large set of decay channels, it would have been possible to explore carefully the entire mass region between 115 and 600 GeV. The plot in (b) shows the projected significance of the observation that CMS would have reached in the presence of a SM Higgs signal in the same mass region [59].

It is worth noticing the extremely challenging situation of the low-mass region, the one favoured by the indirect indications coming from the global electroweak fit. If the Higgs boson had been hidden in the mass region between 115–130 GeV, with $5\,\mathrm{fb}^{-1}$ of data we could have started seeing small excesses of events with a significance of 2-3$\sigma$ only. Therefore, every single channel of some relevance for the search in the low-mass region could have played a significant role in the route to a potential discovery. Similar results were obtained for ATLAS.

This explains why both collaborations invested a huge effort in optimising the most important physics tools, in improving the efficiency in reconstructing each physics object, in extending the sensitivity of the most important channels for the Higgs search towards the low-mass region.

As an example of these efforts, fig. 25 shows the careful studies performed in CMS to extend the efficiency in reconstructing low $p_T$ muons down to values as low as 5 GeV. The motivation for this work comes from the need of extending the sensitivity of the "golden" channel, $H \to ZZ^{(*)} \to \mu^+\mu^-\mu^+\mu^-$, in the very low-mass region.

The signature of this channel is quite striking: two pairs of oppositely charged, isolated muons, with at least one pair yielding an invariant mass compatible with the mass of a $Z$. A 120–130 GeV mass Higgs boson decaying into a final state of 4 muons would pass through the decay of a real $Z$, yielding the usual pair of high $p_T$ muons, and of an off-shell $Z$, whose decay products would be much softer. Since this clean decay mode could yield a handful of events, each gain in efficiency in reconstructing the low $p_T$ muons could have had an impact on the overall result. A single low $p_T$ muon lost in these very rare events could have implied the loss of an opportunity to identify the long sought particle. The efficiency in reconstructing these low $p_T$ muons has been studied using methods based on the reconstruction in data of events with muons coming from $Z$ and $J/\Psi$ *versus* $p_T$ and in various pile-up conditions [60].

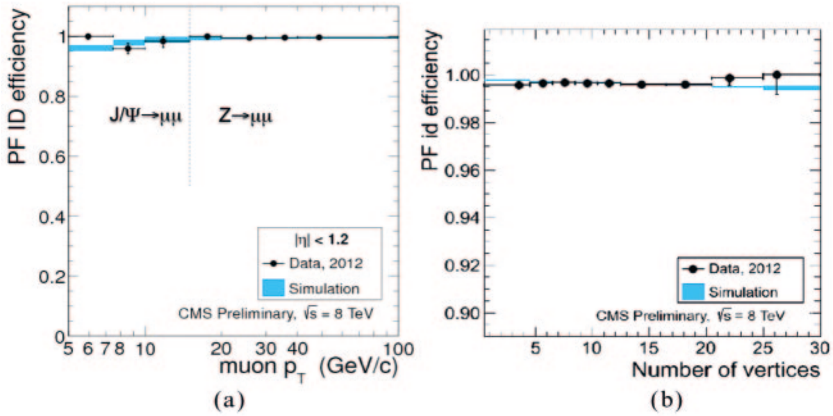


Fig. 25. – (a) CMS study of the reconstruction efficiency for muons *versus* $p_T$ using events with $Z$ and $J/\psi$. (b) Study of the reconstruction efficiency for muons as a function of the number of vertexes in the event [60].

Figure 26 shows instead the studies, performed in ATLAS, on the calibration of the electromagnetic calorimetry. The study is necessary to fully exploit the potential of another key channel for the low-mass region: $H \to \gamma\gamma$. In this case we are looking for a tiny signal superimposed to a steeply falling background of mostly irreducible QCD photons. Each gain in resolution translates immediately in increased sensitivity and this explains why such an incredible effort was put in improving the calibration of the calorimeters and in trying to understand the most subtle systematics effects.

The calorimeter response was carefully studied using electrons from $Z$ and $J/\psi \to e^+e^-$ and from $W \to e\nu$ and the results were used to carefully tune the Monte Carlo description of the detector response. Figure 26(a) shows the comparison between data and MC for the $Z$ in electrons as reconstructed by the ATLAS calorimeter.

These studies yielded an excellent control of the energy scale at the mass of the $Z$,

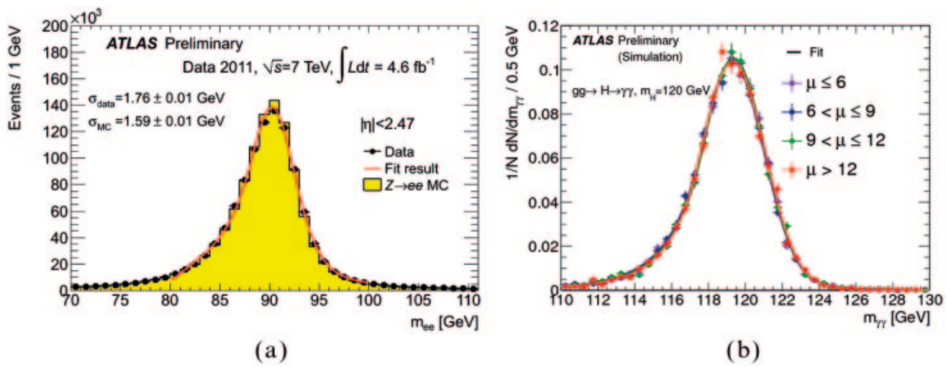


Fig. 26. – (a) Study of the resolution of the electromagnetic calorimeter using electrons in $Z$ events and comparison with the MC simulation. (b) Study of the mass resolution in the reconstruction of a 120 GeV Higgs decaying into photons in various pile-up conditions. The parameter $\mu$ gives the average number of proton-proton collisions per bunch crossing.

known at 0.5%, with a linearity better than 1% and a uniformity (constant term of the resolution) 1% in the barrel and 1.7% in the end-cap calorimeter.

The electron scale and resolution is then transported to photons, using Monte Carlo simulations that take into account the different behaviour of electrons and photons in the detector, and these data are used to evaluate the resolution for a Higgs boson signal of mass 120 GeV in different pile-up conditions, see fig. 26(b).

Detailed studies were performed by both collaborations also on jets, electron, muon and tau reconstruction, jet energy scale calibration, missing transverse energy resolution, $b$-tagging performance etc.

## 10. – First evidence of a neutral 125 GeV new particle

The collection of the first 2.3 $\mathrm{fb}^{-1}$ did not show any significant excess of events in the Higgs boson searches and limits on its mass were set assuming Standard Model production cross sections and decay rates. Preliminary results were shown at the *Lepton-Photon Interactions at High Energies* conference, held in Mumbai (India) in the summer of 2011. ATLAS excluded a SM Higgs boson at 95% confidence level (C.L.) in the mass regions 144–232 GeV, 256–282 GeV and 296–466 GeV [61]. CMS data excluded similar mass regions: 145–216 GeV, 226–288 GeV and 310–400 GeV.

For the quantity of data collected, in the absence of a signal, it was expected to exclude the presence of the Higgs boson signal in the mass range 130–450 GeV. The difference between the expected and observed exclusion mass ranges was explained as consistent with statistical fluctuations in data. The exclusion limit in the mass region $110 < m_H < 135$ GeV was determined by the combination of the $H \to \gamma\gamma$ and $H \to WW^{(*)} \to l\nu l\nu$ decay channels. For $m_H$ up to 180 GeV, the limit was dominated by the $H \to WW^{(*)} \to l\nu l\nu$ decay, while the channels $H \to ZZ^{(*)} \to llll$ and $H \to ZZ^{(*)} \to ll\nu\nu$ dominated the exclusion limit for $m_H > 180$ GeV.

At the end of October 2011, the proton-proton collision campaign was concluded. Thanks to a careful exploration of the main parameters of the machine, the performance of the LHC accelerator throughout the whole year exceeded by far the most optimistic expectations. About 5 $\mathrm{fb}^{-1}$ of data per experiment were collected, to be compared with an official goal of 1 $\mathrm{fb}^{-1}$. For the first time the amount of data was large enough to allow experiments to say something significant on the Higgs boson search in the full mass region. The analysis of the new data was performed with high priority in both experiments to investigate their findings in the mass intervals still not excluded in summer. Preliminary results were available before the end of the year.

Before entering the description of these results, it is worth focusing the attention on the main characteristics of the three bosonic channels: $H \to WW^* \to l^+\nu l^-\nu$, $H \to \gamma\gamma$ and $H \to ZZ^* \to l^+l^-l^+l^-$. These channels are the most sensitive channels for the exploration of the low-mass region and indeed they did play a crucial role both for the first evidence of a signal and for the actual discovery.

**10·1.** $H \to WW^* \to l^+\nu l^-\nu$. – With a series of improvements in lepton identification and missing $E_T$ reconstruction, it was possible to extend the sensitivity of this channel down to 120 GeV. The analysis is split into same and different flavour categories and includes also sub-categories, based on the number of jets present in the event, to exploit different production mechanisms (gluon-gluon fusion and VBF). The zero-jet, electron-muon category has the best signal sensitivity. The main backgrounds for this channel are irreducible non-resonant $WW$ production and reducible $W$ + jets processes, where a jet is misidentified as a lepton. Useful discriminating variables are the opening angle between the two charged leptons in the event, the invariant mass of the two leptons and $m_T$, the transverse mass of the system. Different analysis paths are used to cross check the results: the usual "cut and count" approach and more sophisticated analyses based on the shape of the distributions and on multidimensional fits.

Since a significant missing transverse energy is present in the events due to the two neutrinos produced in the decay, the mass resolution of this channel is quite low (20%). Therefore, even in the presence of a signal, it was not expected to see a narrow peak in the distributions. In this channel the SM Higgs boson would have appeared as a broad excess of events in the low-mass end of the invariant mass distribution of the two leptons or in the transverse mass distribution of the system. To get an unambiguous evidence it was therefore mandatory to cross-check the outcome of the high resolution channels.

**10**˙2. $H \to \gamma\gamma$. – The signature of this decay mode is quite spectacular: two very energetic, isolated photons, accompanied by a number of low $p_T$ tracks associated to the underlying event. A search for a narrow mass peak over a smoothly falling background in the invariant mass distribution of di-photon events was performed. The background is mostly irreducible QCD di-photons and is measured directly from the sidebands of the invariant mass distribution. The challenges for this channel are the photon identification, the right assignment of the vertex and the calibration of the electromagnetic calorimeters (already mentioned in sect. **9**).

To enhance the sensitivity of the analysis, candidate di-photon events are separated into mutually exclusive categories of different expected signal-to-background ratios. Categories were based on the properties of the reconstructed photons and on the presence of two jets satisfying criteria aimed at selecting events in which a Higgs boson is produced through the VBF process. The analysis used multivariate techniques for the selection and classification of the events.

The exclusive di-jet tag selection has the best signal purity, S/N = 1/3, to be compared with the S/N = 1/30 of the standard selection for the gluon-gluon fusion production mechanism. The outstanding resolution of the electromagnetic calorimeters of ATLAS and CMS and the excellent vertexing performances of the two detectors translated into a mass resolution for this channel between 1 and 2%.

**10**˙3. $H \to ZZ^* \to l^+l^-l^+l^-$. – Also for this decay mode the signature is striking: two pairs of oppositely charged, isolated leptons in the event with two high $p_T$ leptons building an invariant mass compatible with a $Z$. The full kinematics of this decay mode is accessible and the invariant mass of the system can be fully reconstructed. The channel is extremely clean with an excellent signal purity (S/N = 1) but the number of expected events is very low ($\sigma$ = 2–5 fb). The main backgrounds are $ZZ^*$ (irreducible) and $Zbb$, $Zcc$, $Z$+jets, $tt$, $WZ$+jets that are suppressed with isolation and impact parameters cuts on two softest leptons. The excellent $p_T$ resolution for electrons and muons of ATLAS and CMS translated in a 1-2% mass resolution also for this channel.

The signature for a low-mass Higgs boson would have been therefore extremely clear: a broad excess in the $H \to WW^* \to l^+\nu l^-\nu$ channel coupled to a coincidence of narrow mass peaks in the same window for the two high resolution channels $H \to \gamma\gamma$ and $H \to ZZ^* \to l^+l^-l^+l^-$.

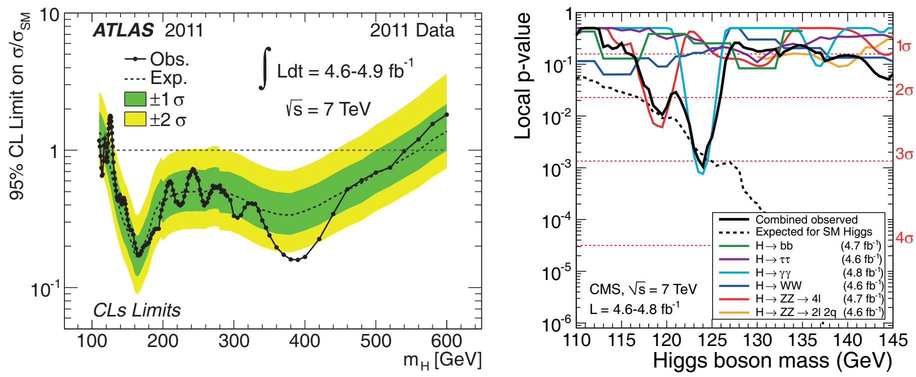


(a) (b)

Fig. 27. – (a) The ATLAS observed (full line) and expected (dashed line) 95% C.L. combined upper limits on the SM Higgs boson production cross section divided by the SM expectation as a function of $m_H$ in the full mass range considered in the analysis [62]. The dotted curves show the median expected limit in the absence of a signal and the green and yellow bands indicate the corresponding $\pm 1$ and $\pm 2$ s.d. intervals. (b) The CMS observed local $p$-value $p_0$ as a function of the SM Higgs boson mass $m_H$ in the range 110–145 GeV. The dashed line shows the expected local $p_0$ values, still as a function on $m_H$ [63].

The preliminary results coming from the 2011 data were available before the end of the year by both ATLAS and CMS. Two important seminars were held at CERN, on December 13, 2011, where the two collaborations showed and discussed these results.

Both collaborations excluded the presence of the SM Higgs boson in the high mass region while it was not possible to exclude it in the region between 115 and 127–129 GeV due to the presence of an excess of events.

The CMS 7 TeV data sample excluded at 95% C.L. a SM Higgs boson with mass $m_H > 127\,\text{GeV}$ and $m_H < 600\,\text{GeV}$, while those recorded by ATLAS excluded this particle with $m_H > 129.2\,\text{GeV}$ up to $m_H = 560\,\text{GeV}$, and of a couple of narrow intervals in the low-mass region (111.4 GeV to 116.6 GeV and 119.4 GeV to 122.1 GeV); see also fig. 27(a).

In the low-mass region, the largest excess was observed by ATLAS for a mass of 126 GeV [62], and by CMS for a mass of 124 GeV [63], yielding a local significance of 3.5 and 3.1 s.d., respectively. Figure 27(b) shows the local significance observed (and expected) by CMS. This excess was seen predominantly in the $H \to \gamma\gamma$ and $H \to ZZ^{(*)} \to llll$ final states, see fig. 28(a) and (b).

The excess seen by both collaborations around 125 GeV was particularly intriguing since it appeared in both data sets with characteristics very similar to the ones expected for a preliminary evidence of a SM Higgs boson.

On the other hand the statistical significance of the two excesses was not large enough to claim anything conclusive. Taking into account the so-called *look elsewhere effect* [65] for the not yet excluded region below 145 GeV, a global significance of 2.5 s.d. (2.1 s.d.) was estimated by ATLAS (CMS).

Both collaborations concluded that more data were needed to explain the nature of this tantalising excess. The call for the 8 TeV run, scheduled for 2012, represented therefore a major appointment with the physics at the Large Hadron Collider.

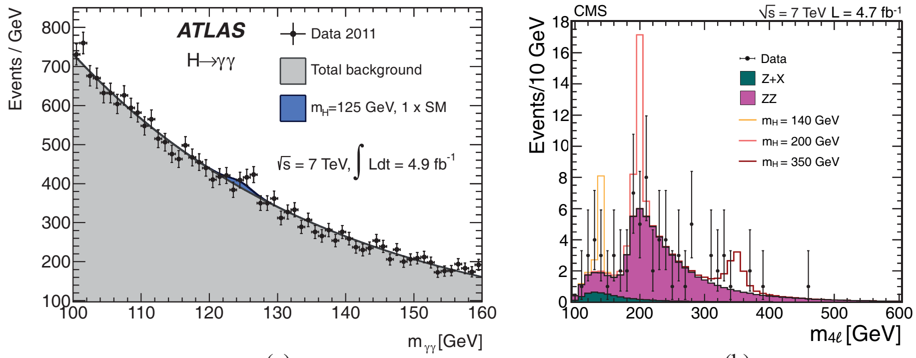


(a) (b)

Fig. 28. – (a): Invariant or transverse mass distributions for the selected candidate events, the total background and the signal expected in the $H \to \gamma\gamma$ channel using the $\sqrt{s} = 7\,\text{TeV}$ data sample recorded by ATLAS [62]. (b): Distribution of the four-lepton reconstructed mass for the sum of the $4e$, $4\mu$ and $2e2\mu$ channels using the $\sqrt{s} = 7\,\text{TeV}$ data sample recorded by CMS [64].

## 11. – July 2012: The discovery of the Higgs Boson

In 2012, the proton-proton collision center-of-mass energy of the LHC was raised from 7 TeV to 8 TeV. Accordingly, the production cross section for $m_H$ values around 125 GeV would have increased by 27%.

The Higgs boson searches were performed by ATLAS and CMS with extraordinary care over the entire mass interval, with a particular attention to the low-mass region, where the 7 TeV data indicated an intriguing excess, as discussed in the previous section.

The data were recorded with instantaneous luminosities up to $6.8 \times 10^{33}\,\text{cm}^{-2}\,\text{s}^{-1}$, and they were affected by significant event pile-up. In the 7 TeV data, the average number of interactions per bunch crossing was approximately 10; this value increased to approximately 20 in the 8 TeV data.

The reconstruction, identification and isolation criteria for electrons and photons were improved to mitigate the effects of these multiple *pp* collisions. Similarly, the data analysis used for the search for the Higgs particle in the bosonic channels were optimised to compensate the effects induced by the pile-up. Searches were conducted also in the fermionic final states, $H \to \tau\tau$ and $H \to b\bar{b}$, following the analyses made for the 7 TeV data set. Detector calibrations were refined, in particular the electromagnetic calorimeters, to further improve the reconstruction of diphoton and 4-lepton events where electrons are present.

Both ATLAS and CMS analyses were performed in a "blind" way: the event selection was optimised and finalised studying data control sample and Monte Carlo simulation, before looking at the results in the kinematic region dedicated to the signal search.

The search was performed using the first $5\,\text{fb}^{-1}$ recorded by the two experiments at $\sqrt{s} = 8\,\text{TeV}$, including the full $5\,\text{fb}^{-1}$ data set taken at 7 TeV.

A concise review of the main results that led to the discovery of a new neutral particle with mass near 125 GeV is given below. The details of the data analyses are available in the original papers from ATLAS [66] and CMS [67] (CMS published afterwords a *long-version* paper of this analysis [68]).

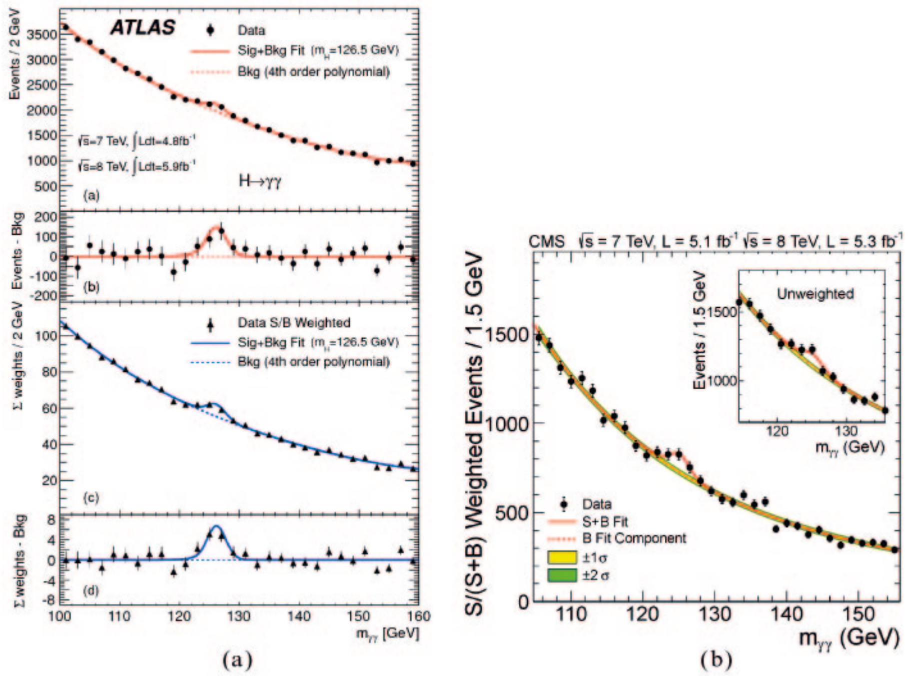


Fig. 29. – Left plot: the ATLAS distributions of the invariant mass of diphoton candidates after all selections for the combined 7 TeV and 8 TeV data sample. The inclusive sample is shown in a) and a weighted version of the same sample in c); the weights are explained in the text. The result of a fit to the data of the sum of a signal component fixed to $m_H = 126.5$ GeV and a background component described by a fourth-order Bernstein polynomial is superimposed. The residuals of the data and weighted data with respect to the respective fitted background component are displayed in b) and d) [66]. Right plot: the CMS diphoton invariant mass distribution with each event weighted by the $S/(S+B)$ value of its category. The lines represent the fitted background and signal, and the coloured bands represent the $\pm 1$ and $\pm 2$ standard deviation uncertainties in the background estimate. The inset shows the central part of the unweighted invariant mass distribution [67].

**11˙1.** *The $H \to \gamma\gamma$ decay channel.* – The distributions of the invariant mass, $m_{\gamma\gamma}$, of the diphoton events for ATLAS and CMS are shown in fig. 29, for all event categories.

A significant excess of events was observed by ATLAS and CMS in this decay channel for a value of $m_H$ around 125 GeV. ATLAS observed a local $p$-value of 4.5 standard deviations at $m_H = 126.5$ GeV, while CMS observed a value corresponding to 4.1 standard deviations assuming $m_H = 125$ GeV. The expected local $p$-values for a SM Higgs boson were 2.5 and 2.8 standard deviations, respectively, evaluated at the stated Higgs boson mass.

The background was estimated from data by fitting the diphoton mass spectrum in the mass range 100–160 GeV by ATLAS, and 100–180 GeV by CMS. The choice of the function(s) used to model the background was based on a study of the possible bias introduced in the measured signal strength. A fourth-order Bernstein polynomial function was chosen by ATLAS [69], while CMS adopted a polynomial function. The degree was chosen by requiring that the potential bias be at least a factor of 5 smaller than

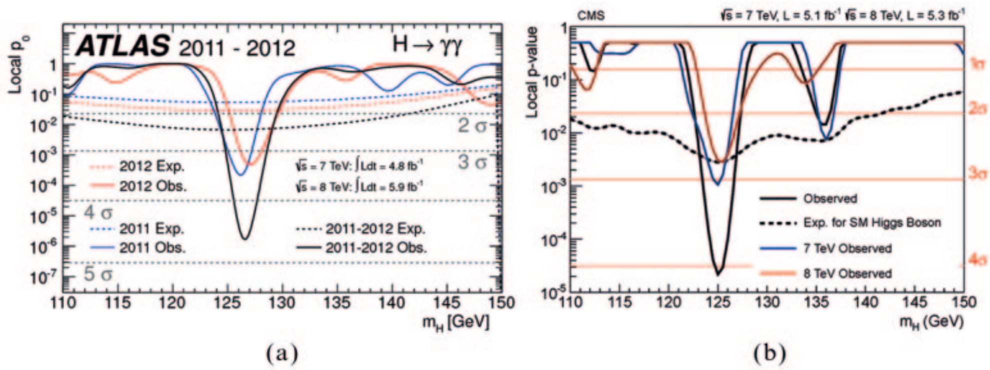


Fig. 30. – The observed local $p_0$ as a function of the hypothesised Higgs boson mass $m_H$ for the $H \to \gamma\gamma$ channel. The dashed curves show the expected local $p_0$ under the hypothesis of a SM Higgs boson signal at that mass. Results are shown separately for ATLAS [66] (left plot) and CMS [67] (right plot) for the 7 TeV (blue) and 8 TeV data (red), and their combination (black). The dashed lines show the expected local $p_0$ for the combined data sets, should a SM Higgs boson exist with mass $m_H$. The additional lines show the values for the two data sets taken individually. The dashed lines show the expected local $p$-value for the combined data sets, should a SM Higgs boson exist with mass $m_H$.

the statistical accuracy of the fit prediction, and it ranged from 3 to 5. The description of the Higgs boson signal was obtained from Monte Carlo simulation. The shape of the diphoton system invariant mass has been modelled by the sum of a Crystal Ball function [70]. The expected full width at half-maximum (FWHM) was 3.9 GeV for the inclusive ATLAS sample; similarly for CMS.

The dominant experimental uncertainty on the signal yield (±8%, ±11%) came from the photon reconstruction and identification efficiency, which was determined from data using $Z \to ee$ decays. Pile-up modelling also affected the expected yield and contributed to the uncertainty (±4%).

In order to enhance the sensitivity of the analysis to the different Higgs boson production modes and final state topologies, events were separated into several mutually exclusive categories, having different mass resolutions and different signal-to-background ratios.

The weight $w_i$ used to plot the ATLAS results in fig. 30(a) was estimated for each category $i$ to be $\ln(1+S_i/B_i)$, where $S_i$ is 90% of the expected signal for $m_H = 126.5$ GeV, and $B_i$ is the integral in the window containing $S_i$ of a background-only fit to the data. The CMS distribution, shown in fig. 30(b), was obtained using a very similar procedure: the events are weighted according to the category $i$ in which they fall with a factor proportional to $S_i/(S_i + B_i)$. Both collaborations showed also the results obtained with unweighted events.

**11·2.** *The $H \to ZZ^{(*)} \to llll$ decay channel.* – As already explained, in the $H \to ZZ^{(*)} \to llll$ decay mode, a search is made for a narrow four-lepton mass peak on top of a small and smooth background. The excellent mass resolution of the two detector played a crucial role in searches for new particles decaying to multi-lepton final states.

Only the search in the mass region 110–160 GeV was performed. The background affecting this search has been already illustrated in the previous section. The $ZZ^*$

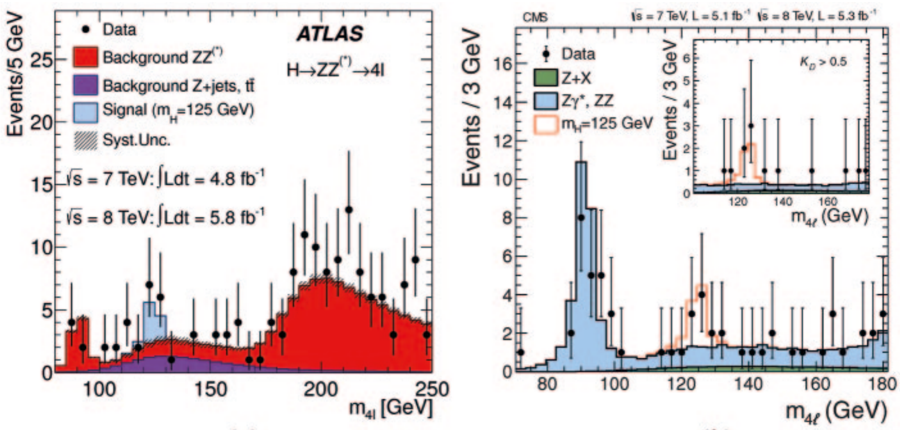


(a) (b)

Fig. 31. – Left plot: the ATLAS distribution of the four-lepton invariant mass, $m_{4l}$, or the selected candidates, compared to the background expectation in the 80 to 250 GeV mass range, for the combination of the $\sqrt{s} = 7\,\text{TeV}$ and $\sqrt{s} = 8\,\text{TeV}$ data. The signal expectation for a SM Higgs with $m_H = 125\,\text{GeV}$ is also shown. From ATLAS Collaboration (Aad G. *et al.*), *Phys. Lett. B*, **716** (2012) 1, `http://dx.doi.org/10.1016/j.physletb.2012.08.020`. Right plot: the CMS distribution of the four-lepton invariant mass for the $H \to ZZ^{(*)} \to llll$ analysis. The points represent the data, the filled histogram represent the background, and the open histogram shows the signal expectation for a Higgs boson of mass $m_H = 125\,\text{GeV}$, added to the expected background. The inset shows the $m_{4l}$ distribution after the selection of events performed by a multi-variate analysis. From CMS Collaboration (Chatrchyan S. *et al.*), *Phys. Lett. B*, **716** (2012) 30, `http://dx.doi.org/10.1016/j.physletb.2012.08.021`.

continuum was estimated using the MC simulation normalised to the theoretical cross section prediction, while $Z+$jets and $t\bar{t}$ yields were evaluated using control data samples. The uncertainties on the integrated luminosity corresponding to the data used in the analysis were determined to be 1.8% for the 7 TeV sample, and 3.6% for the 8 TeV sample. The uncertainties on the lepton reconstruction and identification efficiencies, as well as the lepton momentum scale and resolution, have been determined with samples of $W$, $Z$ and $J/\Psi$ decays to electron and muon final states. The uncertainty for muons, in ATLAS was found to be below 1% for each of the three possible sub-channels $4\mu$ and $2e2\mu$. For electrons, it was found to be around 2% for $4e$ and $2\mu 2e$ final states. The impact of the lepton energy scale was found to be at similar level. Similar figures were found by CMS.

The theoretical uncertainties on the background prediction was calculated to be $\pm 5\%$ (QCD scale) on the total yield, while the effect of the PDFs and $\alpha_S$ was $\pm 4\%$ ($\pm 8\%$) for the processes initiated by quarks (gluons).

Figure 31 shows the distribution of the four-lepton invariant mass after event selection found by ATLAS (left plot) and CMS (right plot). There is a clear peak at the $Z$ boson mass where the rare decay $Z \to 4l$ is reconstructed, and its related event yield was found in agreement with SM predictions. This represented a strong test of the capability of the detector and the analysis to detect a 4-lepton resonance as expected. The figure shows also an excess of events well above the expected background again around a mass of 125 GeV.

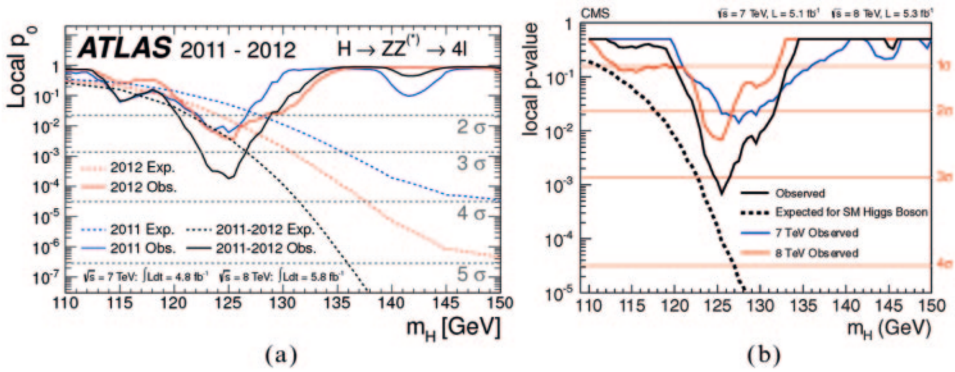


Fig. 32. – The observed local $p_0$ as a function of the hypothesised Higgs boson mass $m_H$ for the $H \to ZZ^{(*)} \to llll$ channel. The dashed curves show the expected local $p_0$ under the hypothesis of a SM Higgs boson signal at that mass. Results are shown separately for ATLAS [66] (left plot) and CMS [67] (right plot) for the 7 TeV (blue) and 8 TeV (red) data, and their combination (black). The dashed lines show the expected local $p_0$ for the combined data sets, should a SM Higgs boson exist with mass $m_H$.

ATLAS observed a local $p$-value of 3.8 standard deviations at $m_H = 125.0\,\text{GeV}$, while CMS observed a value corresponding to 3.2 standard deviations at $m_H = 125.6\,\text{GeV}$. The expected local $p$-values for a SM Higgs boson were 2.7 and 3.8 standard deviations, respectively, at the stated Higgs boson mass. These results are also shown in fig. 32.

**11·3.** *The $H \to WW^{(*)} \to l\nu l\nu$ decay channel.* – For a Higgs boson mass of 125 GeV, the $H \to WW^{(*)} \to l\nu l\nu$ decay has the second largest branching fraction and is an important final state to test the nature of the resonance observed in the $\gamma\gamma$ and 4-lepton final states. ATLAS and CMS analysed final states where the lepton is either an electron or a muon.

Finding such a signal in the complex environment of a hadron collider and in the presence of a significant event pile-up is challenging. A complete reconstruction of all the final-state particles is not possible because of the presence of neutrinos which are not directly detected. Kinematic observables such as the opening angle between the two charged leptons in the transverse plane, the dilepton mass $m_{ll}$, and the transverse mass of the system, $m_T$, of the two leptons and the neutrinos, were used to distinguish not only the Higgs boson signal from background processes with similar signature, but also between the SM Higgs boson hypothesis and other narrow exotic resonances with different spin or parity.

The Drell-Yan (DY) process is the dominant source of events with two identified leptons, and has an important contamination with same-flavour lepton pairs. The DY background is strongly reduced in events of different flavour lepton pairs, $e\mu$, as they arise from the production of $\tau^+\tau^-$ pairs. For this reason, the data have been studied in two different categories, the $ee/\mu\mu$ category and the $e\mu$ category. Since the $e\nu\mu\nu$ channel provides most of the sensitivity of the search, only this final state was used by ATLAS in the analysis of the 8 TeV data.

Events were classified counting the number of jets reconstructed in the event in three different sub-categories: $n_{\text{jet}} = 0$, $n_{\text{jet}} = 1$ and $n_{\text{jet}} \geq 2$. The ggF Higgs boson production mode contributes mainly in the $n_{\text{jet}} = 0, 1$ sub-categories. Important backgrounds are

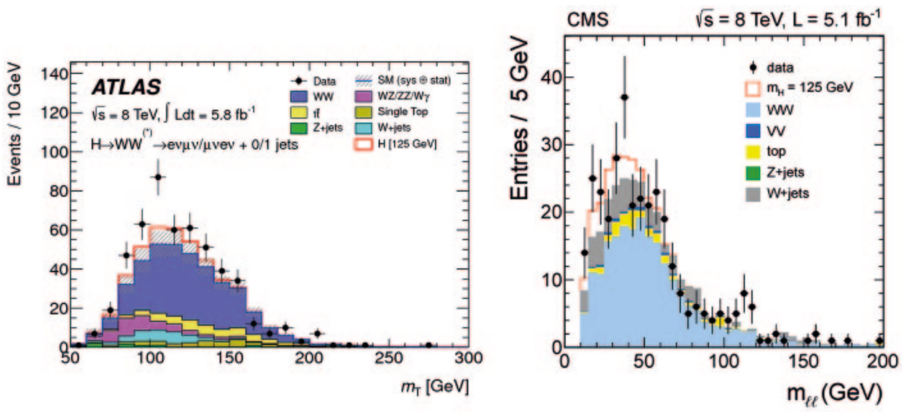


(a) (b)

Fig. 33. – Left: the ATLAS distribution of the transverse mass, $m_T$, in the 0-jet and 1-jet analyses of the $e\nu\mu\nu$ final state events satisfying all selection criteria [66]. The expected signal for $m_H = 125\,\text{GeV}$ is shown stacked on top of the background prediction. The $W +$ jets background is estimated from data, and $WW$ and top background Monte Carlo predictions are normalised to data using control regions. The hashed area indicates the total uncertainty on the background prediction. Right: the CMS Distribution of the invariant mass of the dilepton system, $m_{ll}$, for the 0-jet category $e\nu\mu\nu$ category using 8 TeV data [67]. The signal expected from a SM Higgs boson with mass $m_H = 125\,\text{GeV}$ is shown on top of the expected background.

also $t\bar{t}$ production and $W +$ jet(s) events with one mis-identified lepton. The contamination from top quark processes was reduced vetoing $b$-tagged jets. The VBF Higgs production was selected mainly in the $n_{\text{jet}} \geq 2$ sub-category. Top quark events represent the most important background to multijet final states. The irreducible $pp \to WW$ background is present in all categories, and it contributed significantly in the 0-jet selection.

Given the complexity of this signature and the fact that Monte Carlo expectations were (and are still) affected by large theoretical uncertainties, most of the backgrounds were modelled by normalising predictions to data in control regions. Contributions from $W +$ jet(s) and multijet backgrounds have been fully determined using data only.

A transverse mass variable, $m_T$, was used by ATLAS to test for the presence of a signal [71]. The observed distribution of $m_T$ is shown in fig. 33(a) after all selection criteria in the 0-jet and 1-jet channels combined. Similar tests were made by CMS. Figure 33(b) shows the observed distribution obtained by CMS using another discriminating variable, the invariant mass of the dilepton system ($e\mu$ in this case) after all selection cuts. A broad excess was observed by both experiments, consistent with the production and decay of a SM Higgs boson with 125 GeV mass. The CMS observed (expected) significance for a 125 GeV mass SM Higgs boson was 2.4 s.d. (1.6 s.d.), while for ATLAS was 2.8 s.d. (2.3 s.d.).

**11**$\cdot$4. *$H \to b\bar{b}$ and $H \to \tau\tau$ final states.* – The third-generation Higgs boson decays $H \to b\bar{b}$ and $H \to \tau\tau$ were the only fermionic final states searched for with the 7 TeV and early 8 TeV LHC data. Tau and $b$-jet pairs suffer from the huge background, mainly from jets produced in QCD processes, $t\bar{t}$ and $Z$-boson decays $Z \to \tau^+\tau^-$, $b\bar{b}$. These challenging final states were investigated therefore using production processes, like vector-boson fusion and associated production with a vector boson, that offer significantly better signal-to-background ratio for these decay modes. It must be noted, however, that the

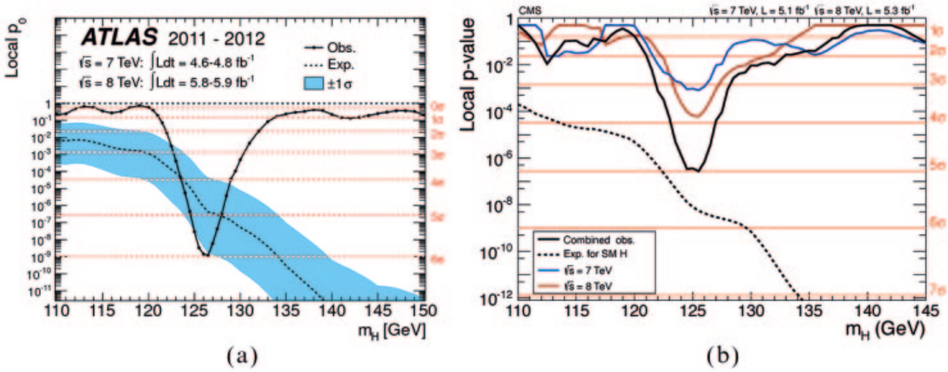


Fig. 34. – Left: The local $p_0$ (solid) observed by ATLAS as a function of $m_H$ and the expectation (dashed) for a SM Higgs boson hypothesis ($\mu = 1$) at the given mass [66]. Right: The local $p_0$ observed by CMS based on the 7 TeV data, 8 TeV data, and their combination, as a function of $m_H$. The dashed line shows the expected $p$-value assuming the SM Higgs boson at the given mass $m_H$ [67].

invariant mass resolution of $b\bar{b}$ and $\tau\bar{\tau}$ systems is poor, of the order of 10% or more, and hence it is not possible to reconstruct a narrow peak. As a consequence, the background is only partially reduced using invariant mass cuts, and moreover it cannot be determined from data with great accuracy through the use of sidebands. No significant excess was found by ATLAS (7 TeV data only analysed) and CMS neither in the $H \to b\bar{b}$ nor $H \to \tau\tau$ final states (observed significance below 1 s.d.), particularly in the low-mass region, in agreement with the expectation for a SM Higgs boson with 125 GeV mass.

**11·5.** *Overall signal strength.* – The individual results from the three decay modes $H \to \gamma\gamma$, $H \to ZZ^{(*)} \to llll$ and $H \to WW^{(*)} \to l\nu l\nu$, as well as from the two fermion final states $H \to \tau\tau$ and $H \to b\bar{b}$ (for ATLAS only the 7 TeV data set was used), were combined using the statistical method described in [72]. The combination assumed the relative branching fractions predicted by the SM and took into account the experimental statistical and systematic, as well as the theoretical uncertainties, which were dominated by the imperfect knowledge of QCD scale and parton distribution functions. The parameter under study was $\mu$, the global signal strength, that acts as a scale factor on the total number of events predicted by the Standard Model for the Higgs boson production and decay. In this way, an event yield fully consistent with a SM Higgs boson would give the value $\mu = 1$, while in case of the background only scenario $\mu = 0$.

Attention was paid by each experiment to take into account correlations of systematic uncertainties across the different channels from theory (*e.g.* PDFs, cross sections, etc.) and from experimental sources (*e.g.* integrated luminosity, jet and lepton energy scale, etc.).

An excess of events was seen near $m_H = 125$–$126$ GeV by both ATLAS and CMS. The observed local $p_0$ values are shown in fig. 34 as a function of the hypothesised Higgs boson mass $m_H$ for the low-mass range.

The largest local significance for the combination was found by ATLAS in correspondence of a SM Higgs boson mass $m_H = 126.5$ GeV, where it reached the value of 6.0 standard deviations. The maximum local significance yielded by CMS, 5.0 standard deviations (5.1 excluding the channels $H \to \tau\tau$ and $H \to b\bar{b}$ from the combination) was for a mass $m_H \sim 125$ GeV.

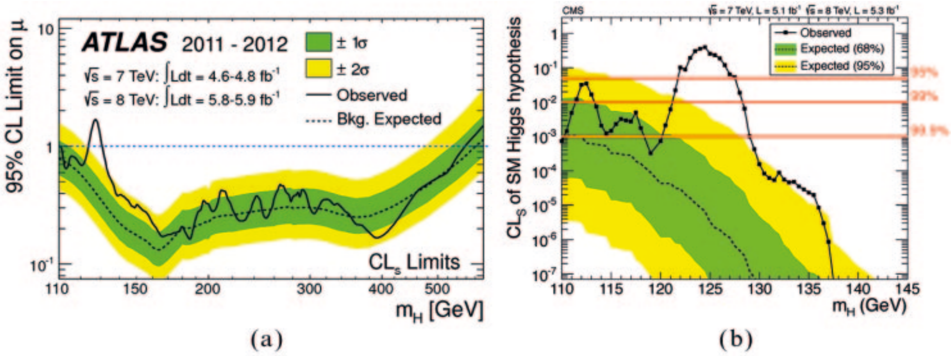


Fig. 35. – The ATLAS [66] (left plot) and CMS [67] (right plot) observed (solid) 95% C.L. limits on the signal strength as a function of $m_H$ and the expectation (dashed) under the background-only hypothesis. The dark and light shaded bands show the $\pm 1$ s.d. and $\pm 2$ s.d. uncertainties on the background-only expectation.

Taking into account the *look-elsewhere effect* [65], a global significance of 5.1 s.d. was estimated by ATLAS in the mass interval 110–600 GeV, and 5.3 s.d. in the mass range 110–150 GeV, while a global significance of 4.5 s.d. was estimated by CMS in the mass interval 110–145 GeV.

The combined 95% C.L. exclusion limits on the production of the SM Higgs boson, expressed in terms of the signal strength parameter $\mu$ as a function of $m_H$ are shown in fig. 35. The excluded mass regions by ATLAS (CMS) were 111–122 GeV and 131–559 GeV (110–121.5 GeV; in the discovery paper CMS limited the search to the mass interval 110–145 GeV).

Three mass regions were excluded by ATLAS at 99% C.L.: 113–144, 117–121 and 132–527 GeV.

**11·6.** *Characterisation of the excess.* – The best-fit signal strength $\hat{\mu}$ has been measured by ATLAS to be $\hat{\mu} = 1.4 \pm 0.3$ for $m_H = 126$ GeV, which is consistent with the Standard Model hypothesis $\mu = 1$. A summary of the individual and combined best-fit values of the strength parameter for a SM Higgs boson of 126 GeV mass is shown in fig. 36(a). Figure 36(b) shows the two-dimensional 68% C.L. regions for the signal strength $\sigma/\sigma_{\mathrm{SM}}$ *versus* $m_H$ (indicated as $m_X$ in the figure) for the $H \to \gamma\gamma$ and the $H \to ZZ^{(*)} \to llll$ channels (the former is shown for the inclusive and the VBF processes).

These results provided a conclusive evidence of the existence of a new particle with mass of about 125 GeV, discovered independently by two experiments at the Large Hadron Collider, based on complementary technology choices.

They were presented for the first time in two seminars held at CERN on July 4th, 2012, and a few days later at the ICHEP Conference 2012, held in Melbourne (Australia).

A new era started in the domain of high-energy physics, characterised by the mission of understanding the nature of this new particle, and, in particular, to ascertain whether it is really the Higgs boson predicted by the Standard Model.

Immediately after the discovery, ATLAS and CMS started a campaign of precision measurement of the physics properties associated to this new particle, in particular its couplings to elementary fermions and bosons.

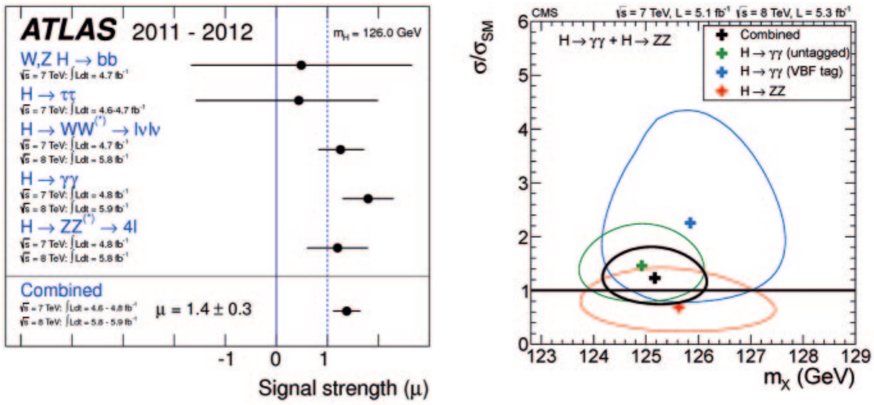


(a) (b)

Fig. 36. – Left: ATLAS measurements of the signal strength parameter $\mu = \sigma/\sigma_{\mathrm{SM}}$ for $m_H = 126\,\mathrm{GeV}$ for the individual channels and their combination [66]. Right: the 68% C.L. contours of the signal strength $\mu$ *versus* the boson mass $m_X$ for the untagged $\gamma\gamma$, $\gamma\gamma$ with VBF-like jet selection, $4l$ and their combination, measured by CMS [67]. In both combinations, the relative signal strengths for the processes considered are constrained by the predictions for the SM Higgs boson.

## 12. – Bosonic and fermionic decay modes: Legacy results of Run 1

The LHC accelerator continued its 8 TeV operation for the whole 2012 and new data were collected by ATLAS and CMS bringing the total available statistics, at the end of the year, close to $25\,\mathrm{fb}^{-1}$ for both collaborations: $5.1\,\mathrm{fb}^{-1}$ at 7 TeV + $19.7\,\mathrm{fb}^{-1}$ at 8 TeV for CMS and 4.5 at 7 TeV + $20.3\,\mathrm{fb}^{-1}$ at 8 TeV for ATLAS. Additional data and several refinements of the analyses allowed to produce many new results on the main decay modes of the newly discovered boson. Furthermore, it was possible to measure carefully its properties and couplings to check the level of compatibility of the observed particle with the Higgs boson predicted by the Standard Model, and to further elucidate its role in the electroweak symmetry breaking and in the mechanism that gives mass to fermions. Results with full statistics for the most important channels have been produced by the two collaborations and published in a series of legacy papers summarising the outcome of the first physics run of LHC.

**12·1.** *Bosonic decay modes:* $H \to \gamma\gamma$, $H \to ZZ^{(*)} \to llll$ $H \to WW^{(*)} \to l\nu l\nu$. – With the full Run 1 statistics the Higgs signals in the two high resolution channels, $H \to \gamma\gamma$ and $H \to ZZ^{(*)} \to llll$, yielded an impressive evidence of the new state of matter. A strong signal is seen in the di-photon and in the four-leptons channels. The statistical significance in both cases exceeds the 5 s.d. that would be needed to claim the observation of the new boson in a single channel.

Compared with the results shown at the time of the discovery, not only the statistics is much higher but new, refined analyses have yielded also higher sensitivity. A couple of examples of these new results are shown in fig. 37. The statistical significance for the signal is 5.2 s.d. for the channel $H \to \gamma\gamma$ in ATLAS and 6.8 s.d. for the decay mode $H \to ZZ^{(*)} \to llll$ in CMS. The final Run 1 data analysis results for $H \to \gamma\gamma$ and $H \to ZZ^{(*)} \to llll$ in ATLAS and CMS are available in refs. [73, 74] and [75, 60], respectively.

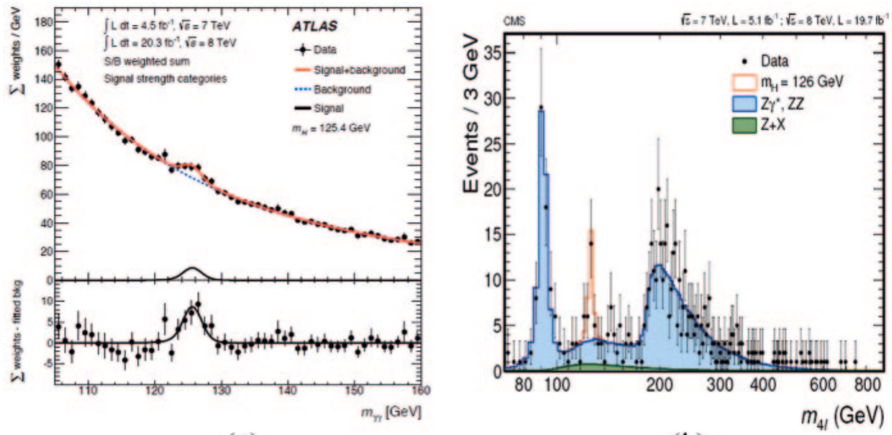


(a) (b)

Fig. 37. – (a) Diphoton invariant mass spectrum observed in ATLAS in the sum of 7 TeV and 8 TeV data [73]. Each event is weighted by the signal-to-background ratio in the data set and category it belongs to. The solid red curve shows the fitted signal plus background model when the Higgs boson mass is fixed at 125.4 GeV. The background component of the fit is shown with the dotted blue curve. The bottom plot shows the data after subtraction of the background component. (b) Distribution of the four-lepton reconstructed mass in the full mass range $70 < m_{4l} < 1000$ GeV explored by CMS using 7 TeV and 8 TeV data for the sum of the $4e$, $2e2\mu$ and $4\mu$ channels [60]. Shaded histograms represents the backgrounds, and the unshaded histogram represents the signal expectation for a mass hypothesis of 126 GeV. Signal and $ZZ$ background are normalised to the SM expectation; the $Z + X$ background to the estimation from data.

With the increased statistics of the full data set and further improvements in the analysis, both collaborations were able to report significant Higgs signals also in the $H \to WW^{(*)} \to l\nu l\nu$ channel.

A clear excess of events above background appears in the distributions of the most sensitive variables. As an example fig. 38 shows the distribution of $m_T$, the transverse mass of the system as measured by ATLAS, and the global exclusion plot for this decay mode produced by CMS.

The broad, un-ambiguous excess of events seen in both experiments, is consistent with the presence of the Higgs boson signal with a significance of 6.1 (4.3) standard deviations in ATLAS and CMS, respectively. These results provide therefore a very strong evidence for a Higgs-like boson decaying to a $W$-boson pair. The final Run 1 data analysis results of $H \to WW^{(*)} \to l\nu l\nu$ search from ATLAS and CMS are available in refs. [76, 77], respectively.

**12**˙2. *Main fermionic modes: $H \to \tau^+\tau^-$, $H \to b\bar{b}$.* – With data available at the time of the discovery it was not possible to establish un-ambiguously that the newly discovered boson couples to fermions through a Yukawa interaction, giving rise to the masses of quarks and leptons. Indirect evidence for the Higgs coupling to the top quark is implied by an overall agreement of the gluon-gluon fusion production channel cross section with the standard model prediction. However, the masses of down-type fermions may come about through different mechanisms in theories beyond the Standard Model. Since the decay of a Higgs boson with a mass around 125 GeV to top quarks is kinematically not allowed, the most abundant fermionic decays will be to third-generation quarks and leptons, namely to bottom quark-antiquark pairs and to tau lepton-antilepton pairs.

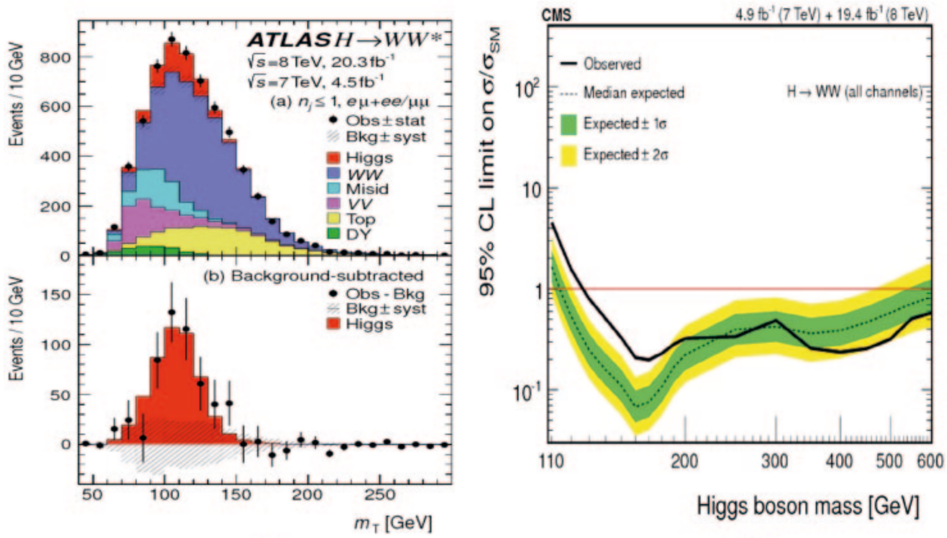


(a) (b)

Fig. 38. – (a) Post-fit combined transverse mass distributions observed in ATLAS for all lepton-flavour in the 7 and 8 TeV data [76]. The bottom plot shows the data after subtraction of the background component. (b) CMS expected 95% C.L. upper limits on the $H \to WW$ production cross section relative to the SM expectation, as a function of the SM Higgs boson mass hypothesis [77].

These decay modes were therefore studied carefully by both experiments using the full available statistics.

The search for $H$ decaying to tau lepton pairs is a very complex task. All combinations of leptonic ($\tau \to l\nu\bar{\nu}$, with $l = e, \mu$) and hadronic ($\tau \to hadrons + \nu$) tau decays are considered. Furthermore, the search is designed to be sensitive to the major production processes, *i.e.* production via gluon fusion (ggF), vector-boson fusion (VBF), and associated production (VH) with $V = W$ or $Z$. These production processes lead to different final-state signatures, which are exploited by defining an event categorisation. Dedicated categories are considered to achieve both a good signal-to-background ratio and good resolution for the reconstructed invariant mass. The VBF category, enriched in events produced via vector-boson fusion, is defined by the presence of two jets with a large separation in pseudorapidity. The boosted category contains events where the reconstructed Higgs boson candidate has a large transverse momentum. It is dominated by events produced via gluon fusion with additional jets from gluon radiation. In view of the signal-to-background conditions, and in order to exploit correlations between final-state observables, multivariate analysis techniques are used to extract the final results. As a cross-check, separate analyses where cuts on kinematic variables are applied, are carried out. An excess of events over the expected background from other Standard Model processes is found by both collaborations with an observed (expected) significance of 4.5 (3.4) standard deviations for ATLAS and 3.2 (3.7) for CMS (fig. 39). These results provide evidence for the direct coupling of the recently discovered Higgs boson to fermions. The measured signal strengths, normalised to the Standard Model expectation, of $1.43^{+0.43}_{-0.37}$ for ATLAS and $0.78 \pm 0.27$ for CMS are consistent with the predicted Yukawa coupling strength in the Standard Model [78, 79].

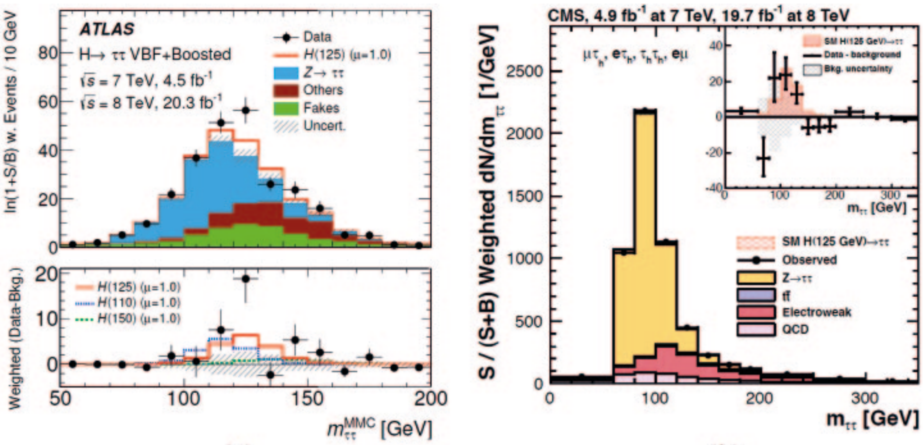


(a) (b)

Fig. 39. – (a) Distributions of the reconstructed invariant mass, $m_{\tau\tau}$ in ATLAS [78]. Events are weighted for each category according to the expected signal-to-noise ratio. The bottom panel shows the difference between weighted data events and weighted background events (black points), compared to the weighted signal yields. (b) Combined observed and predicted $m_{\tau\tau}$ distributions for different channels ($\mu\tau_h$, $e\tau_h$, $\tau_h\tau_h$, and $e\mu$) in CMS [79]. Also in this case the events are weighted according to the expected signal-to-noise ratio. The inset shows the corresponding difference between the observed data and expected background distributions, together with the signal distribution for a SM Higgs boson with $m_H = 125\,\text{GeV}$.

The inclusive production of a Higgs boson decaying into a $b\bar{b}$ quark pair is extremely hard to exploit due to the overwhelming direct production of $bb$ quark pairs, as predicted by QCD. For this reason, present searches target the VH production mode in which the Higgs boson is produced in association with a $W$ or a $Z$ boson, identified via its leptonic decay. Requiring the presence of additional leptons with high transverse momentum provides an effective handle to reduce the QCD background. The Higgs-boson candidate is reconstructed from two jets of particles, each of which has been identified as having a high probability of arising from the hadronisation of a bottom quark. The identification is based on properties of hadrons containing bottom quarks, such as their long lifetimes which lead to displaced vertexes, or their decay to muons, both producing distinctive signatures that the LHC detectors are sensitive to. Owing to the 10% mass resolution of the identified pair of $b$-quark jets, the Standard Model Higgs boson signal is expected to produce a broad enhancement over the background in the $b\bar{b}$ invariant mass distribution. The result of the analysis performed on the full available statistics shows an excess over the background expectation for Higgs boson mass hypotheses, $m_H$, in the range of 120–135 GeV, with an observed (expected) significance of 2.1 (2.1) standard deviations for CMS (see fig. 40(a)) and 1.4 (2.6) standard deviation for ATLAS, at a mass of 125 GeV [80, 81]. Correspondingly, the strength of this excess relative to the expectation for the Standard Model Higgs boson observed by ATLAS is $0.52 \pm 0.32(\text{stat}) \pm 0.24(\text{syst})$, while for CMS is $1.0 \pm 0.5$ (where here the uncertainty includes the effect of both statistical and systematic sources of uncertainty).

The CMS Collaboration has combined together their results for the decay modes $H \to b\bar{b}$ and $H \to \tau^+\tau^-$ under the assumption that the Higgs boson is produced as expected in the Standard Model. The combination provides further strong evidence for

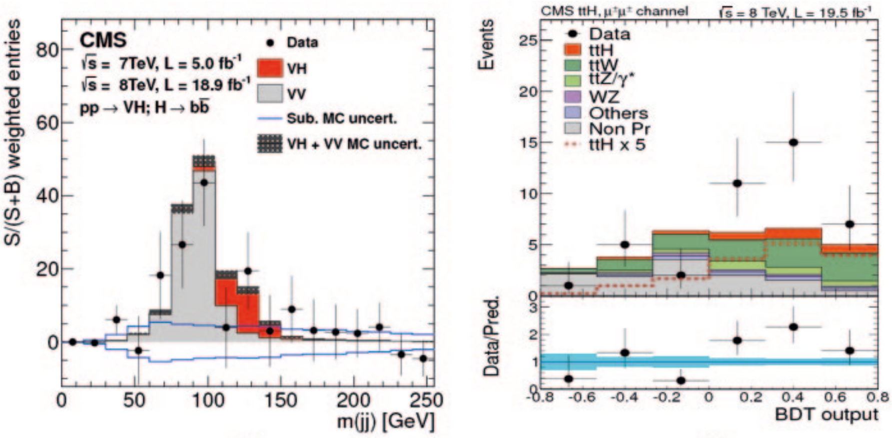


(a) (b)

Fig. 40. – (a) Distribution of $m_{jj}$, invariant mass of $b$-tagged jets in CMS produced in association with a boosted $W$ or $Z$ [80]. All channels are combined and events are weighted for each category according to the expected signal-to-noise ratio. The histogram shows the number of events observed in data to that of the Monte Carlo prediction for signal and backgrounds with all backgrounds, except di-bosons, subtracted. The small excess of events on the right-hand shoulder of the expected di-boson distribution is consistent with a $WH/ZH$ associated production for a $m_H = 125\,\text{GeV}$. (b) Distribution of the BDT discriminant used in CMS to enhance the sensitivity to $t\bar{t}H$ for same-sign di-lepton events and final states with muons [83]. The red dotted line shows the expected Higgs signal in $t\bar{t}H$ for this channel magnified by a factor of 5. This particular channel dominates the excess reported by CMS in this search.

the direct coupling of the 125 GeV Higgs boson to down-type fermions, with an observed (expected) significance of 3.8 (4.4) standard deviations [82]. In conclusion, the existing searches for a Higgs boson decaying into bottom quarks and tau leptons are consistent with the Standard Model prediction of a Yukawa structure, where the fermionic couplings are proportional to the fermion masses.

**12**˙3. *Further fermionic modes:* $pp \to t\bar{t}H$, $H \to \mu^+\mu^-$, $H \to e^+e^-$. – Additional channels dealing with fermionic modes that were studied by ATLAS and CMS included $pp \to t\bar{t}H$, and the rare decay modes $H \to \mu^+\mu^-$ and $H \to e^+e^-$.

Probing the top quark Yukawa coupling directly requires a process that results in both a Higgs boson and top quarks explicitly reconstructed via their final-state decay products. The production of a Higgs boson in association with a top quark pair ($t\bar{t}H$) satisfies this requirement. Furthermore the measurement of this rate provides a direct test of several New Physics scenarios that predict the existence of heavy top quark partners that would alter it significantly. Observation of a significant deviation in the $t\bar{t}H$ production rate with respect to the SM prediction would be an indirect indication of unknown phenomena.

The small $t\bar{t}H$ production cross section, roughly 130 fb at $\sqrt{s} = 8\,\text{TeV}$, makes measuring its rate experimentally challenging. Therefore, it is essential to exploit every accessible experimental signature. For this search lepton+jets, di-lepton and all hadronic final states of the $t\bar{t}$ system could be explored. With respect to the Higgs decay modes, several channels can be considered: $H \to b\bar{b}$, $H \to \tau^+\tau^-$, $H \to \gamma\gamma$ and $H \to WW/ZZ$.

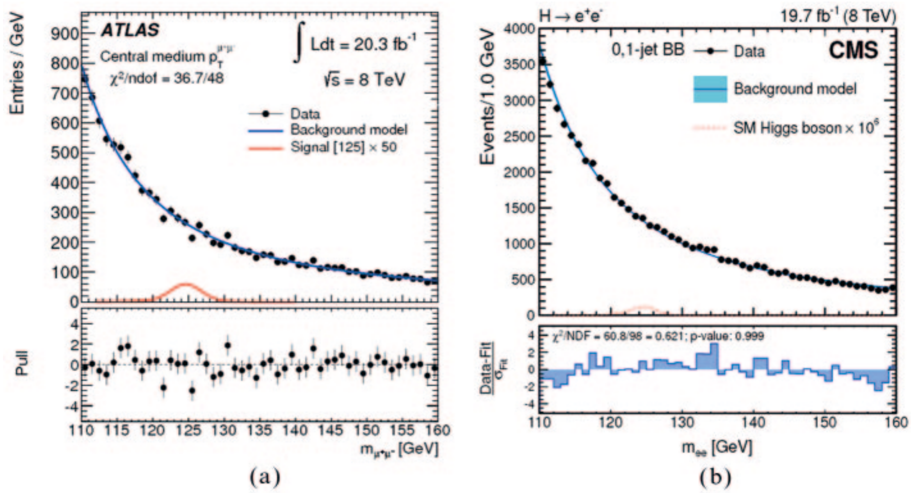


Fig. 41. – (a) ATLAS di-muon invariant mass distribution at 8 TeV and fit of the background model [84]. To increase the sensitivity of the search, the events are subdivided in categories with different signal-to-noise ratio. The plot refers to events with muons in the central region and intermediate $p_T^{\mu^+\mu^-}$. The bottom plot shows the pull for each bin once the background fit is subtracted. The expected signal is shown for $m_H = 125$ GeV and scaled by a factor of 50. (b) CMS di-electron invariant mass distribution at 8 TeV and fit of the background model [83]. The plot shows the 0,1-jet BB categories corresponding to events with both electrons in the barrel part of the electromagnetic calorimeter. The dotted line illustrates the expected SM Higgs boson signal enhanced by a factor of $10^6$, for $m_H = 125$ GeV. The lower histogram shows the residual for each bin normalised by the Poisson statistical uncertainty of the background model.

Multivariate analysis techniques could be used to tag the jets coming from $b$-quark or $\tau$-lepton decays and to separate $t\bar{t}H$ events from the large $t\bar{t}$ + jets backgrounds. MVA techniques can be used also to separate signal leptons arising from $W$-boson, $Z$-boson and $\tau$-lepton decays from background leptons, which may come from $b$-quark or $c$-quark decays, or misidentified jets.

For the study of the $t\bar{t}H$ channel both ATLAS and CMS performed an analysis based on $H \to b\bar{b}$ decay channel. The CMS collaboration published also comprehensive studies considering many final states together, combining $H \to$ multi-leptons, $H \to b\bar{b}$ and $H \to \gamma\gamma$ analyses [83,85-87]. No significant excess above background is found by ATLAS, while CMS reported an excess of events with respect to the background-only hypothesis corresponding to 3.4 standard deviations and a best-fit value for a Higgs signal strength of $2.8 \pm 1.0$ at 68% (fig. 40(b)). Compared to the SM expectation the observed excess is equivalent to a 2-standard-deviation upward fluctuation. Additional data will be needed to better study this important channel.

With respect to the two channels $H \to \mu^+\mu^-$ and $H \to e^+e^-$, the decay modes are far too rare to detect with the available statistics and no signal is observed. For a Higgs boson mass of 125 GeV, it is only possible to set upper limits on the branching ratio of the two decays (fig. 41). The observed limit for $H \to \mu^+\mu^-$ is 7.0 (7.4) times the SM value for ATLAS (CMS), while for $H \to e^+e^-$ CMS sets an upper limit $3.7 \cdot 10^5$ times the SM prediction [84, 83]. These results, together with the evidence for the coupling to tau-leptons, show that the leptonic couplings of the new 125 GeV boson are not flavour-universal, confirming therefore the SM prediction.

## 13. – Measurement of the properties of the new boson

The SM Higgs boson is predicted to have even parity, zero electric charge, and zero spin. All its other properties can be derived once its mass is known. Being the only free parameter of the theory, $m_H$ must be measured with the greatest accuracy to be able to perform precision calculations of the electroweak observables, including the production and decay properties of the Higgs boson itself.

The amount of data available at the time of the discovery was not large enough to measure carefully the quantum numbers of the new particle and to investigate thoroughly its couplings to the SM particles. This work was done by ATLAS and CMS using the full data set collected in the first physics run of LHC. The result of these studies are described in the present section.

**13˙1.** *Measurement of the mass.* – ATLAS and CMS have chosen a model-independent approach to measure the Higgs boson mass. The best determination is obtained by combining the measurements performed in the two high resolution channels: $H \to \gamma\gamma$ and $H \to ZZ^{(*)} \to llll$. In these two channels the Higgs signal appears as a narrow mass peak with a typical experimental resolution of 1.5–2 GeV over a smooth background. Therefore, the information on the mass can be extracted without assumptions on the signal production and decay yields. Interference effects with SM backgrounds are expected to be small for a very narrow state. Coarser measurements of the mass can be obtained using $H \to WW^*$, $H \to \tau\tau$ and $H \to b\bar{b}$.

To extract the value of $m_H$ in a way that is not completely dependent on the SM prediction for the production and decay ratios, the signal strength modifiers for the major production processes ggH, $t\bar{t}H \to \gamma\gamma$, VBF, VH $\to \gamma\gamma$ and $pp \to H \to ZZ^{(*)} \to llll$ are taken as independent, unconstrained, parameters. The signal in all channels is assumed to be due to a single, narrow state with mass $m_H$.

The best-fit value of $m_H$ and its uncertainty are extracted from a scan of the combined test statistic $q(m_H)$ with the three signal strength modifiers profiled together with all other nuisance parameters. Figure 42 shows the results obtained by the two experiments.

For both experiments the two channels yield results that are compatible within errors ($2.0\sigma$ for ATLAS and $1.6\sigma$ for CMS).

CMS measured a mass $m_H = 125.02^{+0.26}_{-0.27}\,\text{GeV(stat)}^{+0.14}_{-0.15}\text{(syst)}$ [89] while the measurement of ATLAS was $m_H = 125.36 \pm 0.37\text{(stat)} \pm 0.18\text{(syst)}\,\text{GeV}$ [88].

Recently the two experiments have combined their measurements. The result is obtained from a simultaneous fit to the reconstructed invariant mass peaks in the two high resolution channels and for the two experiments. The combined measured mass of the Higgs boson is $m_H = 125.09 \pm 0.24\,\text{GeV} = 125.09 \pm 0.21\text{(stat)} \pm 0.11\text{(syst)}\,\text{GeV}$, corresponding to an accuracy better than 0.2%. The total uncertainty is dominated by the statistical term while systematics errors are mostly linked to uncertainties in the energy or momentum scale and resolution for photons and leptons [90].

**13˙2.** *Direct and indirect measurement of the width.* – The natural width of a 125 GeV Higgs boson is so small, 4 MeV, that any attempt to measure it directly, with experimental resolutions orders of magnitude larger, is simply hopeless. However, upper limits on the total width of the Higgs boson can be derived from fits to the mass spectra of the $H \to \gamma\gamma$ and $H \to ZZ^{(*)} \to llll$ decay channels, under the assumption that there is no interference with background processes.

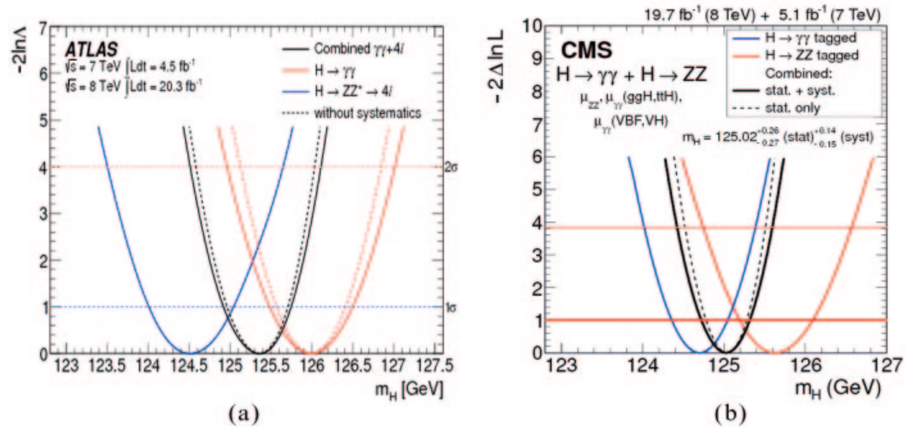


Fig. 42. – (a) The profile likelihood for the individual $H \to \gamma\gamma$ and $H \to ZZ^{(*)} \to llll$ channels in ATLAS and their combination [88]. The signals strengths in the two decay modes are allowed to vary independently. (b) Scan of the test statistic $q(m_H) = -2\Delta \ln L$ *versus* the mass of the boson $m_H$ for the $H \to \gamma\gamma$ and $H \to ZZ^{(*)} \to llll$ final states separately and for their combination in CMS [89]. Three independent signal strengths, (ggH, $t\bar{t}H$) $\to \gamma\gamma$, (VBF, VH) $\to \gamma\gamma$ and $pp \to H \to ZZ^{(*)} \to llll$ are profiled together with all other nuisance parameters.

In the $H \to \gamma\gamma$ channel, an upper limit of 5.0 (6.2) GeV was observed (expected) by ATLAS [73] while the corresponding values for CMS in the same decay mode were 2.4 (3.1) GeV [74]. For the $H \to ZZ^{(*)} \to llll$ channel, the upper limit observed by ATLAS was 2.6 (6.2) GeV [75] while CMS reports an upper limit of 3.4 GeV with 2.8 GeV expected [60].

The Higgs boson width can be severely constrained using indirect methods, in particular by studying its off-shell production and decay to two $Z$ bosons away from the resonance peak.

In the dominant, gluon fusion, production mode, the off-shell production cross section is known to be sizable. This arises from an enhancement in the decay amplitude from the vicinity of the $Z$-boson pair production threshold. A further enhancement comes from the top quark pair production threshold. In these conditions the zero-width approximation is inadequate and the ratio of the off-shell cross section above $2m_Z$ to the on-shell signal is of the order of 8%.

The gluon fusion production cross section depends on $\Gamma_H$ through the Higgs boson propagator, therefore a careful measurement of the relative off-shell and on-shell production in the $H \to ZZ^{(*)} \to 4l$ channel provides direct information on $\Gamma_H$.

In order to enhance the sensitivity to the gg production in the off-shell region, a likelihood discriminant (MELA) based on the angular distributions of the leptons in the final states was used. The effect of this discriminant in the high mass end of the $m_{4l}$ distribution for $\Gamma_H = 10 \times \Gamma_H^{SM}$, can be seen in fig. 43.

Similar methods can be used to extract information on $\Gamma_H$ studying the high mass region of $H \to ZZ^{(*)} \to 2l2\nu$ and $H \to WW^{(*)} \to l\nu l\nu$.

The outcome of these studies for ATLAS was $\Gamma_H < 22.7$ MeV [92] while the combined fit for CMS yields $\Gamma_H < 22$ MeV which is 5.4 times the expected width of the SM Higgs boson [91]. These results improve by more than two orders of magnitude upon the previous experimental constraints from the direct measurement at the resonance peak.

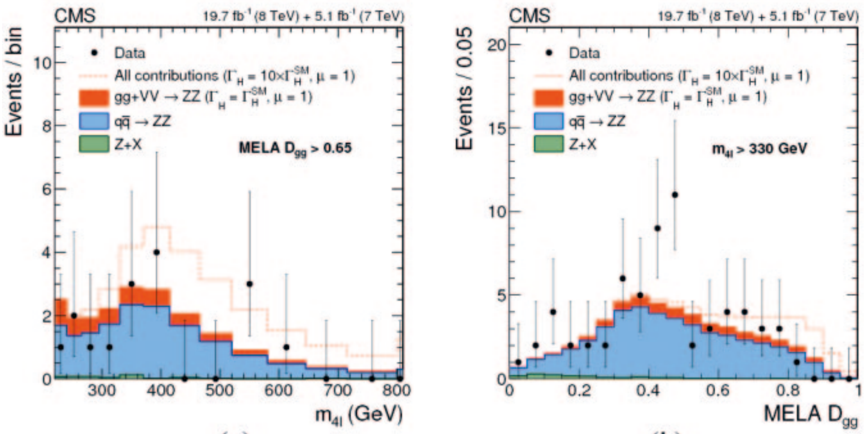


(a) (b)

Fig. 43. – (a) CMS distributions of the four-lepton invariant mass after a selection requirement on the MELA likelihood discriminant. (b) Distribution of the MELA likelihood discriminant for a four-lepton invariant mass > 330 GeV. In both cases a $\Gamma_H = 10 \times \Gamma_H^{\mathrm{SM}}$ is assumed [91].

**13**˙3. *Study of the spin and parity of the new particle.* – The four-lepton decay mode, with the full kinematics of the Higgs boson and its decay products well measurable in the detector, provides many independent observables that can be used also to study the quantum numbers of the new resonance. In particular the angular correlations of its decay products carry useful information that can be used to experimentally establish the consistency of its spin and parity quantum numbers with respect to the SM predictions. Additional information can be extracted studying the angular distributions of the decay products in $H \to \gamma\gamma$ and $H \to WW^{(*)} \to l\nu l\nu$.

In these studies the Standard Model spin-parity $J^P = 0^+$ hypothesis is compared to several alternative hypotheses with $J^P = 0^-, 1^+, 1^-, 2^+$. The measurements are based on the kinematic properties of the three final states $H \to ZZ^{(*)} \to 4l$, $H \to \gamma\gamma$ and $H \to WW^{(*)} \to l\nu l\nu$. To improve the sensitivity several final states are combined. Signal models yielding spin-0, spin-1 and even graviton-inspired spin-2 resonances are simulated taking into account the main production and decay processes and the kinematics of the decay. The spin-1 hypotheses are considered under the assumption that the resonance decaying into four leptons is not necessarily the same resonance observed in the $H \to \gamma\gamma$ channel as $J = 1$ in the latter case is prohibited by the Landau-Yang theorem.

Figure 44 illustrates the method used to compare the various hypotheses while the summary of the results obtained by CMS in comparing several spin-parity models is shown in fig. 45. Similar studies have been performed by ATLAS.

The conclusion of the studies performed by ATLAS and CMS on the spin and parity of the new boson is that all observations are consistent, within their uncertainties, with the expectations for the SM Higgs boson [93-96, 74]. Data favour the pure scalar hypothesis when compared to several other spin-parity hypotheses. The hypotheses of a pseudoscalar and all tested spin-1 boson hypotheses are excluded at the 99% C.L. or higher. All tested spin-2 boson hypotheses are excluded at the 95% C.L. or higher. The fraction of a CP-odd contribution to the decay amplitude is consistent with the expectation for the SM Higgs boson.

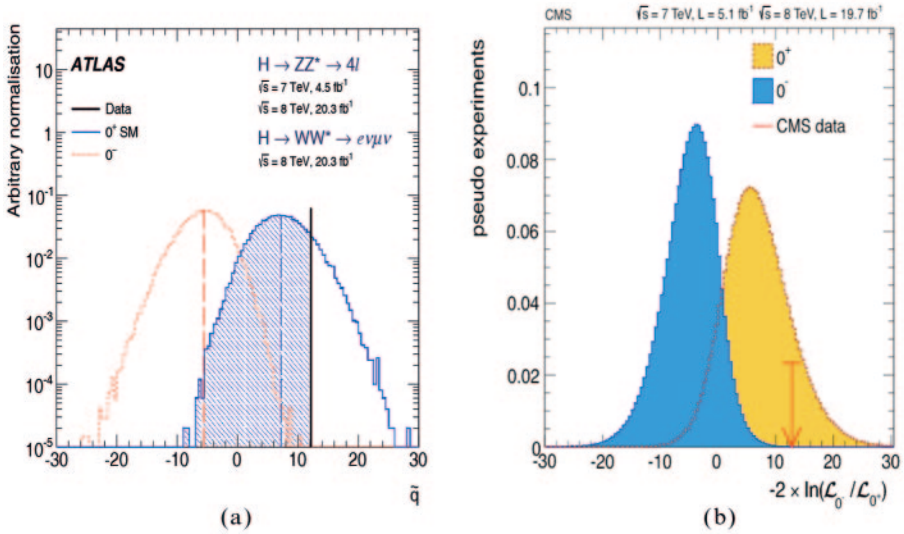


Fig. 44. – (a) Expected distributions of the logarithm of the ratio of profiled likelihoods, $\tilde{q}$, under the $J^P = 0^+$ and $0^-$ hypotheses for ATLAS. The observed value is indicated by the vertical solid line and the expected medians by the dashed lines [93]. (b) Similar distributions produced for CMS. In both cases the data are fully compatible with the $J^P = 0^+$ expected for the SM Higgs and the $J^P = 0^-$ solution is strongly disfavoured by data [60].

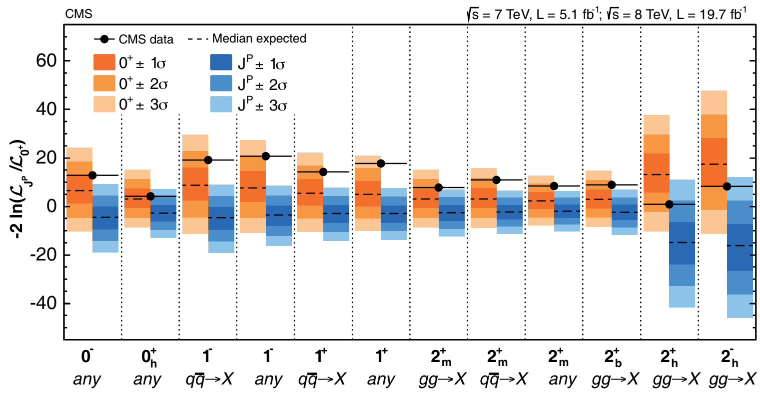


Fig. 45. – Summary of the expected and observed values for the test-statistic distributions for the twelve hypotheses tested by CMS as alternative with respect to the SM Higgs boson [60]. The orange (blue) bands represent the 1, 2, 3$\sigma$ bands around the median expected value for the SM Higgs boson hypothesis (alternative hypothesis). The black point represents the observed value.

**13**·4. *Study of the Higgs boson couplings.* – The study of the coupling of the Higgs with the full available statistics includes all major production modes (gg, VBF, VH and ttH) and the most important decay modes ($\gamma\gamma$, $WW^{(*)}$, $ZZ^{(*)}$, $\tau\tau$ and $b\bar{b}$).

Following the framework and benchmarks recommended in ref. [97], the measurements of the couplings were performed using a leading-order motivated approach. The framework is based on the following assumptions:

– The signals observed in different search channels originate from a single narrow resonance with mass of about 125.5 (125.8) GeV in the case of ATLAS (CMS).

– Modifications of coupling strengths are considered, while the tensor structure of the Lagrangian is assumed to be the same as in the Standard Model; this implies in particular that the observed state is a CP-even scalar.

– The width of the particle is assumed to be negligible, justifying the use of the narrow-width approximation. Hence the predicted rate for a given channel can be decomposed as follows:

$$\sigma \cdot B\ (i \to H \to f) = \frac{\sigma_i \cdot \Gamma_f}{\Gamma_H}\,, \tag{17}$$

where $\sigma_i$ is the production cross section through the initial state $i$, $B$ and $\Gamma_f$ are the branching ratios and partial decay width into the final state $f$, respectively, and $\Gamma_H$ the total width of the Higgs boson.

The leading-order coupling scale factors, $\kappa_i$, are defined in such a way that the cross sections $\sigma_i$ and the partial decay width $\Gamma_i$ associated to the Standard Model elementary particle $i$ scale with $\kappa_i^2$ when compared to the corresponding SM expectation. More details can be found in [98].

Using this notation, for the process $gg \to H \to \gamma\gamma$ one would write the production cross section as follows:

$$\frac{\sigma \cdot B\ (gg \to H \to \gamma\gamma)}{\sigma_{\mathrm{SM}}(gg \to H) \cdot B_{\mathrm{SM}}(H \to \gamma\gamma)} = \frac{\kappa_g^2 \cdot \kappa_\gamma^2}{\kappa_H^2}\,. \tag{18}$$

The compatibility of the observed yields with the SM Higgs boson hypothesis has been studied using the common signal strength modifier $\hat{\mu}$ defined in sect. **11**. The best fit value for $\hat{\mu}$ obtained from the combined analysis of all channels, provides the simplest compatibility test.

The event yields obtained in the different analyses tagging specific decay modes and production mechanisms are consistent with those expected for the Standard Model Higgs boson. Detailed studies on the subject can be found in refs. [98, 75, 73, 76, 99, 89]. An example of these studies is shown in fig. 46. The combined best-fit signal relative to the Standard Model expectation is $1.18 \pm 0.15$ for ATLAS, at the measured mass of 125.36 GeV, and $1.00 \pm 0.14$ for CMS at the mass of 125.02 GeV. It is worth noticing the consistency of the signal strength, for all major decay modes, with the SM predictions.

At the time of the discovery both experiments reported an intriguing hint of an excess in the $H \to \gamma\gamma$ channel ($\hat{\mu}_{\gamma\gamma} = 1.8 \pm 0.5$ for ATLAS and $\hat{\mu}_{\gamma\gamma} = 1.6 \pm 0.4$ for CMS). This coincidence triggered a lot of interest, since this channel is extremely sensitive to contributions coming from heavy charged particles that could enter the loops and modify the signal strengths. With the full available statistics these hints have vanished. Both experiments report now $\hat{\mu}_{\gamma\gamma}$ values fully consistent with the SM expectations: $1.17 \pm 0.27$ for ATLAS and $1.12 \pm 0.24$ for CMS.

Many other tests on the signal strengths modifiers have been performed to test the most important production mechanisms and the possible role of different sources of New Physics.

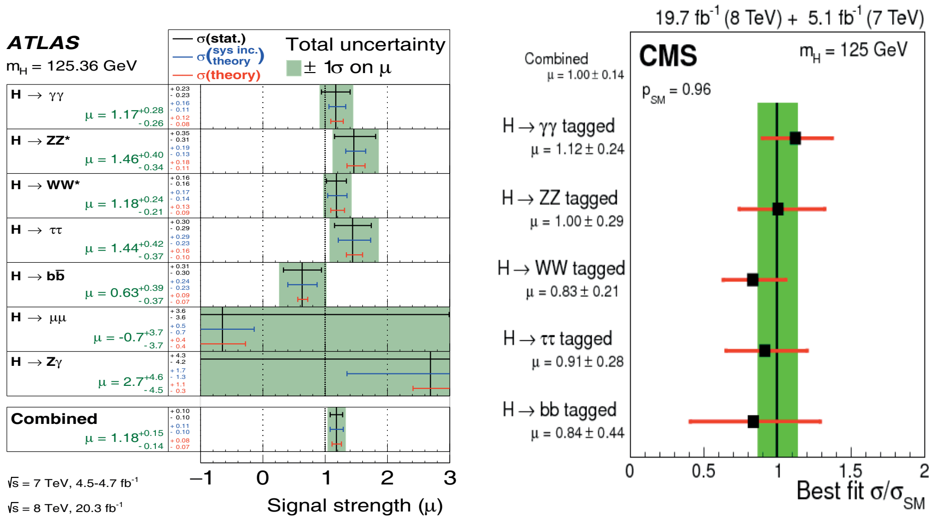


(a) (b)

Fig. 46. – (a) Signal strengths for a Higgs boson of mass $m_H = 125.36\,\text{GeV}$, normalised to the SM expectations, as measured in ATLAS for several decay modes [99]. (b) Similar results produced by CMS for the most important decay modes assuming a Higgs boson mass $m_H = 125\,\text{GeV}$ [89].

In the SM, the Higgs sector possesses an approximate $SU(2)_L \times SU(2)_R$ global symmetry, which is broken by the Higgs vacuum expectation value to the diagonal subgroup $SU(2)_{L+R}$. As a result, the tree-level ratio of the $W$ and $Z$ boson masses, $m_W/m_Z$, and the ratio of their couplings to the Higgs boson, $g_W/g_Z$, are protected against large radiative corrections, a property known as "custodial symmetry", an essential feature of the SM Higgs boson that must be checked carefully.

The test is done studying two scaling factors, $k_W$ and $k_Z$, that could modify the couplings of the SM Higgs to the $W$ and $Z$ bosons, therefore differing significantly from 1 in several models of New Physics.

The dominant production mechanism populating the 0-jet and 1-jet channels of the $H \to WW^{(*)} \to l\nu l\nu$ analysis and the untagged channels of the $H \to ZZ^{(*)} \to 4l$ is gluon-gluon fusion. Therefore, the ratio of event yields in these channels provides a nearly model-independent measurement of $\lambda_{WZ} = k_W/k_Z$. The likelihood scan *versus* $\lambda_{WZ}$ is shown in fig. 47(a). CMS measures $\lambda_{WZ} = 0.94^{+0.22}_{-0.18}$, while the value measured by ATLAS is $\lambda_{WZ} = 1.00^{+0.15}_{-0.11}$. Both results are in excellent agreement with expectations for the SM Higgs boson.

In the SM, the Yukawa coupling between the Higgs boson and the fermions is proportional to the mass of the fermion while the coupling to weak bosons involves the square of the mass of the weak boson. Some BSM models predict completely different couplings to fermions and massive vector bosons with respect to those foreseen in the SM. These models can be tested assuming a common modifier for all vector bosons, $k_V$, and a common modifier for all fermions, $k_f$ and checking whether or not they are consistent with 1. Many compatibility tests can be performed on the two common modifiers including the combined analysis in the different decay modes shown in fig. 47(b) yielding results, once more, fully consistent with the SM expectations.

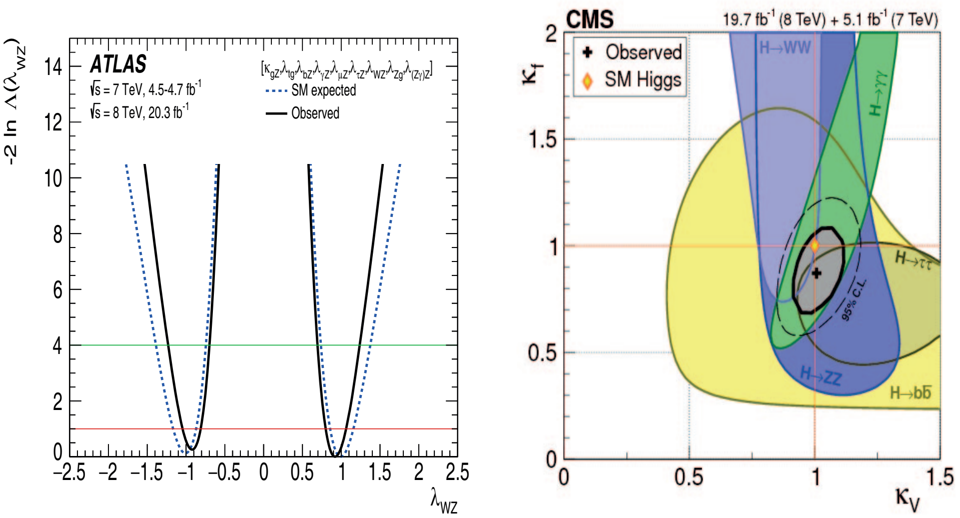


(a) (b)

Fig. 47. – (a) Likelihood scans *versus* $\lambda_{WZ}$, the ratio of the coupling scaling factors to $W$ and $Z$ bosons to test the custodial symmetry in ATLAS [99]. (b) The 68% C.L. confidence regions for individual channels (coloured areas) and for the overall combination (thick curve) for the $k_V$ and $k_f$ parameters as measured by CMS [89]. The cross indicates the global best-fit values. The dashed contour bounds the 95% C.L. confidence region for the combination. The diamond represents the SM expectation.

The results of the various fits for the couplings can be plotted also *versus* the particle masses showing in the same plot both Yukawa and weak bosons couplings. Since $g_V \sim k_V 2m_V^2/v$ and $\lambda_f \sim k_f m_f/v$ adopting a "reduced" weak boson coupling $\sqrt{g_V/(2v)} = k_V^{1/2} m_V/v$, fermions and weak bosons results can be plotted together, as shown in fig. 48. Although the error bars for the fermions couplings are still quite large, the agreement with the Standard Model expectations over many order of magnitudes is really spectacular.

The studies of the production and decay rates and of the spin-parity quantum numbers of the new boson show that, within the present level of uncertainty, all its properties are definitely compatible with those expected for the SM Higgs boson.

## 14. – Search for other Higgs-like bosons at LHC

The Standard Model has an outstanding record of consistency with experimental observations. However, it is not a complete theory, and since the discovery of the SM-like Higgs boson with 125 GeV mass, deep investigations of the mechanism responsible for the electroweak symmetry breaking has become a goal of paramount importance in particle physics.

The experimental directions to pursue this physics programme include the Higgs characterisation analyses discussed in the previous section and the searches for new particles such as the partners of an extended Higgs sector as predicted by several extensions of the SM.

In many of these extensions, the Higgs sector includes two scalar doublets [100]. The two-Higgs-doublet model (2HDM) [101] is a specific example of this type of SM

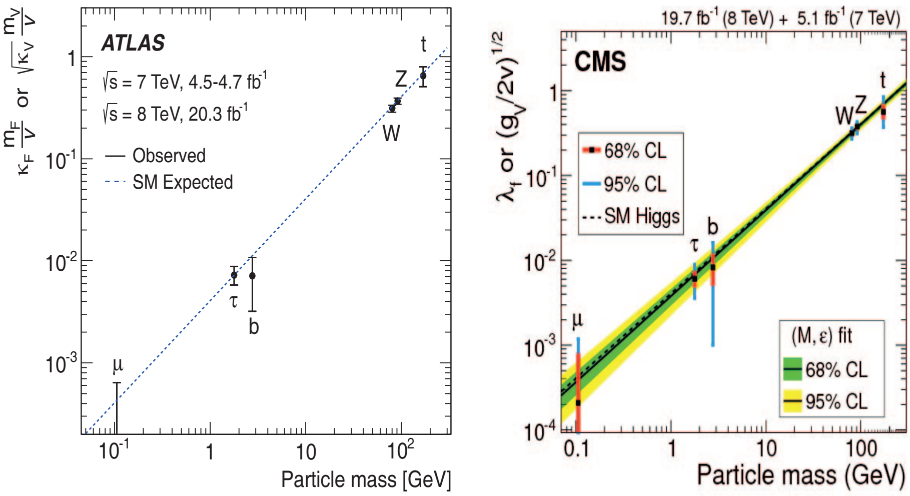


(a) (b)

Fig. 48. – (a) ATLAS fit results for the reduced coupling strength scale factors as a function of the particle mass, assuming a SM Higgs boson with a mass of 125.36 GeV. The dashed line indicates the predicted mass dependence for the SM Higgs boson [99]. (b) Similar results produced for CMS assuming a Higgs boson mass of 125.02 GeV. In both cases the data are fully compatible with the expectations for a Standard Model Higgs boson [89].

extensions. In this model, five physical Higgs particles are expected after electroweak symmetry breaking: two neutral CP-even scalars ($h^0$, $H^0$), one neutral CP-odd scalar ($A^0$) and two charged scalars ($H^+$, $H^-$) [102]. In the context of the Supersymmetry theories (SUSY), the *minimal supersymmetric extension of the Standard Model* (MSSM) predicts a family of Higgs partners, with masses up to 1 TeV, that can be produced and observed at the LHC.

In many of these models it is often assumed that the observed, SM-like, 125 GeV Higgs boson, is the lightest CP-even neutral scalar, the $h^0$ (the so-called *alignment limit*). In these models $\tan\beta$ is defined as the ratio of the vacuum expectation values associated to the two Higgs boson doublets. Depending on the parameters of the model (scalar boson masses, $\tan\beta$ and couplings), both the neutral heavy scalar $H^0$ and pseudoscalar $A^0$ can decay to $\gamma\gamma$, $\tau\tau$, 4-lepton, $t\bar{t}$ final states, as well as to electroweak bosons, including the recently discovered Higgs boson. The branching fractions of $H^0$ and $A^0$ into final states containing one or more Higgs bosons $h^0$ often dominate when kinematically accessible.

The decays of the charged Higgs depend strongly on its mass. For masses $m_{H^\pm} < (m_t + m_b)$ (where $m_t$ and $m_b$ are the pole top and bottom mass, respectively), the charged Higgs can be produced in top quark decays ($t \to H^+ b$) and the subsequent decay $H^+ \to \tau^+\nu$ is the most robust and sensitive final state. For masses $m_{H^\pm} > (m_t + m_b)$ the decay $H^+ \to t\bar{b}$ is the final state with the highest branching fraction and is fully accessible to experiments.

ATLAS and CMS performed extensive searches of neutral and charged partners of the 125 GeV Higgs boson, treating the newly discovered particle as background.

No excess of events has been observed: the data are well described, within uncertainties, by the predictions based on the Standard Model. Therefore limits have been set on

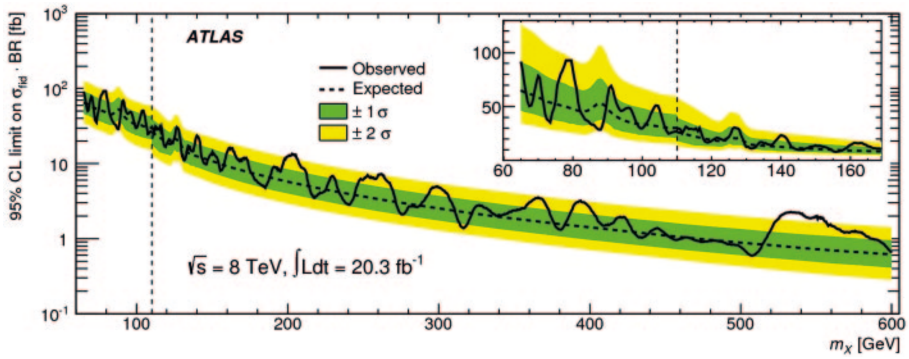


Fig. 49. – ATLAS observed and expected 95% C.L. limit on the fiducial cross section times branching ratio $\mathrm{BR}(\phi \to \gamma\gamma)$ as a function of the $\phi$ particle mass $m_{\gamma\gamma}$ in the range $65 < m_{\gamma\gamma} < 600\,\mathrm{GeV}$ [103]. The discontinuity at $m_{\gamma\gamma} = 110\,\mathrm{GeV}$ is due to the transition between the different low-mass and high-mass analyses adopted to enhance the sensitivity in the two different kinematic regimes. The green and the yellow bands show the 1 s.d. and 2 s.d. uncertainties on the expected limit. The inset shows a zoom on the limit.

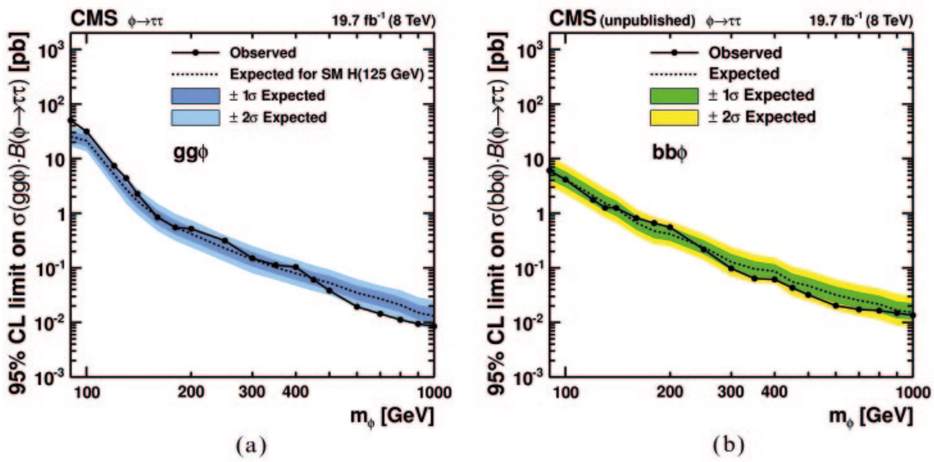


Fig. 50. – CMS C.L. limit on $\sigma(gg\phi) \times \mathrm{BR}(\phi \to \tau\tau)$, where $\phi$ denotes a generic Higgs-like state [104]. The expected limit is also shown for background contribution including a SM Higgs boson with 125 GeV mass. The left plot (a) shows the result for the ggF production mode (leaving free in the fit the associated production mode with $b$-quarks), while the right plot (b) shows the result for the bbH associated production mode (leaving free in the fit the ggF contribution).

the production cross sections and on the mass of these additional scalars. The results have been interpreted using different 2HDM implementations.

It is not in the scope of this paper to provide an exhaustive compilation of these investigations: only some representative results are provided in the following.

Figure 49 shows the observed and expected limit on the production cross section $\times$ B.R. in $\gamma\gamma$ final states of a generic Higgs-like state $\phi$, searched in a wide interval of $m_{\gamma\gamma}$ values, from 65 to 600 GeV by ATLAS [103]. The analysed data are well described by

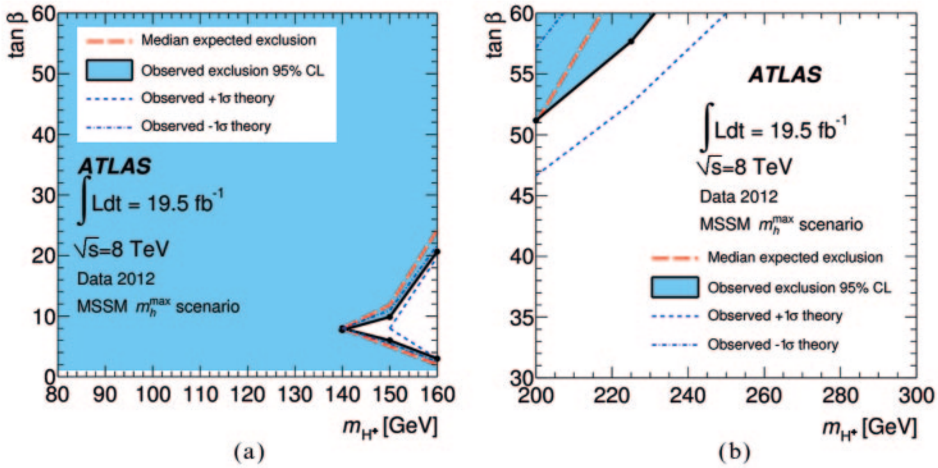


Fig. 51. – The ATLAS 95% C.L. exclusion limits on $\tan\beta$ as a function of $m_{H^+}$ [105]. Results are shown in the context of the $m_h^{\max}$ MSSM scenario, for (a) the $H^+$ low mass region, and (b) the $H^+$ high mass region.

the Standard Model expectations which include a Higgs boson with 125 GeV mass. No significant excess is observed in the wide mass interval under investigation.

Figure 50(a) shows the 95% C.L. limits on the production cross section and decay of a generic Higgs-like particle $\phi$ studied by CMS. The particle is searched through the decay $\phi \to \tau\tau$, while different production mechanisms are considered as a function of the $\phi$ mass: gluon-gluon fusion and associated production with $b$-quarks. The expected limit, assuming only SM processes (including the $H$ boson with $m_H = 125\,\text{GeV}$), is also shown [104].

Figure 51 shows the results by ATLAS on the search for the charged Higgs boson looking at $\tau\nu$ final states [105]. The analysis here has been done in the context of the so-called $m_h^{\max}$ scenario, where the $h^0$ boson mass $m_h$ gets the highest possible mass for fixed $\tan\beta$ and large mass of the $A^0$ boson [106].

## 15. – First implications of the discovery

The discovery of the Higgs boson marks a new success of the Standard Model of the elementary particles. With the inclusion of the fundamental scalar all particles predicted by the theory have been actually discovered. However, in the exact moment in which we celebrate this last triumph, we know that, even including the Higgs, the Standard Model is far from being perfect. It still appears as an incomplete theory, not able to explain many phenomena that play big roles in the evolution of our universe: the mechanism responsible for the inflation, the origin of dark matter and dark energy, the source of the large asymmetry between matter and antimatter, the role of gravity and so on.

We know therefore, that sooner or later an answer to some of these fundamental questions will be found and the SM will become a low energy case of a more general theory of matter. As of today we do not know at which energy scale this will happen but, from now on, any theory of New Physics will be further constrained by the need to include this very special object. In the following we will discuss some of the first implications of the discovery and its impact on some New Physics scenarios.

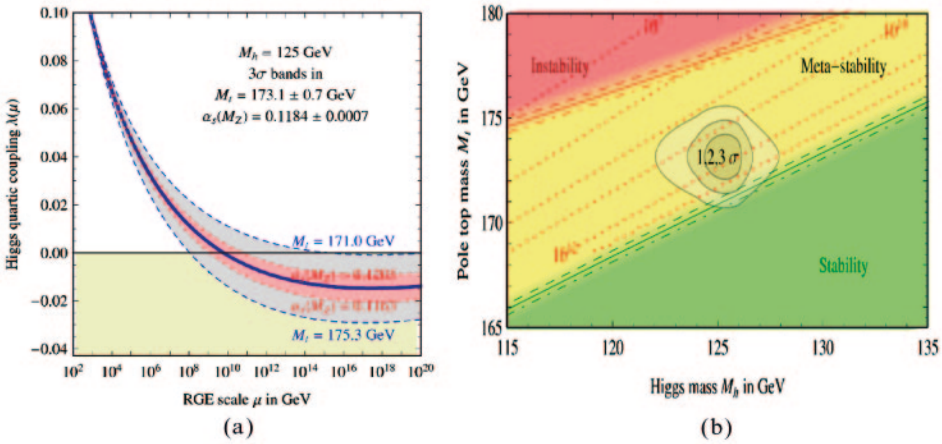


Fig. 52. – (a) RG evolution of $\lambda$ varying $M_t$ and $\alpha_s$ by $\pm 3\sigma$. (b) Regions of absolute stability, meta-stability and instability of the SM vacuum in the ($M_t$, $M_h$)-plane. The dotted colour lines show the instability scale $\Lambda$ in GeV assuming $\alpha_s = 0.1184$ [108].

**15**˙1. *Electroweak vacuum stability*. – The question of the stability of the electroweak vacuum has been studied thoroughly since many years. Now that we know the mass of the new boson, the evolution of the Higgs quartic coupling with energy can be studied more in detail. Updated evaluations have been recently made with a complete NNLO analysis [107, 108]. The measured value of the Higgs mass, $m_H = 125.09 \pm 0.24$ GeV, is close to the minimum value that ensures absolute stability of the electroweak vacuum within the Standard Model, which in turn implies a vanishing Higgs quartic coupling $\lambda$ at the Planck scale. It is intriguing to note that, with the current central values of the Higgs and top mass, $\lambda$ seems to be very small at $M_{Pl}$ while a fully vanishing Higgs self-coupling is not favoured (fig. 52). With a heavy top quark and a 125 GeV Higgs the EWK vacuum in our Universe appears to be in a meta-stable state. The Higgs potential could develop an instability around $10^{(11\text{-}12)}$ GeV, with a lifetime still much longer than the age of the Universe. However, taking into account theoretical and experimental errors, stability up to the Planck scale cannot be excluded.

Further improvements in the computation could come from a better precision in the measurement of the key parameters, namely $\alpha_s$, the Higgs mass itself and, mostly, the top quark mass, $M_t$.

In the future it would be extremely important to test the hypothesis that a light boson could in principle rule its self-interaction and the Yukawa interactions with fermions in such a way that the theory could remain weakly coupled up to the Planck scale without any dynamics appearing beyond the EWK scale. If we could be able to prove this hypothesis, this would be in itself an outstanding discovery: for the first time we would have a phenomenon that could be described by the same theory over 15 orders of magnitude in energy. Although possible, this scenario would be severely constrained by the need that the couplings of the boson must be finely tuned to very well predicted values.

Precision measurements of the couplings could lead to unambiguous hints of the presence of New Physics beyond the EWK scale. The Higgs boson properties must be therefore studied in great detail with the goal of a $< 1\%$ accuracy in the couplings.

It must be noted however, that all these studies, and, in particular, the extrapolation of the Standard Model up to the Planck scale, requires very strong assumptions that might be challenged by any New Physics discovery.

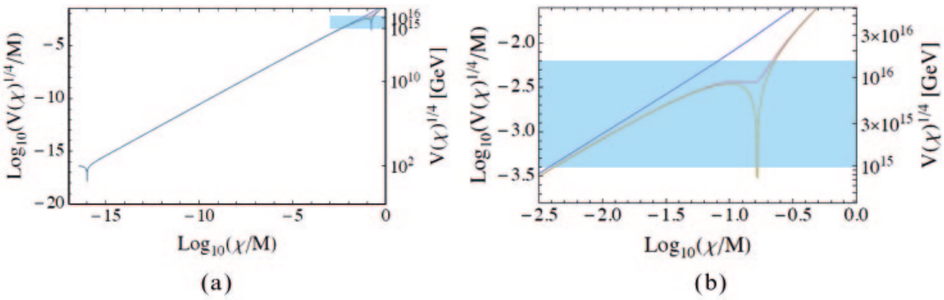


Fig. 53. – (a) Higgs potential as a function of the Higgs field value $\chi$. Assumed values for $m_t = 171.8\,\text{GeV}$ and, from top to bottom lines, $m_H = 125.2, 125.158, 125.157663\,\text{GeV}$. (b) Magnification of the false EWK vacuum region [110].

**15**˙2. *Could the Higgs be the inflaton?* – The newly discovered Higgs boson is the first fundamental particle with the properties of a scalar. Inflation is known to be driven by a negative-pressure vacuum energy density that could be produced by a slowly rolling scalar field. The hypothesis that the Higgs field could have played a role during inflation is therefore quite intriguing.

This could have happened through different mechanisms [109-112]. A non-minimal coupling to gravity could flatten the Higgs potential close to $M_{\text{Pl}}$ while keeping $\lambda$ always positive. Alternatively, the Higgs potential could have developed another false EWK minimum close to the Planck scale. The scalar boson, sitting in this second, unstable minimum could have driven the inflation to reach later the EWK minimum in which is still today. An intriguing component of this scenario is that the appearance of the second false minimum seems to be possible only for values of $m_H$ strictly compatible with the 125 GeV particle effectively discovered (see fig. 53).

Both hypotheses, however, although possible, seem not to be fully compatible with present data. New experimental measurements as well as updated computations will be crucial components to produce further developments on this subject.

**15**˙3. *SUSY and a light Higgs boson.* – A 125 GeV Higgs puts strong constraints on many models for new physics including SUSY. While in the SM, the Higgs mass is essentially a free parameter, in many implementations of MSSM, in which the Higgs sector is extended to contain three neutral and two charged scalar bosons, the lightest CP-even Higgs particle is bounded from above to mass values $\leq 110$–$135\,\text{GeV}$.

Figure 54(a) shows that there is still room to accommodate this relatively heavy object, but several classes of models have been already excluded by this discovery [113]. It must be noted however that, for the models compatible with all constraints, large mixing parameters for the *stop* are favoured (see fig. 54(b)).

It must be lastly considered that virtual loops of the new heavy particles predicted by SUSY would modify the coupling of the Higgs, therefore precision measurements of the couplings will add important additional constrains.

The combination of direct and indirect searches for SUSY, and the implications for SUSY coming from the measurement of the couplings of the new boson, will likely lead either to a discovery of super-symmetry or to a drastic revision of some of its paradigms.

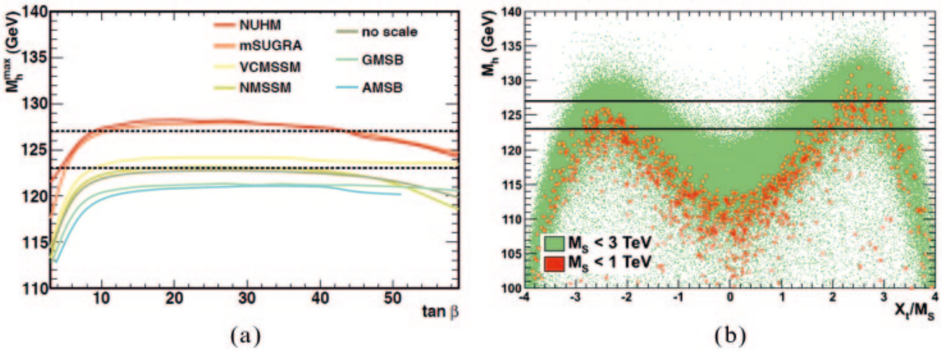


Fig. 54. – (a) The maximum value of the $h$ mass shown as a function of $\tan\beta$ for the various constrained MSSM models. (b) The maximum value of the $h$ boson mass as a function of the mixing parameter $X_t/M_S$ in the pMSSM when all other soft SUSY-breaking parameters and $\tan\beta$ are scanned [113].

## 16. – Future prospects

The discovery of the 125 GeV Higgs boson opens a new era in particle physics. Data collected so far, within the so-called LHC Run 1, indicate a full consistency of the new particle with the Higgs boson predicted by the Standard Model. If confirmed to be an elementary object, this particle would be the only fundamental scalar ever observed in nature. At the time of writing this paper, the LHC is opening a new era in high-energy physics, producing proton-proton collisions at the unprecedented energy of $\sqrt{s} = 13\,\text{TeV}$. Further machine developments will be made during the next years to increase the energy of the accelerator to 14 TeV, the design value.

Precision measurements are now essential to confirm the Standard Model properties of this Higgs boson, and to probe for possible, subtle effects produced by New Physics phenomena, an approach fully complementary to the direct search for new particles.

Table III. – *Summary of the physics-based targets for Higgs boson couplings to vector bosons, top quarks, and bottom quarks. It is assumed here that no other exotic electroweak symmetry breaking state (e.g. new Higgs bosons or $\rho$ particle) is found at LHC, except for the SM-like Higgs boson resonance just discovered. For the $\Delta h\bar{b}b$ values of supersymmetry, the superscript "a" refers to the case of* $\tan\beta > 20$ *and no superpartners are found at the LHC, and the superscript "b" refers to all other cases, with the maximum* 100% *value reached for the special case of* $\tan\beta \simeq 5$ [114]. *The fourth row reports the uncertainty evaluated at LHC with the* 7 *and* 8 TeV *data (Run 1, for* 1 *experiment only), while the last row reports anticipated uncertainties at* 14 TeV *and* 300 $\text{fb}^{-1}$ *of data, based on the studies presented in refs.* [115, 116].

| | $\Delta hVV$ | $\Delta h\bar{t}t$ | $\Delta h\bar{b}b$ |
|---|---|---|---|
| Mixed-in singlet | 6% | 6% | 6% |
| Composite Higgs | 8% | tens of % | tens of % |
| Minimal supersymmetry | $< 1\%$ | 3% | $10\%^a$, $100\%^b$ |
| LHC Run 1 | $\sim 15\%$ | $\sim 40\%$ | $\sim 30\%$ |
| LHC 14 TeV 300 $\text{fb}^{-1}$ | $\sim 6\%$ | $\sim 15\%$ | $\sim 12\%$ |

TABLE IV. – *Summary of the anticipated Higgs boson couplings to vector bosons ($W$, $Z$ and $\gamma$), top and bottom quarks, tau and muon leptons at the LHC, for two different luminosity scenarios, $L = 300$ and $3000\,\mathrm{fb}^{-1}$, respectively. In this model, no Higgs boson decay modes are permitted other than those predicted by Standard Model. The findings reported here are based on predictions available in refs.* [115, 116].

| | $\Delta hVV$ | $\Delta h\bar{b}b$ | $\Delta h\bar{t}t$ | $\Delta h\bar{\tau}\tau$ | $\Delta h\mu\mu$ |
|---|---|---|---|---|---|
| $L = 2\times10^{34}\,\mathrm{cm}^{-2}\,\mathrm{s}^{-1}$, $300\,\mathrm{fb}^{-1}$ | 6% | 12% | 15% | 10% | 22% |
| $L = 5\times10^{34}\,\mathrm{cm}^{-2}\,\mathrm{s}^{-1}$, $3000\,\mathrm{fb}^{-1}$ | 3% | 5% | 7% | 5% | 8% |

One obvious question that arises is how well we need to measure the couplings to elementary particles of this new object. Quite a few papers are available in the literature to address this point; for example, ref. [114] suggests various, highly motivated scenarios for New Physics: supersymmetry, mixed-in hidden sector Higgs bosons, and a composite Higgs boson. Table III summarises the result of the study, and compares it with the present uncertainties and with the uncertainties expected by the end of LHC physics programme [115, 116], in 2022. The results take into account the luminosity upgrade of the machine, planned in 2018-2019, to increase the instantaneous luminosity to $L = 2\times10^{34}\,\mathrm{cm}^{-2}\,\mathrm{s}^{-1}$, and to collect about $300\,\mathrm{fb}^{-1}$ of data.

To reach the ultimate precision on the Higgs couplings, strong efforts will be needed to improve both the experimental measurements and the theory calculations.

On the experimental side, high precision measurements can be achieved with the large statistics data sample that can be produced with the final luminosity upgrade of LHC, HL-LHC [117, 118]. Within this project, still to be formally approved, the LHC instantaneous luminosity would increase to values close to $L = 10^{35}\,\mathrm{cm}^{-2}\,\mathrm{s}^{-1}$, and the plan is to collect up to $3000\,\mathrm{fb}^{-1}$ of data, starting from 2025, after a long shutdown of about two years.

On the theoretical side, a significant reduction of the uncertainty on the Higgs boson production cross section, due to QCD scale variations at NNLO (in particular for the gluon-fusion process), and to the current level of PDF knowledge, is mandatory. Recent preliminary $N^3LO$ gluon-gluon calculations [119-122] indicate that the cross section uncertainty due to the QCD scale can be reduced by a factor of about 3, down to 3%. Similarly, new preliminary PDF fits indicate that the uncertainty on the Higgs boson production can be reduced by a factor of about 3 [123].

Table IV shows the summary of the expected accuracy on Higgs coupling fits based on the independent studies made by ATLAS [115] and CMS [116] already mentioned. In the model under investigation, no Higgs boson decay is permitted other than those predicted by the Standard Model. Coupling ratios are largely model independent, and hence they also are studied in detail at the LHC and HL-LHC. The deterioration of some of the performance expected from the large pile-up predicted for HL-LHC (in average about 140 overlapping inelastic events at $L = 5\times10^{34}\,\mathrm{cm}^{-2}\,\mathrm{s}^{-1}$) will be largely compensated by the overall superior performance of the upgraded LHC detectors. Moreover, the large statistics sample that will be produced by HL-LHC will allow more accurate background determination from data, thus allowing an important reduction of the experimental systematics affecting the results of the first LHC run. The scenario with reduced theory uncertainties is considered in this summary.

It should be stated that the projections currently available from ATLAS and CMS are based on the data analyses that were available at the time of the discovery. They do not take into account the improvements that can be obtained with more aggressive analyses, and with the study of several additional processes that have been already included in the legacy results of the 7 and 8 TeV data.

Measurements of the Higgs couplings with an accuracy down to the sub-% level will likely require dedicated projects, *e.g.* experiments at new electron-positron collider(s). Furthermore collisions of electrons and positrons would probe directly the Higgs invisible width and allow for a precise measurement of the natural width, less affected by model dependencies.

The Higgs boson self-coupling plays a crucial role in probing the origin of the electroweak symmetry breaking. In the Standard Model, the value of this coupling is fully determined when the Higgs boson mass is assigned. At particle colliders, it can be experimentally extracted measuring the Higgs boson pair production. This process is extremely rare and the measurement extremely difficult, however it is of paramount importance since the parameter is particularly sensitive to effects predicted by several theoretical implementations of physics beyond the Standard Model.

The total SM HH production cross section at the LHC is predicted to be 41 fb (with an error of $\pm 8.5\%$ from QCD scale uncertainties and $\pm 7\%$ from PDF $+\,\alpha_S$) [124, 125]. With $3000\,\mathrm{fb}^{-1}$, 120 K Higgs boson pairs would be produced at the HL-LHC. Many final states are possible, but only a limited number of processes are experimentally accessible [126, 127]. In many cases the results obtained with preliminary analyses appear limited by statistics. It is likely therefore, that to reach an evidence of the HH production at the HL-LHC, and to target, its observation, the combination of many different final states will not be enough. It will be, maybe, necessary the deployment of new ideas and, very likely, the combination of the results of the two general purpose experiments.

In any case the result on HH of HL-LHC will be the only one available on this important process for several decades. Any future collider, if approved, will require collision energies of 1 TeV (or larger) for $e^+e^-$ machines, or at least 50 TeV for hadron colliders, to produce results significantly superior than those expected from HL-LHC.

Future facilities for the research programme in high-energy physics are widely discussed in the community. Examples are the *Update of the European strategy for particle physics* [128], the *Report of the Particle Physics Project Prioritisation Panel (P5)* [129] and the recent *What Next: White Paper of the INFN-CSN1* [130].

Appropriate decisions will be discussed within the scientific community when 13 TeV results will be available, to get guidance from data at the highest energy possible before defining the strategy for the future.

In conclusion, we summarise in the following the most important milestones for the new analyses of the 125 GeV boson, in a scenario that assumes LHC delivering up to $3000\,\mathrm{fb}^{-1}$ of data:

$100\,\mathrm{fb}^{-1}$ *of data*:

- Observation of the Higgs boson decays $H \to \tau\tau$ and $H \to b\bar{b}$.
- Evidence for ttH production.
- Differential cross sections.

$300\,\mathrm{fb}^{-1}$ *of data*:

- Possible observation of ttH production.
- Evidence for $H \to \mu\mu$.
- Precision measurement of Higgs couplings with about 10% accuracy.

$3000\,\mathrm{fb}^{-1}$ *of data*:

- Observation of ttH production.
- Observation of $H \to \mu\mu$ and $H \to Z\gamma$.
- Precision measurement of Higgs couplings with few % accuracy.
- Evidence for HH production.

## 17. – Conclusions

In 2012, the experiments ATLAS and CMS at the Large Hadron Collider at CERN discovered a new neutral particle with mass $m_H = 125.09 \pm 0.21(\mathrm{stat}) \pm 0.11(\mathrm{syst})\,\mathrm{GeV}$, whose properties to date are fully consistent, within theoretical and experimental uncertainties, with the expectations for the Standard Model Higgs boson at that mass. All available information is so far consistent with the hypothesis that we have discovered a fundamental scalar field that pervades all corners of our universe.

With the discovery of this new particle, the Standard Model is complete and all its main parameters can be experimentally measured. The theory can be therefore fully constrained or challenged by current and future precision data. This is an unprecedented situation in high-energy physics opening new lines of research in the quest of understanding matter and the universe.

In this context establishing the true nature of the new boson is of paramount importance and answer a list of open questions that are already on the table: Is the new particle alone, or is it accompanied by other partners? Is it elementary or composite? Is it precisely the SM Higgs boson or will some subtle anomaly in its properties imply the existence of New Physics beyond the Standard Model?

The development of the scientific programme needed to address these questions will require the collection of a large statistics of data from the LHC collisions at the highest possible energy. These data will allow the search for new phenomena at the multi-TeV scale, while probing the couplings of the 125 GeV particle to elementary fermions and bosons at the level of a few percent. This new set of results will shed light on the deepest nature of the new particle, thus providing essential information to identify the best strategy for future facilities in particle physics.

## REFERENCES

[1] Glashow S., *Nucl. Phys.*, **22** (1961) 579.
[2] Weinberg S., *Phys. Rev. Lett.*, **19** (1967) 1264.
[3] Salam A., in *Weak and electromagnetic interactions in Elementary particle theory: relativistic groups and analyticity*, edited by Svarthlom N. (Almqvist & Wiksell) 1968.
[4] 't Hooft G. and Veltman M., *Nucl. Phys. B*, **44** (1972) 189.
[5] Gaillard M. K., Grannis P. D. and Sciulli F. J., *Rev. Mod. Phys.*, **71** (1999) S96.
[6] Beringer J. *et al.*, *Phys. Rev. D*, **86** (2012) 010001.

[7] Ellis J., Gaillard M. K. and Nanopoulos D. V., KCL-PH-TH-2012-04, LCTS-2012-01, CERN-PH-TH-2012-009, LBNL, UCB-PTH-12-01, ACT-1-12, MIFPA-12-01 (2012).
[8] Tonelli G., *Europhys. News*, **43N5** (2012) 20.
[9] Checchia P., *Int. J. Mod. Phys. A*, **30** (2015) 1530003.
[10] 't Hooft G., *Nucl. Phys. B*, **35** (1971) 167 `http://www.sciencedirect.com/science/article/pii/0550321371901398`.
[11] Goldstone J., *Nuovo Cimento*, **19** (1961) 154.
[12] Sundaresan M. K. and Watson P. J. S., *Phys. Rev. Lett.*, **29** (1972) 1122 `http://link.aps.org/doi/10.1103/PhysRevLett.29.1122`.
[13] Adler S. L., Dashen R. F. and Treiman S., *Phys. Rev. D*, **10** (1974) 3728.
[14] Sato K. and Sato H., *Prog. Theor. Phys.*, **54** (1975) 1564.
[15] Kohler D., Watson B. A. and Becker J. A., *Phys. Rev. Lett.*, **33** (1974) 1628 `http://link.aps.org/doi/10.1103/PhysRevLett.33.1628`.
[16] Barbieri R. and Ericson T., *Phys. Lett. B*, **57** (1975) 270 `http://www.sciencedirect.com/science/article/pii/0370269375900738`.
[17] Hasert F. *et al.*, *Phys. Lett. B*, **46** (1973) 138.
[18] Hasert F. *et al.*, *Phys. Lett. B*, **46** (1973) 121 `http://www.sciencedirect.com/science/article/pii/0370269373904942`.
[19] Aubert J., Becker U., Biggs P., Burger J. and Chen M. *et al.*, *Adv. Exp. Phys.*, **5** (1976) 128.
[20] Augustin J. *et al.*, *Phys. Rev. Lett.*, **33** (1974) 1406.
[21] Ellis J., Gaillard M. K. and Nanopoulos D. V., *Nucl. Phys. B*, **106** (1976) 292.
[22] Trost H. J. (for the Crystal Ball Collaboration), in *Proceedings of the 22nd International Conference on High Energy Physics*, July 19-25, 1984, edited by Meyer A. and Wieczorek E., Vol. **1** (Leipzig, Zeuthen, East Germany, Akad. Wiss) 1984.
[23] CUSB Collaboration, in *Proceedings of the XXIV International Conference on High Energy Physics*, *Munich, Fed. Rep. of Germany, August 4-10 1988*, edited by Kuhn Jens H., 1989.
[24] Alam M. *et al.*, *Phys. Rev. D*, **40** (1989) 712.
[25] Egli S. *et al.*, *Phys. Lett. B*, **222** (1989) 533.
[26] Buskulic D. *et al.*, *Phys. Lett. B*, **384** (1996) 427.
[27] Abreu P. *et al.*, *Nucl. Phys. B*, **421** (1994) 3.
[28] Acciarri M. *et al.*, *Phys. Lett. B*, **385** (1996) 454.
[29] Alexander G. *et al.*, *Z. Phys. C*, **73** (1997) 189.
[30] ALEPH, DELPHI, L3 and OPAL Collaborations, The LEP Working Group for Higgs Boson Searches (Editors), *Searches for Higgs bosons: preliminary combined results using LEP data collected at energies up to 202 GeV.CERN-EP/2000-055*, unpublished, 2000.
[31] Barate R. *et al.*, *Phys. Lett. B*, **565** (2003) 61.
[32] Tevatron Higgs Working Group (Editor), *Combined CDF and D0 Upper Limits on Standard Model Higgs Boson Production with up to 8.6 fb$^{-1}$ of Data. FERMILAB-CONF-11-354-E*, 2011.
[33] Goebel M., *PoS-ICHEP 2010* (2010) 570.
[34] Asner A., Baconnier Y., Barbalat O., Bassetti M. and Benvenuti C. *et al.*, CERN-84-10-V-1, ECFA-84-85, CERN-YELLOW-84-10-V-1 (1984).
[35] Evans L., *Rev. Accel. Sci. Tech.*, **3** (2010) 261.
[36] Bruning O. S., Collier P., Lebrun P., Myers S. and Ostojic R. *et al.*, CERN-2004-003-V-1, CERN-2004-003 (2004).
[37] Bruning O. S., Collier P., Lebrun P., Myers S. and Ostojic R. *et al.*, CERN-2004-003-V-2, CERN-2004-003 (2004).
[38] Benedikt M. E., Collier P. E., Mertens V. E., Poole J. E. and Schindl K. E., CERN-2004-003-V-3, CERN-2004-003 (2004).
[39] Aad G. *et al.*, *JINST*, **3** (2008) S08003.
[40] Chatrchyan S. *et al.*, *JINST*, **3** (2008) S08004.
[41] Alves A. and Augusto J. *et al.*, *JINST*, **3** (2008) S08005.

[42] Aamodt K. *et al.*, *JINST*, **3** (2008) S08002.
[43] Anelli G. *et al.*, *JINST*, **3** (2008) S08007
`http://stacks.iop.org/1748-0221/3/i=08/a=S08007`.
[44] Adriani O. *et al.*, *JINST*, **3** (2008) S08006
`http://stacks.iop.org/1748-0221/3/i=08/a=S08006`.
[45] Dittmaier S. *et al.*, (2011)
`http://arxiv.org/abs/1101.0593`.
[46] Heuer R., DESY-PROC-2010-01 (2010)
`http://dx.doi.org/10.3204/DESY-PROC-2010-01/1`.
[47] Aad G. *et al.*, *JHEP*, **1012** (2010) 060.
[48] Khachatryan V. *et al.*, *JHEP*, **1101** (2011) 080.
[49] Aad G. *et al.*, *JHEP*, **1307** (2013) 032.
[50] Chatrchyan S. *et al.*, *JHEP*, **1406** (2014) 009.
[51] Aad G. *et al.*, *Eur. Phys. J. C*, **71** (2011) 1763.
[52] Chatrchyan S. *et al.*, *Phys. Rev. D*, **84** (2011) 092004.
[53] Aad G. *et al.*, *Phys. Rev. D*, **90** (2014) 112006.
[54] Chatrchyan S. *et al.*, *Eur. Phys. J. C*, **73** (2013) 2610.
[55] Aad G. *et al.*, *JHEP*, **1303** (2013) 128.
[56] Aad G. *et al.*, *Phys. Rev. Lett.*, **105** (2010) 252303.
[57] Chatrchyan S. *et al.*, *Phys. Rev. C*, **84** (2011) 024906.
[58] Airapetian A. *et al.*, CERN-LHCC-99-15, ATLAS-TDR-15 (1999).
[59] CMS Collaboration, Chatrchyan S. *et al.*, CMS-NOTE-2010-008, CERN-CMS-NOTE-2010-008 (2010).
[60] Chatrchyan S. *et al.*, *Phys. Rev. D*, **89** (2014) 092007.
[61] Nisati A., *Pramana J. Phys.*, **79** (2012) 541.
[62] Aad G. *et al.*, *Phys. Rev. D*, **86** (2012) 032003.
[63] Chatrchyan S. *et al.*, *Phys. Lett. B*, **710** (2012) 26.
[64] Chatrchyan S. *et al.*, *Phys. Lett. B*, **710** (2012) 403.
[65] Gross E. and Vitells O., *Eur. Phys. J. C*, **70** (2010) 525.
[66] Aad G. *et al.*, *Phys. Lett. B*, **716** (2012) 1.
[67] Chatrchyan S. *et al.*, *Phys. Lett. B*, **716** (2012) 30.
[68] Chatrchyan S. *et al.*, *JHEP*, **1306** (2013) 081.
[69] Bernstein S. N., *Comm. Soc. Math. Kharkov*, **13** (1912).
[70] Gaiser J., *Charmonium spectroscopy from radiative decays of the $J/\Psi$ and $\Psi'$*, Ph.D. thesis, SLAC-R-255, SLAC (1982).
[71] Aad G. *et al.*, *Phys. Rev. Lett.*, **108** (2012) 111802.
[72] ATLAS and Collaborations C., Tech. Rep. ATLAS and CMS `http://cds.cern.ch/record/1375842`, ATLAS and CMS (2011).
[73] Aad G. *et al.*, *Phys. Rev. D*, **90** (2014) 112015.
[74] Khachatryan V. *et al.*, *Eur. Phys. J. C*, **74** (2014) 3076.
[75] Aad G. *et al.*, *Phys. Rev. D*, **91** (2015) 012006.
[76] Aad G. *et al.*, CERN-PH-EP-2014-270 (2014)
`http://arxiv.org/abs/1412.2641`.
[77] Chatrchyan S. *et al.*, *JHEP*, **1401** (2014) 096.
[78] Aad G. *et al.*, *JHEP*, **1504** (2015) 117.
[79] Chatrchyan S. *et al.*, *JHEP*, **1405** (2014) 104.
[80] Chatrchyan S. *et al.*, *Phys. Rev. D*, **89** (2014) 012003.
[81] Aad G. *et al.*, *JHEP*, **1501** (2015) 069.
[82] Chatrchyan S. *et al.*, *Nature Phys.*, **10** (2014) 557.
[83] Khachatryan V. *et al.*, *JHEP*, **09** (2014) 087 (Erratum: *JHEP*, **10** (2014) 106).
[84] Aad G. *et al.*, *Phys. Lett. B*, **738** (2014) 68.
[85] Aad G. *et al.*, *Phys. Lett. B*, **740** (2015) 222.
[86] Aad G. *et al.*, CERN-PH-EP-2015-047 (2015).
[87] Aad G. *et al.*, CERN-PH-EP-2015-109 (2015).
[88] Aad G. *et al.*, *Phys. Rev. D*, **90** (2014) 052004.

[89] Khachatryan V. *et al.*, *Eur. Phys. J. C*, **75** (2015) 212.
[90] Aad G. *et al.*, *Phys. Rev. Lett.*, **114** (2015) 191803.
[91] Khachatryan V. *et al.*, *Phys. Lett. B*, **736** (2014) 64.
[92] Aad G. *et al.*, CERN-PH-EP-2015-026 (2015).
[93] Aad G. *et al.*, *Eur. Phys. J. C*, **75** (2015) 476 http://arxiv.org/abs/1506.05669.
[94] Aad G. *et al.*, *Phys. Lett. B*, **726** (2013) 120.
[95] Aad G. *et al.*, *Eur. Phys. J. C*, **75** (2015) 231.
[96] Chatrchyan S. *et al.*, *Phys. Rev. Lett.*, **110** (2013) 081803.
[97] Heinemeyer S. *et al.*, CERN-2013-004, FERMILAB-CONF-13-667-T (2013) http://arxiv.org/abs/1307.1347.
[98] Aad G. *et al.*, *Phys. Lett. B*, **726** (2013) 88.
[99] Aad G. *et al.*, (2015) http://arxiv.org/abs/1507.04548.
[100] Branco G., Ferreira P., Lavoura L., Rebelo M. and Sher M. *et al.*, *Phys. Rep.*, **516** (2012) 1.
[101] Craig N. and Thomas S., *JHEP*, **1211** (2012) 083.
[102] Craig N., Evans J. A., Gray R., Kilic C. and Park M. *et al.*, *JHEP*, **1302** (2013) 033.
[103] Aad G. *et al.*, *Phys. Rev. Lett.*, **113** (2014) 171801.
[104] Khachatryan V. *et al.*, *JHEP*, **1410** (2014) 160.
[105] Aad G. *et al.*, *JHEP*, **1503** (2015) 088.
[106] Carena M., Heinemeyer S., Stål O., Wagner C. and Weiglein G., *Eur. Phys. J. C*, **73** (2013) 2552.
[107] Elias-Miro J., Espinosa J. R., Giudice G. F., Isidori G., Riotto A. and Strumia A., *Phys. Lett. B*, **709** (2012) 222.
[108] Degrassi G., Di Vita S., Elias-Miro J., Espinosa J. R., Giudice G. F., Isidori G. and Strumia A., *JHEP*, **08** (2012) 098.
[109] Bezrukov F. L. and Shaposhnikov M., *Phys. Lett. B*, **659** (2008) 703.
[110] Masina I. and Notari A., *Phys. Rev. Lett.*, **108** (2012) 191302.
[111] Hamada Y., arXiv:1504.04246 (2015).
[112] Notari A., *Phys. Rev. D*, **91** (2015) 063527 http://link.aps.org/doi/10.1103/PhysRevD.91.063527.
[113] Arbey A., Battaglia M., Djouadi A., Mahmoudi F. and Quevillon J., *Phys. Lett. B*, **708** (2012) 162.
[114] Gupta R. S., Rzehak H. and Wells J. D., *Phys. Rev. D*, **86** (2012) 095001.
[115] ATLAS Coll., ATL-PHYS-PUB-2014-016 (2014) http://cds.cern.ch/record/1956710.
[116] CMS Coll., CMS-NOTE-13-002 (2013) http://arxiv.org/abs/1307.7135.
[117] Rossi L. and Brüning O.,, ATS-2012-236 (2012) https://indico.cern.ch/event/175067/call-for-abstracts/153/file/0.
[118] Brüning O. and Rossi L., *The High Luminosity Large Hadron Collider: The New Machine for Illuminating the Mysteries of Universe* (World Scientific) 2015.
[119] Anastasiou C., Buehler S., Herzog F. and Lazopoulos A., *JHEP*, **1112** (2011) 058.
[120] Anastasiou C., Duhr C., Dulat F., Furlan E. and Gehrmann T. *et al.*, *Phys. Lett. B*, **737** (2014) 325.
[121] Anastasiou C., Duhr C., Dulat F., Furlan E. and Gehrmann T. *et al.*, *JHEP*, **1503** (2015) 091.
[122] Anastasiou C., Duhr C., Dulat F., Herzog F. and Mistlberger B., *Phys. Rev. Lett.*, **114** (2015) 212001.
[123] Forte S., *talk at the XXIII International Workshop on Deep-Inelastic Scattering and Related Subjects* (2015) https://indico.cern.ch/event/341292/session/3/contribution/250.

[124] de Florian D. and Mazzitelli J., *Phys. Rev. Lett.*, **111** (2013) 201801.
[125] Grigo J., Melnikov K. and Steinhauser M., *Nucl. Phys. B*, **888** (2014) 17.
[126] ATLAS Coll., ATL-PHYS-PUB-2014-019 (2014)
`http://cds.cern.ch/record/1956733`.
[127] CMS Coll., CERN-LHCC-2015-010; LHCC-P-008 (2015)
`http://cds.cern.ch/record/2020886`.
[128] Krammer M., *Phys. Scr.*, **2013** (2013) 014019
`http://stacks.iop.org/1402-4896/2013/i=T158/a=014019`.
[129] U.S. Department of Energy (2014)
`http://www.usparticlephysics.org/p5/`.
[130] Andreazza A. *et al.*, *Frascati Phys. Ser.*, **60** (2015) 1.